

Effect of Hydrogen Spillover on Acidic Properties of Silica-supported Tungsten oxide
Catalysts: *In situ* DRIFTS study



A Dissertation Submitted in Partial Fulfillment of the Requirements
for the Degree of Doctor of Engineering in Chemical Engineering
Department of Chemical Engineering
FACULTY OF ENGINEERING
Chulalongkorn University
Academic Year 2020
Copyright of Chulalongkorn University

ผลของไฮโดรเจนสปีลล์โอเวอร์ต่อสมบัติความเป็นกรดของตัวเร่งปฏิกิริยาทั้งสแตนด์อัลโตนอกไซด์บนตัว
รองรับซิลิกาโดยการวิเคราะห์ด้วยเทคนิค *In situ* DRIFTS



วิทยานิพนธ์นี้เป็นส่วนหนึ่งของการศึกษาตามหลักสูตรปริญญาวิทยาศาสตรดุษฎีบัณฑิต
สาขาวิชาวิศวกรรมเคมี ภาควิชาวิศวกรรมเคมี
คณะวิศวกรรมศาสตร์ จุฬาลงกรณ์มหาวิทยาลัย
ปีการศึกษา 2563
ลิขสิทธิ์ของจุฬาลงกรณ์มหาวิทยาลัย

Thesis Title Effect of Hydrogen Spillover on Acidic Properties of
Silica-supported Tungsten oxide Catalysts: *In situ* DRIFTS
study
By Mr. Sirawat Boonpai
Field of Study Chemical Engineering
Thesis Advisor Professor PIYASAN PRASERTHDAM, Dr.Ing.

Accepted by the FACULTY OF ENGINEERING, Chulalongkorn University in
Partial Fulfillment of the Requirement for the Doctor of Engineering

..... Dean of the FACULTY OF
ENGINEERING
(Professor SUPOT TEACHAVORASINSKUN, D.Eng.)

DISSERTATION COMMITTEE

..... Chairman
(Sippakorn Wannakao, Ph.D.)

..... Thesis Advisor
(Professor PIYASAN PRASERTHDAM, Dr.Ing.)

..... Examiner
(Professor JOONGJAI PANPRANOT, Ph.D.)

..... Examiner
(Professor SUTTICHAJ ASSABUMRUNGRAT, Ph.D.)

..... Examiner
(Professor BUNJERD JONGSOMJIT, Ph.D.)

ศิริวัฒน์ บุญผาย : ผลของไฮโดรเจนสปิลล์โอเวอร์ต่อสมบัติความเป็นกรดของตัวเร่ง
 ปฏิริยาทั้งสแตนออกไซด์บนตัวรองรับซิลิกาโดยการวิเคราะห์ด้วย
 เทคนิค *In situ* DRIFTS. (Effect of Hydrogen Spillover on Acidic Properties of
 Silica-supported Tungsten oxide Catalysts: *In situ* DRIFTS study) อ.ที่ปรึกษา
 หลัก : ศ. ดร.ปิยะสาร ประเสริฐธรรม

การศึกษาบทบาทของไฮโดรเจนสปิลล์โอเวอร์ต่อสมบัติความเป็นกรดบนพื้นผิวตัวเร่ง
 ปฏิริยาโลหะและโลหะออกไซด์มีความสำคัญและเป็นประโยชน์อย่างยิ่งต่อปฏิริยาที่มีความ
 เกี่ยวข้องกับไฮโดรเจน เนื่องจากความเป็นกรดของตัวเร่งปฏิริยามีบทบาทสำคัญต่อเคมีพื้นผิวและ
 สมบัติของตัวเร่งปฏิริยา อย่างไรก็ตามตัวเร่งปฏิริยาโลหะออกไซด์ยังคงมีการศึกษาไม่แพร่หลาย
 มากนัก ดังนั้นวัตถุประสงค์ของงานวิจัยนี้คือเพื่อศึกษาผลของไฮโดรเจนสปิลล์โอเวอร์ต่อสมบัติ
 ความเป็นกรดของตัวเร่งปฏิริยาทั้งสแตนออกไซด์โดยการวิเคราะห์ด้วยเทคนิค *In situ* DRIFTS
 จากผลการศึกษาพบว่าไฮโดรเจนสปิลล์โอเวอร์ส่งผลให้เกิดการเปลี่ยนรูปของกรดลิวอิสไปเป็น
 กรดบรอนสเตดบนตัวเร่งปฏิริยาทั้งสแตนออกไซด์ได้แก่ W/HY-500 W/SiO₂ W/HY-15
 W/MCM-22 W/Al₂O₃ W/SSP และ W-SSP โดยการเปลี่ยนรูปของกรดลิวอิสมีความสัมพันธ์ต่อ
 ปริมาณของไซต์เร่งปฏิริยาได้แก่ช่องว่างของออกซิเจนและทั้งสแตนออกไซด์ที่มีเลขออกซิเดชันห้า
 บวก ซึ่งไซต์เร่งปฏิริยาเหล่านี้สามารถเกิดขึ้นได้โดยการเตรียมตัวเร่งปฏิริยาและการปรับสภาพ
 ด้วยไฮโดรเจนและไนโตรเจน นอกจากนี้งานวิจัยนี้ยังพบว่าไฮโดรเจนสปิลล์โอเวอร์ส่งผลให้เกิด
 การเพิ่มขึ้นของหมู่ไฮดรอกซิลบนตัวรองรับซิลิกา ซึ่งอินเตอร์เฟซของทั้งสแตนออกไซด์และตัว
 รองรับมีบทบาทสำคัญต่อการเพิ่มขึ้นของหมู่ไฮดรอกซิลโดยไฮโดรเจนสปิลล์โอเวอร์บางส่วนสามารถ
 ไปดูดซับที่บริเวณอินเตอร์เฟซของทั้งสแตนออกไซด์และตัวรองรับจึงส่งผลให้เกิดการเพิ่มขึ้นของ
 หมู่ไฮดรอกซิล โดยงานวิจัยนี้เป็นประโยชน์ต่อการเข้าใจบทบาทของไฮโดรเจนที่มีต่อพื้นผิวตัวเร่ง
 ปฏิริยาทั้งสแตนออกไซด์ซึ่งสามารถนำไปสู่การออกแบบและพัฒนาตัวเร่งปฏิริยาให้มีสมบัติที่
 เหมาะสมยิ่งขึ้นในอนาคต

สาขาวิชา วิศวกรรมเคมี
 ปีการศึกษา 2563

ลายมือชื่อนิสิต
 ลายมือชื่อ อ.ที่ปรึกษาหลัก

5971446121 : MAJOR CHEMICAL ENGINEERING

KEYWORD: Tungsten oxide, Silica, Lewis acid, Hydrogen spillover

Sirawat Boonpai : Effect of Hydrogen Spillover on Acidic Properties of Silica-supported Tungsten oxide Catalysts: *In situ* DRIFTS study. Advisor: Prof. PIYASAN PRASERTHDAM, Dr.Ing.

The knowledge and understanding about hydrogen spillover on the acidic property over surface metal and metal oxide catalysts are beneficial information in catalytic reactions with hydrogen. The perception of the nature of the surface acidity is a key role in catalytic properties and surface chemistry. However, metal oxide catalyst is still not widely studied on this issue. Therefore, the aim of this work is to investigate the effect of hydrogen spillover on their acidic property over silica-supported W catalysts by *in situ* DRIFTS. The results of *in situ* DRIFTS experiments have confirmed that the acidic property of silica-supported W catalysts was affected by hydrogen spillover. The Lewis acid site can be changed to the Brønsted acid site upon hydrogen exposure of activated catalysts (i.e., W/HY-500, W/SiO₂, W/HY-15, W/MCM-22, W/Al₂O₃, W/SSP, and W-SSP). The Lewis acid transformation performance correlates with oxygen vacancy and tungstate W⁵⁺ active species. This active site could be generated by catalyst preparations and activating the process of H₂ and N₂ pretreatments. Additionally, molecular hydrogen can be dissociated to form hydrogen spillover onto surface catalysts leads to form the new Si-OH species. It was postulated that the Si-O-W species is a major importance for new Si-OH formation. Some H atoms should be adsorbed around the Lewis acid site of Si-O-W species leads to the Si-OH formation.

Field of Study: Chemical Engineering

Student's Signature

Academic Year: 2020

Advisor's Signature

ACKNOWLEDGEMENTS

The author would first like to thank the advisor, Prof. Piyasan Praserttham, whose expertise was invaluable in formulating the research questions and methodology. His insightful feedback pushed the author to sharpen my thinking and brought the work to a higher level. The author would like to acknowledge the professor at Chulalongkorn University, Prof. Bunjerd Jongsomjit, Prof. Joongjai Panpranot, and Prof. Suttichai Assabumrungrat. Their supports and discussions are valuable information to complete the thesis and research publications.

The author appreciated the SCG Chemical Co., Ltd., for financial support and a great opportunity to do research in a doctoral degree. The author would like to acknowledge Dr. Kongkiat Suriye and Dr. Sippakorn Wannakao including all employees and friends who work at SCG – CHULA ENGINEERING Research Center. The author would also like to thank Prof. Alexis T. Bell accepted me to be visiting student researcher at the University of California at Berkeley including his supports for research publication. Also, the author would like to acknowledge Dr. Prael Chirawatkul from the Synchrotron Light Research Institute (SLRI) to support results and discussion.

Additionally, the author would like to thank parents. Finally, the author could not have completed this dissertation without the support of friends, Adisak Guntida and Victor Márquez, who help me in research, experiment, and publication.

Sirawat Boonpai

TABLE OF CONTENTS

	Page
.....	iii
ABSTRACT (THAI).....	iii
.....	iv
ABSTRACT (ENGLISH).....	iv
ACKNOWLEDGEMENTS.....	v
TABLE OF CONTENTS.....	vi
LIST OF TABLES.....	ix
LIST OF FIGURES.....	x
CHAPTER I INTRODUCTION.....	1
1.1 Rational.....	1
1.2 Objective.....	2
CHAPTER II THEORY AND LITERATURE REVIEWS.....	3
2.1 Hydrogen spillover on heterogeneous catalysts.....	3
2.2 Formation of hydroxyl groups.....	5
2.3 Transformation of Lewis acid to Brønsted acid.....	6
2.4 Supported tungsten oxide catalyst.....	9
CHAPTER III RESEARCH SCOPES AND METHODOLOGY.....	13
3.1 Research scopes.....	13
3.2 Benefits.....	14
3.3 Research methodology.....	15
CHAPTER IV EXPERIMENTAL.....	15

4.1 Chemicals and materials	16
4.2 Catalyst preparation	16
4.3 Catalyst characterizations	18
4.4 <i>In situ</i> DRIFTS experiments	20
CHAPTER V RESULT AND DISCUSSION	22
5.1 Effect of different supports on hydrogen activated supported W catalysts for Lewis acid transformation to Brønsted acid.....	22
5.2 Active Site Formation in WO _x Supported on Spherical Silica Catalysts for Lewis Acid Transformation to Brønsted Acid Activity.....	47
5.3 Influence of isolated tungstate sites on surface Si-OH formation with hydrogen-bonded clusters over spherical silica-supported WO _x catalysts.....	59
5.4 Influence of surface Sn species and hydrogen interactions on the OH group formation over spherical silica-supported tin oxide catalysts.....	69
5.5 Model mechanism of hydrogen spillover on acidic properties.....	84
CHAPTER VI CONCLUSION AND RECOMMENDATION.....	86
6.1 Conclusions	86
6.2 Recommendations.....	87
APPENDIX A.....	88
Supporting information.....	88
A.1) Active Site Formation in WO _x Supported on Spherical Silica Catalysts for Lewis Acid Transformation to Brønsted Acid Activity.....	88
A.2) Influence of isolated tungstate sites on surface Si-OH formation with hydrogen-bonded clusters over spherical silica-supported WO _x catalysts.....	92
A.3) Influence of surface Sn species and hydrogen interactions on the OH group formation over spherical silica-supported tin oxide catalysts.....	96
APPENDIX B.....	100

List of Publications 100

REFERENCES 101

VITA..... 119



LIST OF TABLES

	Page
Table 5.1 Surface characterization by transmission electron microscopy and energy-dispersive X-ray spectroscopy (TEM-EDS) on Supported W catalysts.....	25
Table 5.2 Surface characterization by X-ray photoelectron spectroscopy (XPS) on Supported W catalysts with H ₂ /N ₂ gas pretreatments.....	31
Table 5.3 Percentage of loss of Lewis acid sites over Supported W catalysts for 130 min.....	38
Table 5.4 Relative area of X-ray photoelectron spectroscopy (XPS) of SSP-supported W catalysts with gas pretreatment.	49
Table 5.5 Deconvoluted results of relative peaks ²⁹ Si NMR analysis of catalysts.	61
Table 5.6 Textural properties of SSP-supported Sn catalysts.....	71
Table 5.7 Normalized relative area of XPS and ²⁹ Si NMR analysis of SnO _x supported on SSP catalysts.....	81

LIST OF FIGURES

	Page
Figure 2.1 Hydrogen spillover from an adsorbing metal to an oxide surface [32].	3
Figure 2.2 Producing protons and Ti^{3+} cations by hydrogen spillover from Pt to the TiO_2 [36].	4
Figure 2.3 Hydrogen spillover formed on Ir clusters onto the silica support [44].	5
Figure 2.4 Hydrogen spillover to active sites on the periphery of Ru on SBA-15 in H_2 [48].	6
Figure 2.5 Structures of Lewis acid sites and Brønsted acid sites on the surface of SO_4-ZrO_2 [36].	7
Figure 2.6 A model for the formation of a protonic acid site from molecular hydrogen on Pt/SO_4-ZrO_2 [52].	8
Figure 2.7 Proposed mechanism of ammonia migration on Lewis acid to Brønsted acid sites.[54]	9
Figure 2.8 Structures of WO_x species on SiO_2 of W/SiO_2 catalyst. (a) Dioxo WO_4 , (b) mono-oxo WO_5 , and (c) crystalline WO_3 nanoparticles.	11
Figure 2.9 Proposed model of the acid site of tungsten oxide structure [66].	11
Figure 2.10 Proposed model of tungstate species on alumina [69].	12
Figure 5.11 H_2 -TPR profiles of the Supported W catalysts.	23
Figure 5.12 XRD patterns of the Supported W catalysts (colored continuous lines) and Supported W catalysts with H_2/N_2 gas pretreatments (dotted lines) and standard data reference from JCPDS (black continuous lines)	24
Figure 5.13 TEM images (top) and high-resolution TEM image (bottom) of the Supported W catalysts.	25

Figure 5.14 UV-Vis DRS patterns of the Supported W catalysts; (a) Supported W catalysts, (b) Supported W catalysts with H ₂ /N ₂ gas pretreatments.....	27
Figure 5.15 XPS spectra of W 4f _{7/2} and W 4f _{5/2} for Supported W catalysts with H ₂ /N ₂ gas pretreatments; W/Al ₂ O ₃ (a), W/MCM-22 (b), W/HY-15 (c), W/SiO ₂ (d), W/HY-500 (e).	29
Figure 5.16 XPS spectra of O 1S for Supported W catalysts with H ₂ /N ₂ gas pretreatments; W/Al ₂ O ₃ (a), W/MCM-22 (b), W/HY-15 (c), W/SiO ₂ (d), W/HY-500 (e)....	30
Figure 5.17 O ₂ -TPD profiles of the Supported W catalysts.	32
Figure 5.18 H ₂ -TPD profiles of the catalysts; Supported W catalysts (a) and only supports (b).....	33
Figure 19 FTIR spectra of ammonia adsorbed during the introduction of hydrogen at 100 °C for 130 min over the Supported W catalysts; W/Al ₂ O ₃ (a), W/MCM-22 (b), W/HY-15 (c), W/SiO ₂ (d), W/HY-500 (e).	36
Figure 20 Percentages of remaining Lewis acid sites (a), and percentages of generated Brønsted acid sites (b) on Supported W catalysts; W/Al ₂ O ₃ (■), W/MCM-22 (●), W/HY-15 (▲), W/SiO ₂ (▼), W/HY-500 (◆).	37
Figure 21 The effect of the amount of oxygen vacancy on the loss of Lewis acid sites over the Supported W catalysts.....	39
Figure 22 UV-Vis DRS patterns of the Supported W catalysts with H ₂ /N ₂ gas pretreatments at different temperature (175, 250, 350, and 500 °C).....	41
Figure 23 IR spectra of ammonia adsorbed during the introduction of hydrogen at 100 °C for 130 min over the W/SiO ₂ catalysts with H ₂ /N ₂ gas pretreatments at different temperature; (a) 175 °C, (b) 250 °C, (c) 350 °C, (d) 500 °C.....	43
Figure 24 Percentages of remaining Lewis acid sites (a), and percentages of generated Brønsted acid sites (b) on W/SiO ₂ catalysts with H ₂ /N ₂ gas pretreatments at different temperature; 175 °C (■), 250 °C (●), 350 °C (▲), 500 °C (▼).	45
Figure 25 The summarized Lewis acid transformation over the Supported W catalysts.	46

Figure 5.26 SEM images (a, b), TEM images (c, d): (a,c) W/SSP, (b, d) W-SSP.	47
Figure 5.27 Wide-angle XRD patterns (a) and ^{29}Si NMR spectra (b) of SSP-supported W catalysts.	48
Figure 28 In situ DRIFTS spectra of adsorbed NH_3 upon hydrogen exposure for 0-120 min (orange region) and nitrogen purging for 120-180 min (blue region) at 100 °C over catalysts; W-SSP- H_2 (a), W/SSP- H_2 (b), W-SSP- N_2 (c), and W/SSP- N_2 (d).	50
Figure 29 Percentages of decreased Lewis acid sites (yellow), and increased Brønsted acid sites (green) over SSP-supported W catalysts.	52
Figure 30 XPS spectra of W $4f_{7/2}$ and W $4f_{5/2}$ for SSP-supported W catalysts with gas pretreatment; W-SSP- H_2 (a), W/SSP- H_2 (b), W-SSP- N_2 (c), and W/SSP- N_2 (d).	53
Figure 31 Wide-angle XRD patterns (a) and W L_1 edge XANES spectra (b) for SSP-supported W catalysts with gas pretreatment.	56
Figure 32 Activation of active site and Lewis acid transformation to Brønsted acid over SSP-supported W catalysts.	58
Figure 33 TEM images of catalysts (a) 4W-SSP, (b) 4W/SSP, (c) 8W-SSP, (d) 8W/SSP.	60
Figure 34 (a) XRD patterns and (b) Raman spectra of catalysts.	62
Figure 35 (a) Normalized W L_1 edge XANES spectra and (b) ^{29}Si NMR of catalysts.	63
Figure 36 In situ DRIFTS spectra with hydrogen exposure of catalysts; 8W-SSP (a), 4W-SSP (b), 8W/SSP (c), and 4W/SSP (d).	64
Figure 37 In situ DRIFTS spectra with hydrogen exposure of catalysts; 8W-SSP (a), 4W-SSP (b), 8W/SSP (c), and 4W/SSP (d).	66
Figure 38 H_2 -TPD profiles of catalysts.	67
Figure 39 Schematic model of Si-OH formation under hydrogen exposure over SSP-supported WO_x catalysts.	69
Figure 40 SEM images (a, d, g, j), TEM images (b, c, e, f, h, i, k, l), and EDS elemental mapping analysis (m-o): (a-c) IWI-5Sn, (d-f) IWI-10Sn, (g-i) Inc-5Sn, (j-l) Inc-10Sn, (m-o) Inc-5Sn.	70

Figure 41 Wide-angle XRD patterns of SSP-supported Sn catalysts; IWI-10Sn (a), IWI-5Sn (b), Inc-10Sn (c), and Inc-5Sn (d).....	71
Figure 42 UV-vis DRS spectra of SSP-supported Sn catalysts.....	73
Figure 43 (a) Sn3d XPS spectra and deconvoluted peak results (b) O1s XPS spectra of SSP-supported Sn catalysts.....	75
Figure 44 Solid state ^{29}Si NMR spectra and deconvoluted peak results of SSP-supported Sn catalysts; IWI-5Sn (a), IWI-10Sn (b), Inc-5Sn (c), and Inc-10Sn (d).....	76
Figure 45 In situ DRIFT spectra during the introduction of hydrogen at 40 °C for 30 min over the SnO _x supported on SSP catalysts; Inc-10Sn (a), Inc-5Sn (b), IWI-10Sn (c), and IWI-5Sn (d).....	78
Figure 46 Relative area (IR band at 3200 cm ⁻¹) of formation of new OH groups on silica surface over the SSP-supported Sn catalysts.....	79
Figure 47 H ₂ -TPD profiles of SSP-supported Sn catalysts; IWI-10Sn (a), IWI-5Sn (b), Inc-10Sn (c), and Inc-5Sn (d).....	80
Figure 48 Correlation of the amount of Sn–O–Si species ^[a] on the formation of new OH groups ^[b] on silica surface over SSP-supported Sn catalysts. ^[a] XPS analysis, ^[b] Area of IR band 3200 cm ⁻¹ at final.....	81
Figure 49 Summarized the formation of new OH groups on silica surface over SnO _x supported on SSP catalysts.....	84
Figure 50 Model mechanism of hydrogen spillover on acidic properties of silica-supported tungsten oxide catalysts.....	85

CHAPTER I INTRODUCTION

1.1 Rational

The knowledge and understanding about hydrogen spillover on catalyst surface can give beneficial information in catalytic reactions with hydrogen. Since, the hydrogen spillover is common phenomenon in catalytic reactions with hydrogen over supported metals and metal oxides. Generally, metal catalysts (e.g., Pt, Pd, Ir, and Ru) have applied in many catalytic reactions with hydrogen, in which they can serve an active species for hydrogen dissociation [1-6]. However, the metal materials show a disadvantage to use for big scale application due to the its high-cost [7, 8]. Lately, metal oxide catalysts have attracted in catalytic reactions with hydrogen according to their properties such as highly active, acidity, and low-cost catalysts [4, 9-12]. Additionally, the studying of tungsten oxides catalysts has become a popular issue due to nonstoichiometric and oxygen vacancy (WO_{3-x}), which encourages interesting properties for catalytic reactions with hydrogen [13-16]. The unique properties of tungsten oxide are acid sites over their surface [17], which can be explained as Lewis and Brønsted acidity. These acid sites were regarded as a kind of promising property owing to its versatile application [18-20]. Supports of tungsten oxides catalysts (e.g., silica, alumina, and zeolites) are commonly used in catalytic systems [21-23], in which the nature of support can improve the surface tungstate species on their surface. However, the supported WO_x catalyst can active for many reactions with hydrogen such as isomerization, alkylation, dehydration, cracking and metathesis reactions [24-27]. A small amount of WO_3 not only enhances the acid strength, but also introduces Brønsted acid of catalyst [28]. Huang et al. found the HY contents in WO_x supported on Al_2O_3 -HY catalyst modified the interaction between W species and support and changing the Brønsted acidity of catalysts [29]. The interest properties of WO_x applications, WO_x is a versatile and efficient catalyst for the hydrogenation reaction. Hydrogenation activity is governed by WO_x surface with an oxygen vacancy that can easily activate H_2 molecules. Song et al. proposed that WO_x surface with oxygen vacancy can activate H_2 molecules very easily in kinetics and thermodynamics [30].

However, metal oxide catalyst is still not widely studied on hydrogen spillover and acidity over surface catalyst. Therefore, this issue is necessary to study for academic and industry. The perception of the nature of the surface acidity is a key role for catalytic properties and surface chemistry. In addition, a deeper understanding of the hydrogen surface behavior will provide benefits information on the for further catalyst designs.

1.2 Objective

To investigate the effect of hydrogen spillover on their acidic property over tungsten oxide catalyst by *in situ* DRIFTS.



CHAPTER II THEORY AND LITERATURE REVIEWS

2.1 Hydrogen spillover on heterogeneous catalysts

The spillover in heterogeneous catalysis is described as the migration of active species, which was adsorbed or formed from one phase to another phase. The word “spillover” is the migration of H atoms from the metal particles to the support because the H atoms could migrate from a hydrogen-rich to a hydrogen-poor surface [31]. The phase generating the active species (H atoms) is called the initiator/activator, while the phase providing sites for the adsorption of active species is called the acceptor as shown in **Figure 2.1**.

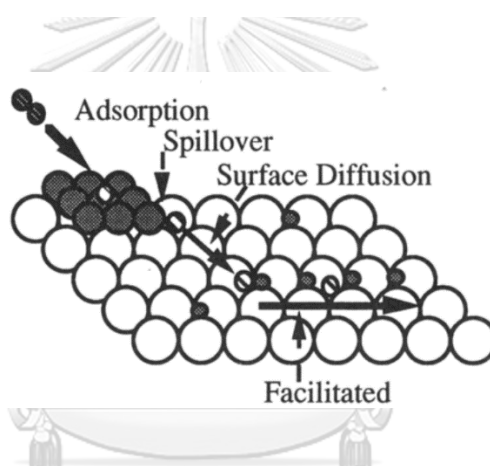
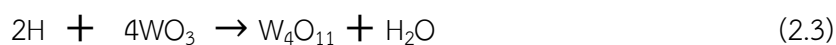


Figure 2.1 Hydrogen spillover from an adsorbing metal to an oxide surface [32].

Usually, H atoms are not produced on the surface of a support, but H atoms are created on a metal/metal oxide surface and migrate to the surface of the support. Khoobiar [33] reported the first evidence of hydrogen spillover by the reduction of WO_3 . Generally, WO_3 could be reduced by hydrogen at temperatures above 200 °C. When WO_3 was mixed with $\text{Pt}/\text{Al}_2\text{O}_3$, they were found to be reduced at lower temperature. However, the low reduction was not found on the $\text{Al}_2\text{O}_3 + \text{WO}_3$ mixture. Therefore, this effect is described by hydrogen spillover, in which hydrogen was dissociated to form H atoms on Pt and migrated onto WO_3 .





Sinfelt and Lucchesi [34] studied the hydrogen spillover of Pt/SiO₂ and ethene hydrogenation. According to hydrogen spillover, the support (i.e., Al₂O₃ and SiO₂) could hydrogenate ethene and benzene under the hydrogen treatment by means of indirect contact with a metal-support catalyst. The hydrogen spillover phenomenon is common in catalysis by supported metals and metal oxides. The function of acceptors of H atoms can be found in adsorbed unsaturated compounds and the metal oxides. Hydrogen spillover from metal particles on a reducible support can lead to full or partial reduction of the reducible support. Huizinga and Prins found the reduction of Pt/TiO₂ at 573K leads to the formation of a Ti³⁺ [35]. The hydrogen spillover onto TiO₂ from Pt site leads to the formation of Ti³⁺ and OH⁻ ions as shown in **Figure 2.2**.

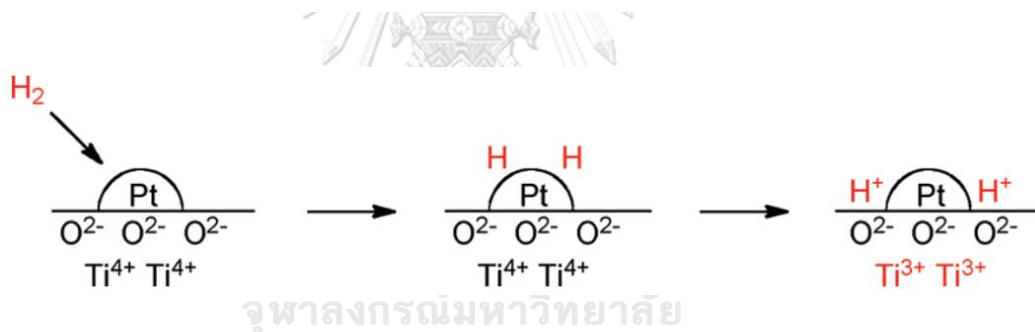


Figure 2.2 Producing protons and Ti³⁺ cations by hydrogen spillover from Pt to the TiO₂ [36].

Recently, Karim et. al. described that hydrogen spillover on the nonreducible support aluminium oxide is vastly slower and limited to short distances than the reducible support titanium oxide.[37] The hydrogen flux decreased over distance to create a concentration gradient on the nonreducible support aluminium oxide. Although, the hydrogen spillover is very slow on the nonreducible support, this phenomenon is common effect in catalysis by supported metals that carried out in the presence of hydrogen.

2.2 Formation of hydroxyl groups

Generally, the final state of hydrogen spillover is the hydroxy-groups (OH) formation because the oxygen ions can serve as H atoms acceptors or ions [31]:



This phenomenon could be explained by the migration of the adsorbed H species across the surface. Surface diffusion is a transportation of this species across a chemically uniform surface [32]. The strength of the interaction between the adsorbed H species and the surface involve the van der Waalls type interactions to more localized bonding between surface atoms and the species [32]. However, the formed OH groups act as effective adsorption or reactive sites for adsorbed species, and can even dominate the activity of these substances [38]. In addition, the surface OH groups on the catalyst can provide valuable information about the properties (i.e., the acid strength) of hydroxyl groups that often act as the catalytic active sites, especially for silica-based catalysts [39-41]. The behavior of silica as a support for catalytic species depends on its physical and chemical surface properties, especially those related to hydroxyl groups [21, 42, 43].

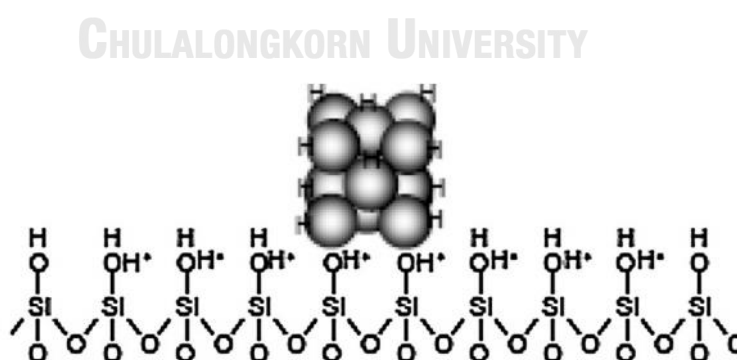


Figure 2.3 Hydrogen spillover formed on Ir clusters onto the silica support [44].

It is noteworthy that the surface OH groups can be formed on silica-supported catalysts in the presence of a hydrogen atmosphere by hydrogen spillover. Wallin et

al. [45] found that the isolated OH groups were formed on the silica surface of Pt/SiO₂ catalyst as proven by FTIR spectroscopy. These new hydroxyl groups appeared on the silica surface during H₂ exposure in the presence of Pt particles. It was suggested that hydrogen molecules dissociate on the Pt particles to form H atoms which then migrate (spillover) to the silica surface and produce new hydroxyl groups. Miyao et al. [44] studied the hydrogen occlusion in hollow silica nano-spheres encapsulating iridium metal clusters (Ir-SiO₂) observed using FTIR. They also found that OH groups are formed by hydrogen spillover caused by the migration of hydrogen atoms formed on Ir clusters onto the silica support as shown in **Figure 2.3**. Wu et al. [46] found that the adsorbed H atoms from dissociated methane were transferred to SiO₂ surface to form surface (-OH) species during the partial oxidation of methane to syngas over Rh/SiO₂ catalyst. These increased hydroxyls could be explained by the hydrogen spillover transferring from the dissociated hydrogen to adsorb at the bridging oxygen atoms of the silica support [46, 47]. The formation of new OH groups on silica surface involves hydrogen spillover that occurs by the dissociation of hydrogen molecules on the metal particles. Recently, Shen et al. reported that the possible structure for active sites of hydrogenation over Ru/SBA-15 catalysts using in situ FTIR experiments with adsorbed H species, in which the formation rate of H species depended on the Ru particle as shown in **Figure 2.4** [48].



Figure 2.4 Hydrogen spillover to active sites on the periphery of Ru on SBA-15 in H₂ [48].

2.3 Transformation of Lewis acid to Brønsted acid

Under hydrogen conditions, the number of Brønsted acid sites could be increased and Lewis acid sites could be decreased by hydrogen spillover effect. Ebitani et al. have studied hydroisomerization of butane to isobutane and pentane to

isopentane on sulfated zirconia ($\text{SO}_4\text{-ZrO}_2$) as shown in **Figure 2.5**. They reported that the number of Brønsted acid sites was increased, while Lewis acid sites was decreased over $\text{Pt}/\text{SO}_4\text{-ZrO}_2$ by hydrogen spillover from the metal to the support [49, 50].

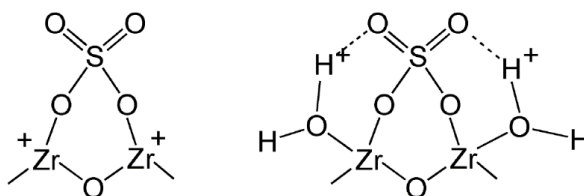


Figure 2.5 Structures of Lewis acid sites and Brønsted acid sites on the surface of $\text{SO}_4\text{-ZrO}_2$ [36].

Also, Satoh et al. explained that the spillover H atoms can react with an electron trapped around Lewis acid site, and then forms the H^- hydride anion [51]. As shown in **Figure 2.6**, Hattori and Shishido studied the promotion of hydrogen molecule on Brønsted acid sites over $\text{Pt}/\text{SO}_4\text{-ZrO}_2$ catalyst including a physical mixture of Pt/SiO_2 and H-ZSM5, and Co-Mo/ $\text{SiO}_2\text{-Al}_2\text{O}_3$ catalysts [52]. They proposed that the hydrogen spillover migrates onto the catalyst surface to Lewis acid sites, where the H atom releases an electron to become a proton. This proton can be stabilized at the O atom around the Lewis acid site. The electron trapped on the Lewis acid site may react with a second hydrogen atom to form a bond H^- -Lewis acid site. Besides, the Lewis acid sites can lose its function and convert to the Brønsted acid sites.

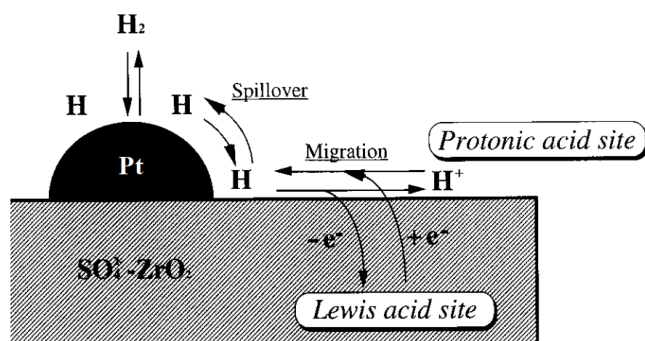


Figure 2.6 A model for the formation of a protonic acid site from molecular hydrogen on Pt/SO₄-ZrO₂ [52].

Additionally, Ueda et al. studied on a physically mixing of SiO₂-supported noble metals catalysts and zeolites/alumina by pyridine IR. They also found that the pyridine on a Lewis acid sites are migrated to the Brønsted acid sites under a hydrogen [53]. It is indicated that hydrogen spillover can enhance the desorption of pyridine adsorbed on the Lewis acid sites, and can supply the Lewis acid sites in the possible form of hydride ion. Guntida et al. studied the transformation of Lewis acid sites to Brønsted acid sites over hybrid Pt/Al₂O₃ catalysts during the introduction of hydrogen by ammonia IR [54]. They found that ammonia was migrated from Lewis acid sites to Brønsted acid sites under hydrogen conditions. As shown in **Figure 2.7**, hydrogen molecules are dissociated on platinum site species to form H atoms and then are migrated onto the support surface to Lewis acid sites. The Lewis acid site is trapped by from H atoms that decomposed to electrons and protons, Finally, ammonia migrate from the Lewis acid sites to adjacent Brønsted acid sites to form ammonium ions.

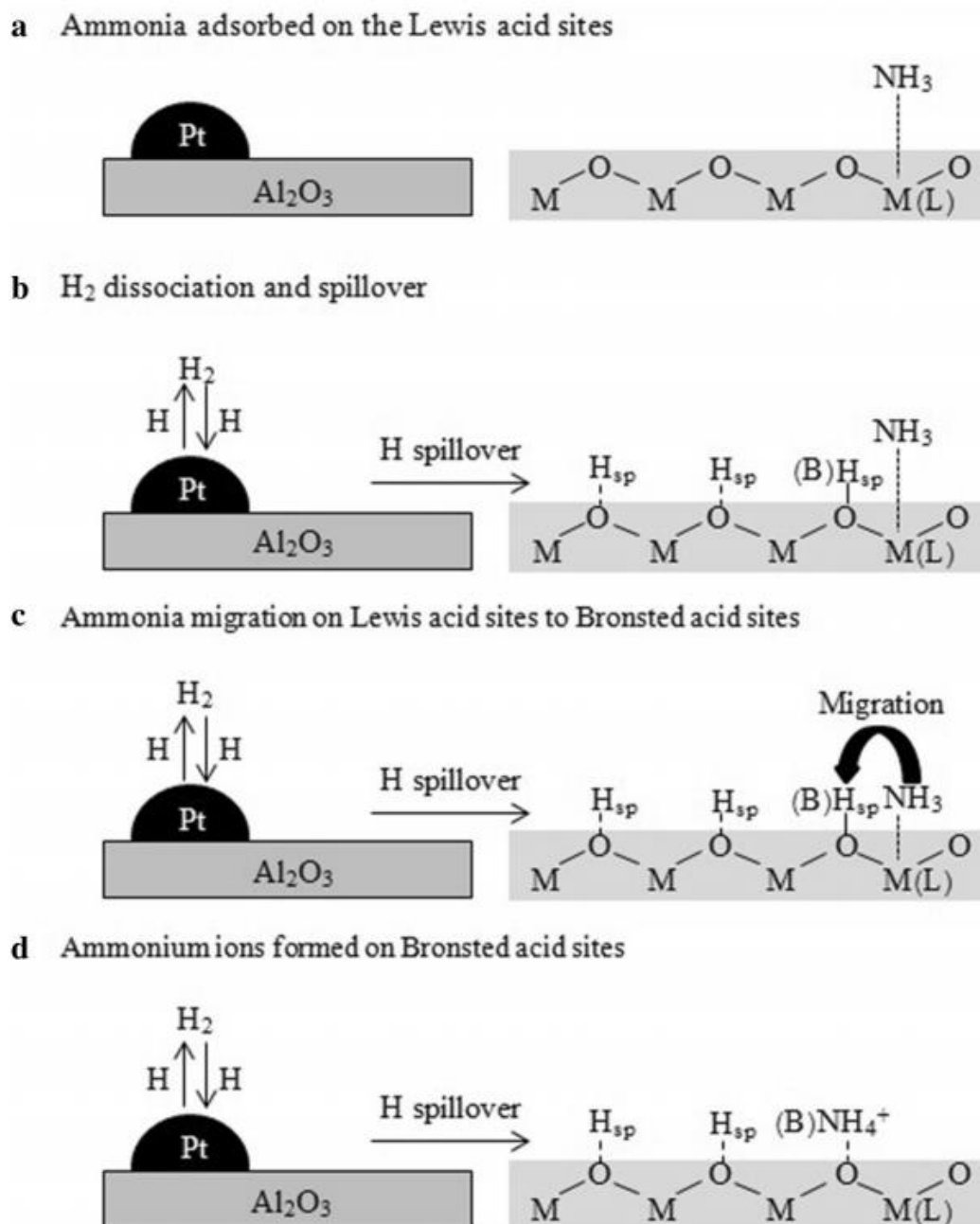


Figure 2.7 Proposed mechanism of ammonia migration on Lewis acid to Brønsted acid sites.[54]

2.4 Supported tungsten oxide catalyst

Tungsten oxide (WO_x) have been used in catalytic reactions for a long time. This catalyst presents an active species for many applications such as hydrocracking,

dehydrogenation, isomerization, reforming, alcohol dehydration, and olefin oligomerization reactions. Many reactions could be activated by the Bulk WO_3 , but required high temperatures because of its low surface area and weak acid sites [55]. Therefore, the partial reduction of tungsten oxides as WO_3 to WO_2 are usually applied for catalytic reactions. The reduction of W^{6+} species on tungsten oxide catalysts lead to increasing of the strength of acid sites and the rate of catalytic reactions [56]. Zaki et al. reported that the formation of $\text{WO}_{2.96}$, $\text{WO}_{2.9}$, and $\text{WO}_{2.72}$ oxidation states, which are partially reduced from WO_3 catalysts, could be generated by controlling the H_2 reduction conditions [57]. Choung and Weller found that some intermediate nonstoichiometric tungsten oxide (WO_{3-x}) was the most active species for propylene self-metathesis reaction that occurred from the N_2 or H_2 pretreatments [58]. Westhoff and Moulijn found that the sample intermediate between WO_3 and $\text{WO}_{2.95}$, which were formed by H_2 pretreatment at 600 °C, provided a high activity in propylene self-metathesis [59]. Recently, the interest properties of new applications, the nonstoichiometric of tungsten oxides with surface oxygen vacancies is a versatile and efficient catalyst for the hydrogenation reaction. Song et al. proposed that WO_x surface with oxygen vacancy can activate H_2 molecules very easily in kinetics and thermodynamics [30]. Tungsten oxide supported on silica (W/SiO_2) comprise surface tungsten oxide species (WO_x) and tungsten oxide crystal (WO_3) [60]. The W/SiO_2 catalyst was used in a large number of industrial applications because of its benefits such as catalyst lifetimes, lower costs, resistance to poisoning, coking and impurities, and regeneration [61]. The surface tungsten oxide species consist of octahedral, tetrahedral and polytungstate species [62]. The surface structures of W/SiO_2 catalyst present for fully oxidized have been measured from the in-situ spectroscopy method (Raman and UV-Vis technique) [63, 64]. The structures of WO_x species on SiO_2 , dioxo ($\text{O}=\text{W}(\text{-O})_2$), mono-oxo $\text{O}=\text{W}(\text{-O})_4$, and crystalline WO_3 nanoparticles species are presented in **Figure 2.8**. For an over loading of tungsten, crystalline WO_3 nanoparticles are present [65]. The tetrahedral tungsten oxide species is mentioned to Brønsted and Lewis acid sites as shown in as shown in **Figure 2.9**. The bond between W and OH (W-OH bond) is indicated to The Brønsted acid sites [66].

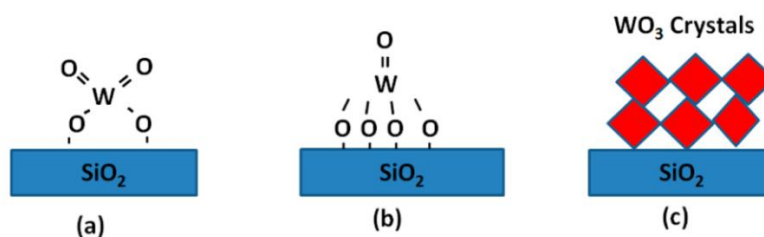


Figure 2.8 Structures of WO_x species on SiO₂ of W/SiO₂ catalyst. (a) Dioxo WO₄, (b) mono-oxo WO₅, and (c) crystalline WO₃ nanoparticles.

Bliss and Dodge reported the catalytic activity of bulk WO₃ catalysts for hydration of ethylene was enhanced by W/Al₂O₃ catalyst [67]. The interest of W species on Al₂O₃ involved the strong interaction between W species and support [68]. Additionally, the W/Al₂O₃ catalysts are active for many catalytic reactions such as isomerization, hydrodesulfurization, hydrodenitrogenation, and metathesis [29, 69-71]. The increasing surface density of W and other related supported phases can develop Brønsted acid sites as reported by Chen et al. [20]. The acidity can be decreased by octahedrally coordinated species of W/Al₂O₃ when each W is connected to 5 Al atoms through W-O-Al bonds as show in **Figure 2.10** [69]. Moreover, Zhu et al. reported that the addition of W to Pt/Al₂O₃ catalyst can show a powerful approach to modify acidic properties with electronic structure, and to control the catalytic performance in glycerol hydrogenolysis [72].

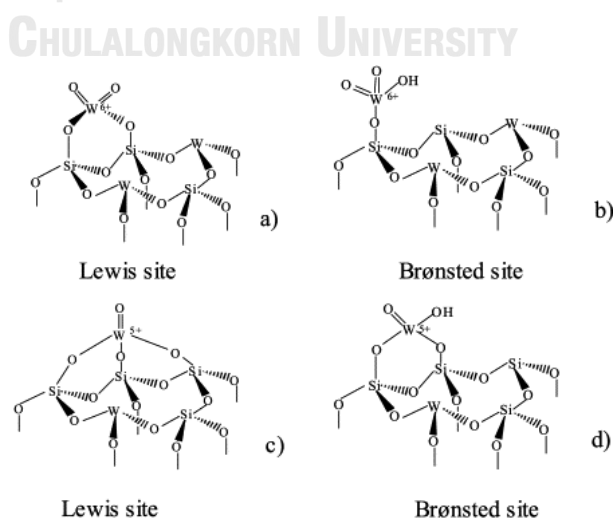


Figure 2.9 Proposed model of the acid site of tungsten oxide structure [66].

Zeolites support show more feasibilities than other supports to modify the properties such as acidity and pore structure. Recently, the noble metal supported on Y-zeolite catalysts have received increasing attention as important industrial aromatic hydrogenation catalysts [73-76]. The use of alumina-zeolite supports can improve the Brønsted acidity of the Supported W catalysts because the zeolites have notable Brønsted acidity. Huang et al. reported that the HY contents in WO_x supported on Al_2O_3 -HY catalyst modified the interaction between W species and support and changing the Brønsted acidity of catalysts [29]. The high HY content in Supported W catalyst can produce the Brønsted acid sites, but reduce the interaction between W species and support [29]. Hu et al. studied the toluene hydrogenation over Pd and Pd-M bimetallic catalysts (M = Cr, W, La, Mn, Mo, Ag) on a mixed Al_2O_3 -HY support [77]. They found all of the bimetallic supported on Al_2O_3 -HY support active for hydrogenation and isomerization. The MCM-22 support show more attention as important industrial catalysts. Asensi et al. studied the skeletal isomerization of 1-butene on two MCM-22 zeolite catalysts synthesized with different Si/Al ratios. They reported the increasing the Si/Al ratios of the zeolite can improve the selectivity to isobutene [78]. Nuntasri et al. reported that the MCM-22 can be an active and highly selective catalyst for the liquid-phase cyclopentene hydration [79]. Some of the metathesis catalyst focus on the MCM-22. Liu et al. studied the influences of support composition on catalytic activity of ethene and butene-2 to propene metathesis reaction. They reported that the $3.0Mo/MCM-22-30\%Al_2O_3$ show the best catalyst activity and stability. The good metathesis activity was obtained by high dispersi70on of Mo species on the support and higher valences of Mo precursor [80].

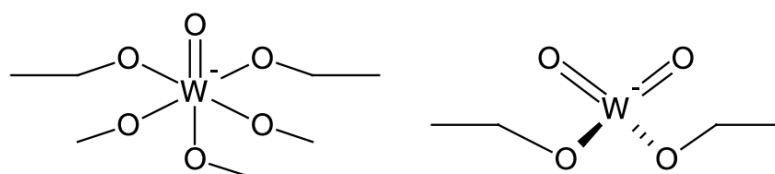


Figure 2.10 Proposed model of tungstate species on alumina [69].

CHAPTER III RESEARCH SCOPES AND METHODOLOGY

3.1 Research scopes

The scopes of the study are shown below.

1. The transformation of Lewis acid was investigated by *in situ* diffuse reflection infrared Fourier transform spectroscopy (DRIFTS) with adsorbed NH_3 under atmospheric pressure at 40 and 100 °C. The decreasing percentage of Lewis acid sites over catalysts was calculated using the deconvoluted area of band around 1622 cm^{-1} , while the increasing percentage of Brønsted acid sites was using the deconvoluted area of bands around 1448 and 1680 cm^{-1} .

- a. The catalysts were prepared by incipient wetness impregnation as WO_x catalysts supported on different supports (HY-15, HY-500, MCM-22, SiO_2 , and Al_2O_3).
- b. The catalysts were synthesized by two methods: (i) incorporation of tungsten oxide to spherical silica using the sol-gel method (W-SSP) and (ii) wetness impregnation method (W/SSP).

2. The formation of new OH groups was investigated using *in situ* diffuse reflection infrared Fourier transform spectroscopy (DRIFTS) with hydrogen exposure under atmospheric pressure. The formation of new OH groups was considered using the deconvoluted IR peaks of OH groups vibrations on silica surface over catalysts.

- a. The catalysts were synthesized by two methods: (i) incorporation of tungsten oxide to spherical silica using the sol-gel method (W-SSP) and (ii) wetness impregnation method (W/SSP).
- b. The catalysts were synthesized by two different methods, incipient wetness impregnation (IWI-Sn) and incorporation (Inc-Sn) of Sn species to SSP support with the sol-gel method.

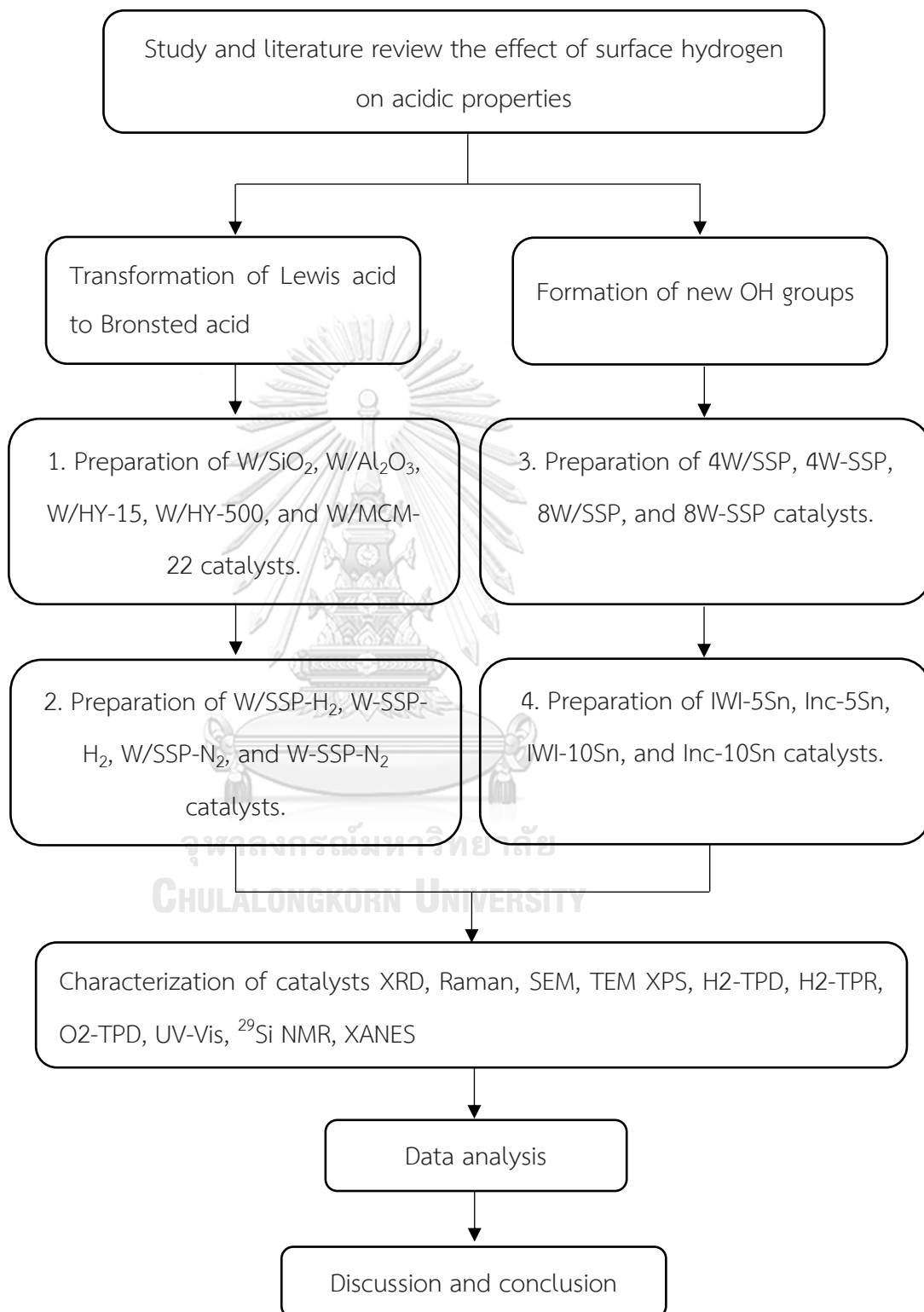
3. The catalysts were discussed and investigated by several analytical techniques such as XRD, Raman, SEM, TEM, XPS, H_2 -TPD, H_2 -TPR, O_2 -TPD, UV-Vis, ^{29}Si NMR, and W L_1 edge XANES techniques.

3.2 Benefits

Understanding of the effect of hydrogen over influence of W species on the support, which is beneficial information for design and control the catalytic performance.



3.3 Research methodology



CHAPTER IV EXPERIMENTAL

4.1 Chemicals and materials

4.1.1 Chemicals

- 1) Ammonium metatungstate, Sigma-Aldrich
- 2) Tin (II) chloride dihydrate, Sigma-Aldrich
- 3) Ethanol, Labscan
- 4) Tetraethoxysilane (TEOS), Sigma-Aldrich
- 5) Cetyl trimethyl ammonium bromide (CTAB), Sigma-Aldrich
- 6) Ammonia, Sigma-Aldrich

4.1.2 Materials

- 1) Boehmite, Sasol
- 2) Silicon dioxide (5-15 nm), Sigma-Aldrich
- 3) HY-500 (Si/Al = 500), Sigma-Aldrich
- 4) HY-15 (Si/Al = 15), Sigma-Aldrich
- 5) MCM-22 (Si/Al = 30), Sigma-Aldrich

4.2 Catalyst preparation

4.2.1 Preparation of WO_x supported on different supports catalyst.

The 9wt% of supported W catalysts were prepared by wetness impregnation method using different supports. Before impregnation, the boehmite was calcined at temperature higher than 530 °C for 4 h with heating rate of 3 °C/min to obtain γ - Al_2O_3 support. Then, porous materials and zeolites having different Si/Al ratios (SiO_2 , HY-15 (Si/Al = 15), HY-15 (Si/Al = 500), MCM-22 (Si/Al = 30)) were used as the supports. The supports were impregnated by aqueous solution of ammonium metatungstate hydrate (Sigma-Aldrich). The impregnated samples were dried with ambient air for 2 h, then kept in an oven at 110 °C for 10 h. Finally, the catalysts supported on different supports were calcined at temperature higher than 530 °C in air for 8 h with heating rate of 10 °C/min.

4.2.2 Preparation of WO_x supported on spherical silica catalyst

The preparation of SSP support was conducted by sol-gel method using tetraethoxysilane (TEOS) as silica source and cetyl trimethyl ammonium bromide (CTAB) as structure directing agent, in which the composition consisted of 1 TEOS:0.3 CTAB:11 NH_3 :58 C_2H_5OH :114 H_2O by mole as reported in the literature [81]. The CTAB was firstly added into the solution of ethanol, de-ionize water, and ammonia, followed by stirring at 350 rpm for 15 min. After that, the TEOS was slowly added into the mixed solution to gain the gel, followed by stirring at 350 rpm for 120 min. Finally, the solution was filtrated and washed with de-ionized water until becomes neutral. To remove the template and surfactant, the obtained sample was then dried in an oven at 110 °C for 10 h and calcined at 550 °C in air for 6 h with heating rate of 2 °C/min. The 12 wt% of impregnated W/SSP was prepared by incipient wetness impregnation method. The SSP was impregnated by aqueous solution of ammonium metatungstate hydrate (Sigma-Aldrich). The impregnated sample was dried under ambient air for 2 h, then kept in an oven at 110 °C for 10 h. Finally, the sample was calcined at 550 °C in air for 8 h with heating rate of 10 °C/min. The 12 wt% of incorporated W-SSP of W species to SSP catalysts was prepared by the modified sol-gel method of SSP synthesis, in which the TEOS and aqueous solution of ammonium metatungstate hydrate were added into the mixed solution simultaneously, then followed by the same filtration, washing, drying. Finally, the incorporated sample was calcined at 550 °C in air for 8 h with heating rate of 2 °C/min.

4.2.3 Preparation of SnO_x supported on spherical silica catalyst

The incorporation of Sn into SSP (Inc-Sn) was performed via the modified sol-gel method of SSP synthesis mentioned above. After the mixture of CTAB, ethanol, de-ionized water, and ammonia solution were stirred at 350 rpm for 15 min, the mixed solution of TEOS and tin chloride dihydrate ($SnCl_2 \cdot 2H_2O$) was added into the mixed solution, followed by the same filtration, washing, drying and calcination steps. To prepare the catalysts by the incipient wetness impregnation method using the analogously prepared SSP support (IWI-Sn), the SSP was impregnated with an aqueous solution of tin chloride dihydrate. The impregnated samples were dried with air for 2 h, then kept in an oven at 110 °C for 10 h. Finally, the samples were heated in air at a

rate of 10 °C/min to 550 °C and maintained at this temperature for 3 h. The prepared samples are denoted as IWI-xSn and Inc-xSn, where “x %” is the nominal Sn content by weight.

4.3 Catalyst characterizations

4.3.1 X-Ray Diffraction Analysis (XRD)

XRD patterns of the catalysts were recorded with a D8 Advance of Bruker AXS using Ni-filter selecting $\text{CuK}\alpha$ radiation. The data were collected in the 2θ range of 20° to 60°.

4.3.2 UV-vis diffuse reflectance spectroscopy (UV-vis DRS)

The UV-vis DRS was used to determine surface structure of tungsten oxide species. The UV-vis spectra were recorded on Lambda 650 spectrophotometer in the range between 200 and 800 nm.

4.3.3 X-ray photoelectron spectroscopy (XPS)

The XPS analysis was performed on an AMICUS photoelectron spectrometer equipped with an Mg $\text{K}\alpha$ X-ray radiation operated at a voltage of 10 kV and a current of 20 mA.

4.3.4 Hydrogen temperature-programmed reduction (H_2 -TPR)

The H_2 -TPR analysis was performed to investigate reducibility of the catalysts. The measurement was carried out in a quartz microreactor by using the Micrometrics Chemisorbs 2750 automated system. First, the sample (200 mg) was pretreated in Ar (99.99%, 25 ml/min) at 500 °C for 1 h, and then cooled down to room temperature. After cooling to room temperature in Ar, it was followed by a temperature-programmed reduction by 10% H_2 in Ar (15 ml/min) from room temperature to 900 °C with a temperature ramp of 10 °C/min. Hydrogen consumption was monitored by a thermal conductivity detector (TCD).

4.3.5 Hydrogen temperature-programmed desorption (H_2 -TPD)

Hydrogen temperature-programmed desorption (H_2 -TPD) analysis was used to determine the adsorption behavior of hydrogen. The sample was carried out in a quartz microreactor by using the Micrometrics Chemisorbs 2750 automated system. The sample was reduced under mixed gas of H_2 flow (99.99%, 25 ml/min) and N_2 flow

(99.999%, 25 ml/min) at 500 °C for 1 h, and then it was heated to 550 °C at a heating rate of 10 °C/min under a pure N₂ gas flow for 30 min. Then, the sample was cooled to the adsorption temperature at 40 °C under a pure N₂ gas flow, followed by purging with pure H₂ gas flow for 30 min for H₂ adsorption. Finally, the sample was purged with a pure N₂ gas flow for 1 h, and then it was heated to 500 °C at a heating rate of 10 °C/min under a pure N₂ gas flow. The signal of H₂ desorption was monitored by a thermal conductivity detector.

4.3.6 Oxygen temperature-programmed desorption (O₂-TPD)

Oxygen temperature-programmed desorption (O₂-TPD) analysis was performed on a Micrometrics Chemisorbs 2750 automated system. This procedure was conducted as similar as for the H₂-TPD steps. After the H₂/N₂ reduction, the sample was cooled to 40 °C under pure He gas flow, followed by the 1% O₂/He gas flow for 30 min at 40 °C for O₂ adsorption. Then, the sample was purged with pure He gas flow for 1 h at 40 °C. Finally, the sample was heated to 500 °C at a heating rate of 10 °C/min under a pure He gas flow. The signal of O₂ desorption was monitored by a thermal conductivity detector.

4.3.7 Transmission electron microscopy (TEM) and Scanning electron microscopy (SEM)

TEM image from a JEOL JEM-2010 microscope equipped with a LaB₆ electron gun operated at 200 kV, were used to investigate the morphology and composition of the sample. The sample were dispersed in ethanol by sonication and a few drops of suspension onto a carbon-coated copper grid followed by natural evaporation. Scanning electron microscopy (SEM), and energy-dispersive X-ray spectroscopy (EDS) were investigated with Hitachi S3400N.

4.3.8 Raman spectroscopy

The Raman investigation was carried out with a Senterra Dispersive Raman Microscopy (Bruker Optics) equipped using the UV line at 532 nm and a TE-cooled CCD detector.

4.3.9 X-ray Absorption Near Edge Structure (XANES)

W L₁-edge XANES measurement was performed in transmission mode at beamlines BL1.1 W at synchrotron light research and institute (Public organization) at

the synchrotron Thailand central lab, which data processing and analysis were performed using Athena software.

4.3.10 Fourier transform nuclear magnetic resonance spectrometer (NMR)

The solid state ^{29}Si and ^1H NMR were determined by Fourier transform nuclear magnetic resonance spectrometer 400 MHz (Solid) using a Bruker AVANCE III HD (Ascend 400 WB) spectrometer using 4 mm MAS probes at a spin rate of 8 kHz.

4.4 *In situ* DRIFTS experiments

4.4.1 Transformation of Lewis acid to Brønsted acid experiment

The changes of acidity were analyzed with IR spectra obtained by the *in situ* diffuse reflectance infrared Fourier transform spectroscopy (*in situ* DRIFTS). The sample was performed in a Bruker Vertex-70 FT-IR spectrometer equipped with a Harrick Praying Mantis attachment for diffuse reflectance spectroscopy. The sample was packed in the *in situ* IR cell with KBr windows under the close circulating system. The sample was firstly pretreated under H_2/N_2 (10 ml/min) or N_2 (10 ml/min) gas flow at 500 °C for 1 h, then heated up to 550 °C under an N_2 flow and hold on 30 min, followed by cooling down to 100 °C. For ammonia adsorption, the sample was adsorbed with mixed 15% NH_3/He gas flow (10 ml/min) for 30 min at 100 °C and then flushed with N_2 gas flow for 1 h to remove physisorbed ammonia. Finally, the sample was introduced with H_2 gas flow at 100 °C for 2 h and was switched to N_2 gas flow for 1 h, in which the changes of IR spectra were automatically monitored every 10 min during this step. All obtained spectra of the adsorbed species were subtracted from the background spectrum. The decreased percentage of Lewis acid sites over catalysts was calculated by Eq. (5) using the deconvoluted area of band around 1622 cm^{-1} , while the increasing percentage of Brønsted acid sites was calculated by Eq. (6) using the deconvoluted area of bands around 1448 and 1680 cm^{-1} .

$$\text{Decreasing of Lewis acid sites (\%)} = \left(\frac{L_0 - L_i}{L_0} \right) \times 100 \quad (5)$$

$$\text{Increasing of Brønsted acid site (\%)} = \left(\frac{B_0 - B_i}{B_0} \right) \times 100 \quad (6)$$

Where L_0 and B_0 indicate the area of Lewis and Brønsted acid sites at initial, while L_i and B_i indicate the area of Lewis and Brønsted acid sites at final, respectively.

4.4.2 Hydroxyl groups formation experiment

The DRIFTS spectra of adsorbed hydrogen were obtained by the *in situ* diffuse reflectance infrared Fourier transform spectroscopy (*in situ* DRIFTS). Spectra were acquired using a Bruker Vertex-70 FT-IR spectrometer equipped with a Harrick Praying Mantis attachment for diffuse reflectance spectroscopy. The sampling was performed in the *in situ* IR cell with KBr windows connected to a close circulating system. To investigate the adsorption of hydrogen, the catalyst was first pretreated in a flow of H₂ (10 mL/min) and N₂ (10 mL/min) at 500 °C for 1 h, and then heated to 550 °C under flowing N₂ for 30 min, followed by cooling to 40 °C. Finally, the catalyst was exposed to a flow of H₂ (10 mL/min) and N₂ (10 mL/min) at 40 °C for 30 min at atmospheric pressure. DRIFTS spectra were collected every 2 min (0-30 min) using a Mercury-Cadmium-Telluride (MCT) detector with a resolution of 4 cm⁻¹ and an accumulation of 128 scans. All DRIFTS spectra were referenced by subtracting the spectrum obtained at 0 min. The deconvoluted peaks of OH groups vibrations on silica surface over catalysts were investigated using the area of deconvoluted bands.

CHAPTER V RESULT AND DISCUSSION

The chapter V was divided in 5 sections (5.1, 5.2, 5.3, 5.4, and 5.5). Firstly, the effect of hydrogen spillover on Lewis acid transformation to Brønsted acid was investigated over the WO_x catalysts supported on different supports (HY-15, HY-500, MCM-22, SiO_2 , and Al_2O_3) in the **section 5.1**. Secondly, the transformation of Lewis acid to new Brønsted acid upon hydrogen exposure of WO_x supported on mesoporous spherical silica nanoparticles (SSP) catalysts was further investigated in the **section 5.2**. The principal goal of this section is to explore the influence of W species on the support and the activating processes involved in the formation of catalytically active sites for Lewis acid transformation. To study of species and positions of acid site formation, the effect of hydrogen spillover on hydroxyl groups (Si-OH) formation was then investigated over WO_x supported on SSP catalysts in the **section 5.3**. Additionally, the proposed model mechanism was applied to further study in the other metal oxide catalyst (silica-supported SnO_x) in the **section 5.4**. Finally, the model mechanism about the effect of hydrogen spillover on acidic properties of silica-supported WO_x catalysts was proposed and described in **section 5.5**.

5.1 Effect of different supports on hydrogen activated supported W catalysts for Lewis acid transformation to Brønsted acid.

5.1.1 Characterization of Supported W catalysts

The interaction between WO_x species and the support, and the reducibility of Supported W catalysts were investigated by the H_2 -TPR. The H_2 -TPR profiles of the catalysts are compared as shown in **Figure 5.1**. In the temperature range studied (40-900 °C), there are the reduction peaks of W species on different supports. The observed peaks at low temperature about 420 and 510 °C on the W/HY-500 and W/ SiO_2 , respectively are assigned to the reduction of W species in octahedral coordination [82, 83]. Comparing between the W/HY-500 and W/ SiO_2 catalysts, the reduction of W species in octahedral coordination of W/ SiO_2 catalyst shifts to higher temperature,

indicating that the reduction of W species in octahedral coordination of W/SiO₂ catalyst was stronger than that of the W/HY-500 catalyst.

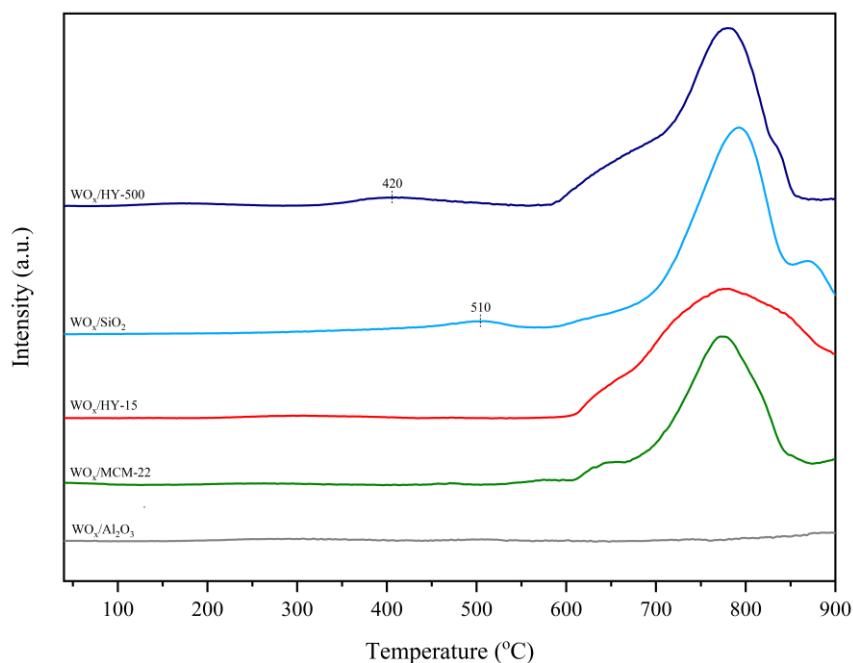


Figure 5.11 H₂-TPR profiles of the Supported W catalysts.

Generally, the broad peaks about 800 °C are assigned to the reduction of the surface amorphous WO₃ species or the WO₃ microcrystallites to the W metal [84, 85]. There are almost no reduction peaks below 800 °C on the W/Al₂O₃ due to the strong interaction between tungsten oxide and alumina support. The WO_x species appear to interact strongly with sites on the alumina support [86]. Therefore, this surface species is difficult to reduce. The low intensities of these peaks indicate the low reducibility of WO₃ crystal on the Supported W catalysts in the following order: W/Al₂O₃ < W/MCM-22 < W/HY-15 < W/SiO₂ < W/HY-500. The existence of reduction peaks of W species on the Supported W catalysts indicated that the Supported W catalysts can be reduced by hydrogen gas.

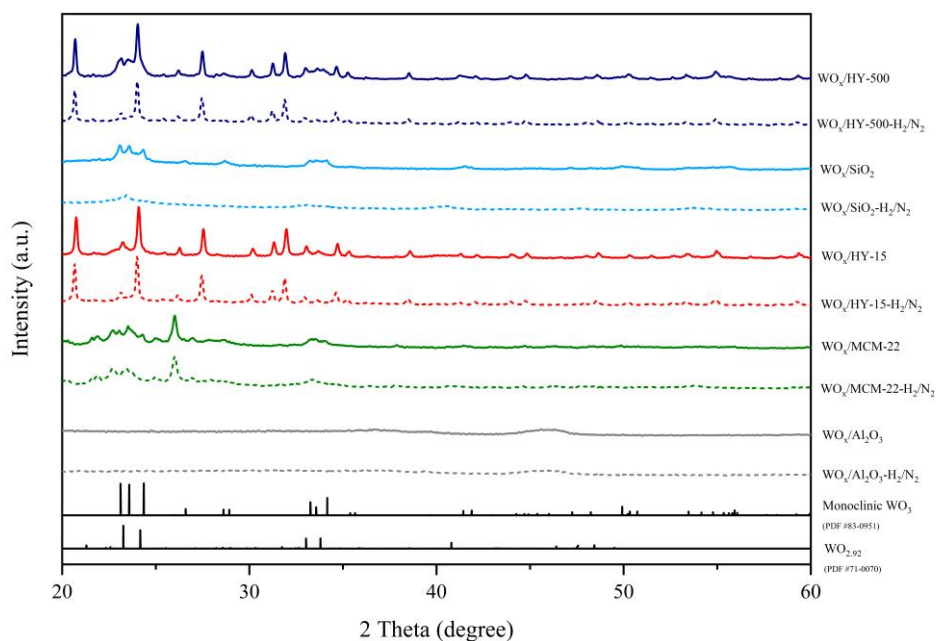


Figure 5.12 XRD patterns of the Supported W catalysts (colored continuous lines) and Supported W catalysts with H_2/N_2 gas pretreatments (dotted lines) and standard data reference from JCPDS (black continuous lines)

The XRD patterns of the Supported W catalysts are shown in Figure 5.2. The diffraction peaks revealed different patterns based on standard data reference in JCPDS. In order to investigate the crystalline phase of tungsten oxide, the W/Support and W/Support- H_2/N_2 were compared. The W/HY-15 and W/ SiO_2 catalysts showed strongly-sharp peaks corresponding to crystalline phase of tungsten oxide. When the W/HY-15 and W/ SiO_2 catalysts were pretreated with H_2/N_2 gas as W/HY-15- H_2/N_2 and W/ SiO_2 - H_2/N_2 , respectively, their XRD patterns clearly changed. Especially, the XRD patterns of W/ SiO_2 - H_2/N_2 catalyst changed as $WO_{2.92}$ phase. It indicated that the partial reduction of WO_3 could occur during the pretreatment under mixed H_2/N_2 gas due to high reducibility of WO_3 crystal on these catalysts, which was consistent with the H_2 -TPR results. Gayapan *et al.* [83] also found that the pretreatment of calcined W/ SiO_2 catalyst under mixed H_2/N_2 gas and pure H_2 exhibited the patterns assigned to $WO_{2.92}$ phase, occurring from the partial reduction of WO_3 , which is the active phase for metathesis reaction. No obvious peaks corresponding to crystalline phase of WO_3 were

detected in the different samples of W/Al₂O₃, W/MCM-22, and W/HY-15, indicating that the W phase was well dispersed on the supports forming either an amorphous phase or microcrystallites or that the WO_x crystallites are too small to be detected [86, 87]. Therefore, when the W/Al₂O₃, W/MCM-22, and W/HY-15 catalysts were reduced with hydrogen gas as W/Al₂O₃-H₂/N₂, W/MCM-22-H₂/N₂, and W/HY-15-H₂/N₂, respectively, their detected XRD patterns were not changed.

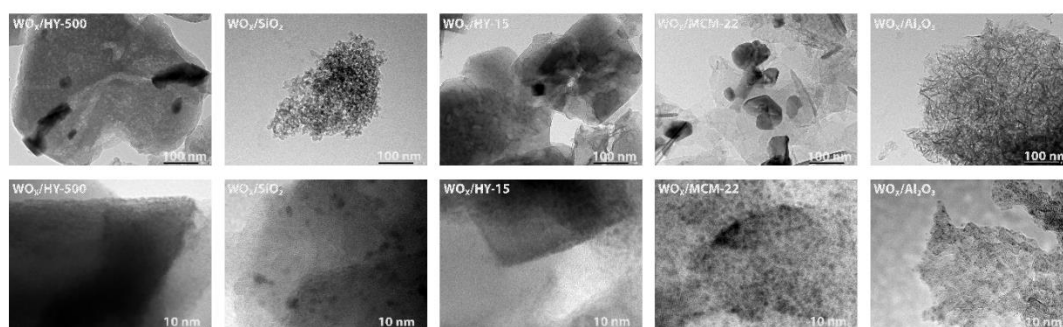


Figure 5.13 TEM images (top) and high-resolution TEM image (bottom) of the Supported W catalysts.

Table 5.1 Surface characterization by transmission electron microscopy and energy-dispersive X-ray spectroscopy (TEM-EDS) on Supported W catalysts

Catalysts	C (at%)	O (at%)	Al (at%)	Si (at%)	Cu (at%)	W (at%)
W/HY-500	80.69	11.92	-	7.26	0.08	0.04
W/SiO ₂	90.28	6.79	-	2.57	0.29	0.08
W/HY-15	30.05	8.90	2.14	56.49	1.87	0.55
W/MCM-22	76.46	12.60	0.33	9.51	0.43	0.68
W/Al ₂ O ₃	63.04	17.97	16.94	-	0.49	1.56

TEM images of various Supported W catalysts are illustrated in **Figure 3**. It was found that the W/HY-15 and W/SiO₂ catalysts showed the agglomeration of tungsten species on the support surface, indicating low dispersion of tungsten species in these catalysts. In contrast, the W/Al₂O₃, W/MCM-22, and W/HY-15 exhibited more highly dispersed tungsten species on the support surface than the others.

The W/Al_2O_3 obviously showed highly dispersed tungsten species on the alumina support. This indicates that the highest tungsten dispersion of Supported W catalysts was found in the W/Al_2O_3 . The results were consistent with the XRD results, which the crystalline phase of tungsten oxide was detected on $W/HY-15$ and W/SiO_2 catalysts, but it was not detected on W/Al_2O_3 , $W/MCM-22$, and $W/HY-15$ catalysts due to the W phase was in the highly dispersed forms. In addition, TEM-EDS were used to investigate the dispersion of tungsten on the supports as shown in **Table 5.1**. The amount of tungsten surface concentration relating to the tungsten dispersion [83, 88], increased with the order of $W/Al_2O_3 > W/MCM-22 > W/HY-15 > W/SiO_2 > W/HY-500$. Therefore, the tungsten dispersion was further confirmed by the results of TEM-EDS, which are consistent with the TEM images and XRD results. Generally, highly dispersed metal oxides entailed the reducibility due to strong interaction with support. The dispersion of the tungsten oxide species and the interaction between tungsten and supports were essentially relevant with the reducibility of tungsten oxide species on supports [89, 90]. Thus, the W/Al_2O_3 showed the highest tungsten dispersion and the strong interaction between tungsten oxide and support, while the $W/HY-15$ exhibited the lowest tungsten dispersion and the weak interaction between tungsten oxide and support, which are consistent with the TPR, XRD, TEM images, and TEM-EDS results.



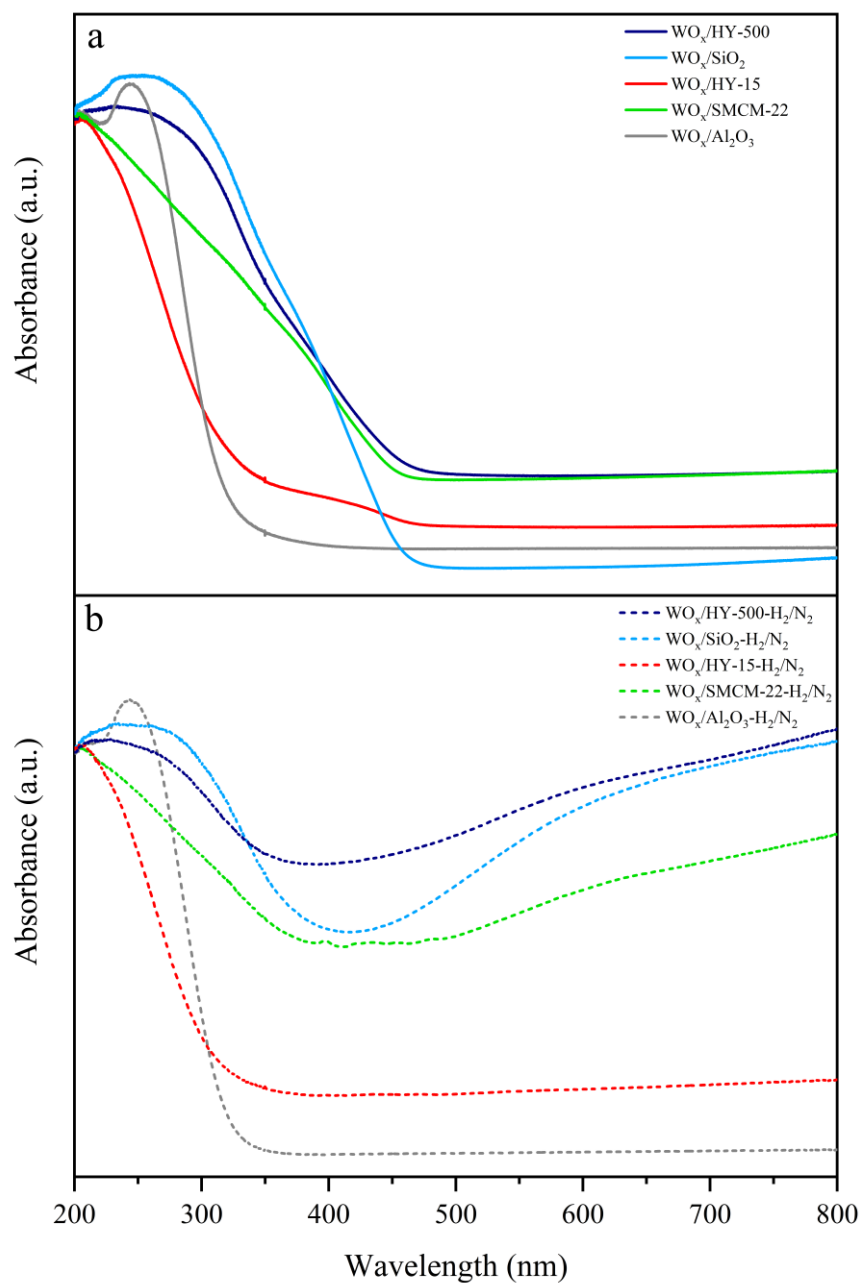


Figure 5.14 UV-Vis DRS patterns of the Supported W catalysts; (a) Supported W catalysts, (b) Supported W catalysts with H_2/N_2 gas pretreatments.

In order to investigate the structure of tungsten species, the Supported W catalysts were analyzed by UV-Vis DRS. The UV-vis DRS spectra are shown in **Figure**

5.4. The samples were compared the UV-vis DRS spectra between W/Support and W/Support-H₂/N₂ as the same of XRD technique. All UV-vis DRS spectra of the catalysts showed two absorption bands at 230 and 270 nm, attributed to isolated tetrahedral [WO₄]²⁻ species and octahedral polytungstate species, respectively [91, 92]. Moreover, this adsorption bands at 230 and 270 nm were attributed to W⁶⁺ species [82]. When the W/Support were pretreated with H₂/N₂ gas as W/Support-H₂/N₂, the UV-vis DRS spectra show the broad bands between 400 and 800 nm. The adsorption bands at 400 nm was assigned to WO₃ crystallites, and the adsorption bands between 400 and 800 nm, which were observed for all W/Support-H₂/N₂ catalysts are assigned to reduction of W species such W⁴⁺ and W⁵⁺ [82, 91, 92]. As shown in **Figure 5.4a** and **Figure 5.4b**, comparing the intensity of adsorption band at 230 and 270 nm between W/Support and W/Support-H₂/N₂ catalysts, it was not much different, excepting for the W/HY-15 and W/SiO₂ catalysts. The W/HY-15-H₂/N₂ and W/SiO₂-H₂/N₂ obviously showed lower intensity band than their fresh catalysts in isolated tetrahedral and octahedral polytungstate species, indicating that the reduction of these species occurred under pretreatment with H₂/N₂ gas, which was consistent with the XRD results. The crystalline tungsten oxide band at 400 nm could be observed for all Supported W catalysts. When the Supported W catalysts were treated with H₂/N₂ gas, the adsorption band at 400 nm was converted to broad bands between 400 and 800 nm, which were described to oxygen vacancies due to the reduction of WO_x and the W⁵⁺ in sub stoichiometric WO_{3-x} [93], excepting for the W/Al₂O₃-H₂/N₂ catalyst. As shown in **Figure 5.4b**, the W/Al₂O₃-H₂/N₂ catalyst showed lower broad bands between 400 and 800 nm than others, indicating that the W⁴⁺ and W⁵⁺ species were less appeared on W/Al₂O₃-H₂/N₂ catalyst and this surface species is difficult to reduce, which was consistent with the TPR result.

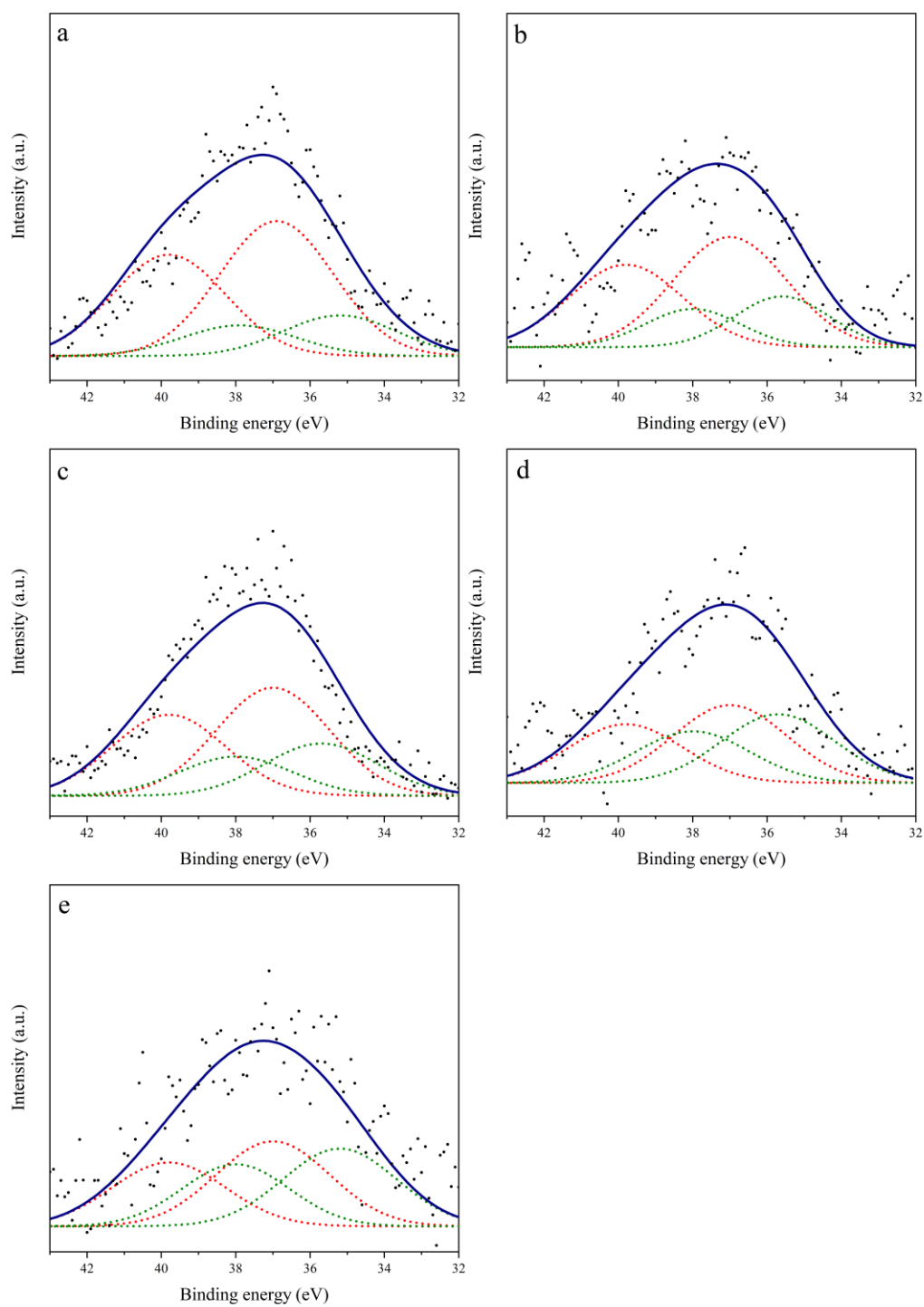


Figure 5.15 XPS spectra of W $4f_{7/2}$ and W $4f_{5/2}$ for Supported W catalysts with H_2/N_2 gas pretreatments; W/ Al_2O_3 (a), W/MCM-22 (b), W/HY-15 (c), W/ SiO_2 (d), W/HY-500 (e).

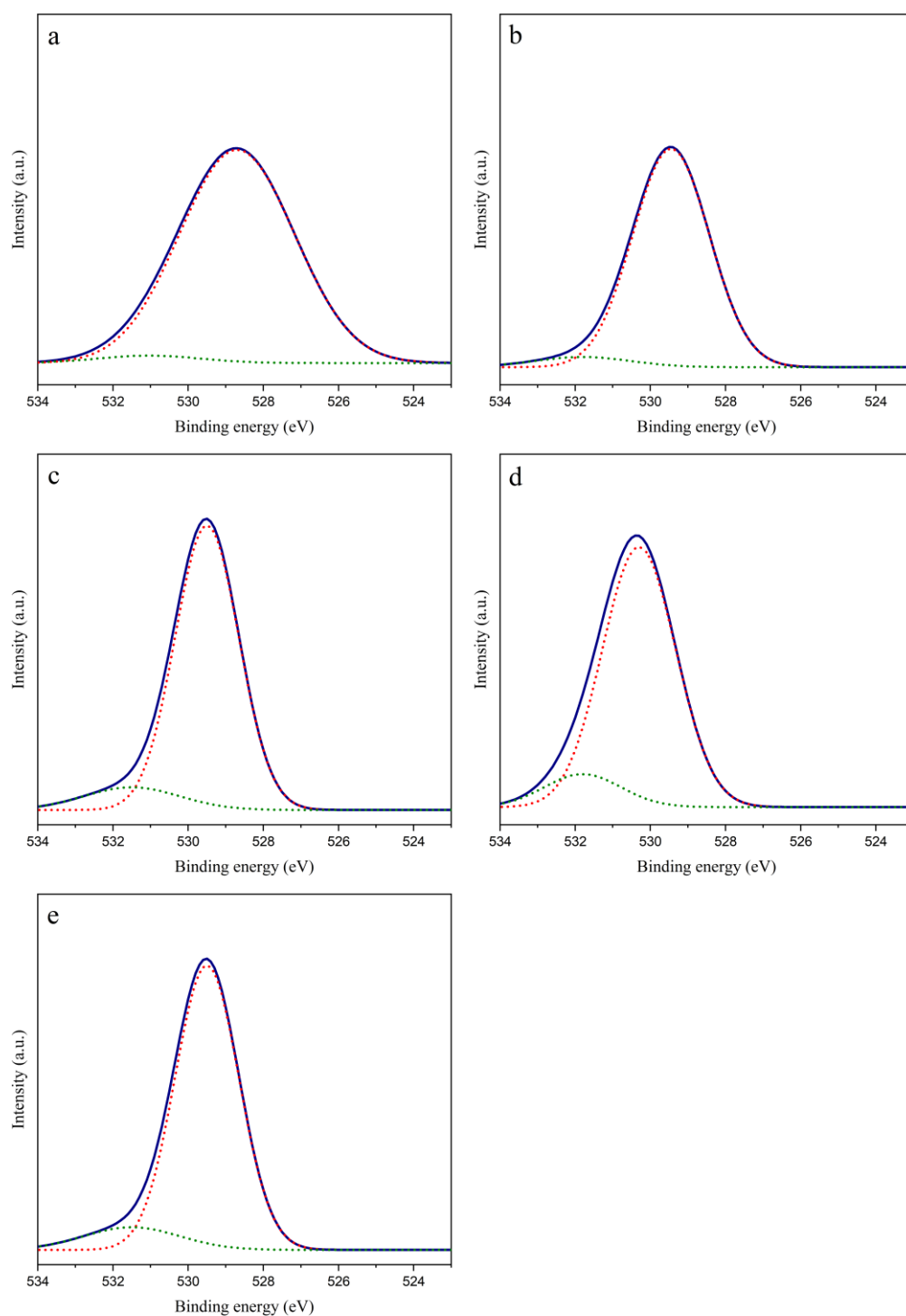


Figure 5.16 XPS spectra of O 1S for Supported W catalysts with H₂/N₂ gas pretreatments; W/Al₂O₃ (a), W/MCM-22 (b), W/HY-15 (c), W/SiO₂ (d), W/HY-500 (e).

Table 5.2 Surface characterization by X-ray photoelectron spectroscopy (XPS) on Supported W catalysts with H₂/N₂ gas pretreatments

Catalysts	O _{ads}	O _{latt}	O _{ads} /O _{latt}	W ⁵⁺ (%)	W ⁶⁺ (%)
W/HY-500	2443	20431	0.12	47.8	52.2
W/SiO ₂	1929	18140	0.11	46.8	53.2
W/HY-15	1370	21001	0.07	32.6	67.4
W/MCM-22	926	15814	0.06	27.8	72.2
W/Al ₂ O ₃	579	18739	0.03	23.2	76.8

The XPS spectra was employed to determine the surface chemical states of tungsten on the surface of Supported W catalysts, which is shown in **Figure 5.5**. The typical patterns of W 4f and O 1s were investigated. Before investigation, the Supported W catalysts were treated with H₂/N₂ gas as W/Support-H₂/N₂. The deconvoluted peaks of XPS spectra of tungsten species at the catalyst surface were based on the full width at half-maximum (FWHM) of 1.7 eV, the binding energy difference between W 4f_{5/2} and W 4f_{7/2} of around 2.7 eV, the peak intensity ratio of W 4f_{5/2} and W 4f_{7/2} [(f_{7/2}) : (f_{5/2})] of 4 : 3, and the binding energy difference between W⁵⁺ 4f_{7/2} and W⁶⁺ 4f_{7/2} peak about 1.3-1.8 eV. Generally, the binding energies of 36.6-37 and 39.8-40.4 eV could be assigned to W⁶⁺ 4f_{7/2} and W⁶⁺ 4f_{5/2} respectively [94, 95], while the ones of 35.2-35.7 and 37.9-38.5 eV could be assigned to W⁵⁺ 4f_{7/2} and W⁵⁺ 4f_{5/2} [96-98]. According to the literature, the exhibition of W⁶⁺ phase was indicated to the WO₃ on the support, while the exhibition of W⁵⁺ and W⁶⁺ phases were indicated to the WO_{3-x} on the support [93]. As shown in **Figure 5.5e**, The W/Al₂O₃-H₂/N₂ catalyst exhibited more W⁶⁺ phase than others, and exhibited W⁵⁺ phase less than the others, indicating that the crystalline tungsten oxide of W/Al₂O₃-H₂/N₂ is difficult to reduce due to strong interaction with sites on the Al₂O₃ support, which was consistent with the UV-Vis results. The W⁵⁺ species were obviously appeared on the W/HY-500-H₂/N₂ and W/SiO₂-H₂/N₂ catalysts. The hydrogen pretreatment of tungsten oxides catalysts by the mixed H₂/N₂ gas leads to the conversion of W⁶⁺ to W⁵⁺ species. As shown in **Table 5.2**, the surface composition results of Supported W catalysts determined by XPS were summarized.

The order of the percentage of W^{5+} species is $W/HY-500-H_2/N_2 > W/SiO_2-H_2/N_2 > W/HY-15-H_2/N_2 > W/MCM-22-H_2/N_2 > W/Al_2O_3-H_2/N_2$. Such results indicated the higher amount of the percentage of W^{5+} species, which was consistent with the reducibility of H_2 -TPR results. Moreover, the UV-Vis results also showed the broad bands between 400 and 800 nm, which are assigned to reduction of W species such W^{4+} and W^{5+} .

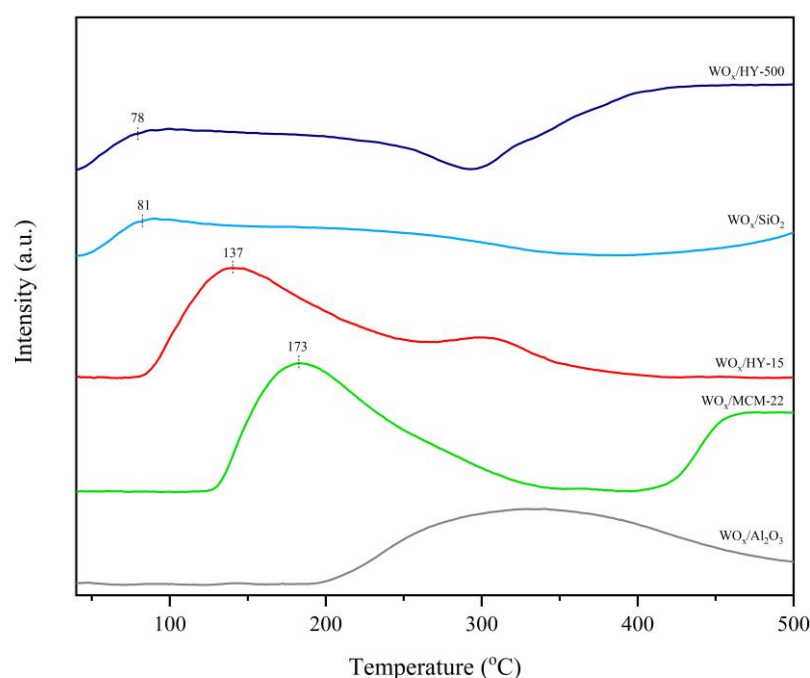


Figure 5.17 O_2 -TPD profiles of the Supported W catalysts.

The existence of surface oxygen vacancies of Supported W catalysts is confirmed by the O 1s spectrum that is shown in the **Figure 5.6**. Before investigation, the Supported W catalysts were treated with H_2/N_2 gas as $W/Support-H_2/N_2$. The first peak around 532-533 eV can be ascribed to surface adsorbed oxygen (O_{ads}), while the one located around 530-531 eV corresponds to lattice oxygen species (O_{latt}) [99, 100]. The formation and increased intensity of the first peak indicated the sequence of $WO_3 \rightarrow WO_2$ [100]. The ratios of O_{ads}/O_{latt} of the different catalysts are shown in **Table 5.2**. Generally, this ratio can be a standard to measure the amount of surface oxygen vacancies [101], thus a higher ratio indicates a larger amount of surface oxygen vacancies. The largest amount of surface oxygen vacancies was found in the $W/HY-$

500-H₂/N₂ catalyst, while the lowest amount of surface oxygen vacancies was found in the W/Al₂O₃-H₂/N₂ catalyst. As shown in **Table 5.2**, the order of surface oxygen vacancy concentration is as following; W/HY-500-H₂/N₂ > W/SiO₂-H₂/N₂ > W/HY-15-H₂/N₂ > W/MCM-22-H₂/N₂ > W/Al₂O₃-H₂/N₂. The relative concentration of surface oxygen vacancies is consistent with the percentage of W⁵⁺ species and the reducibility of H₂-TPR results as mentioned above.

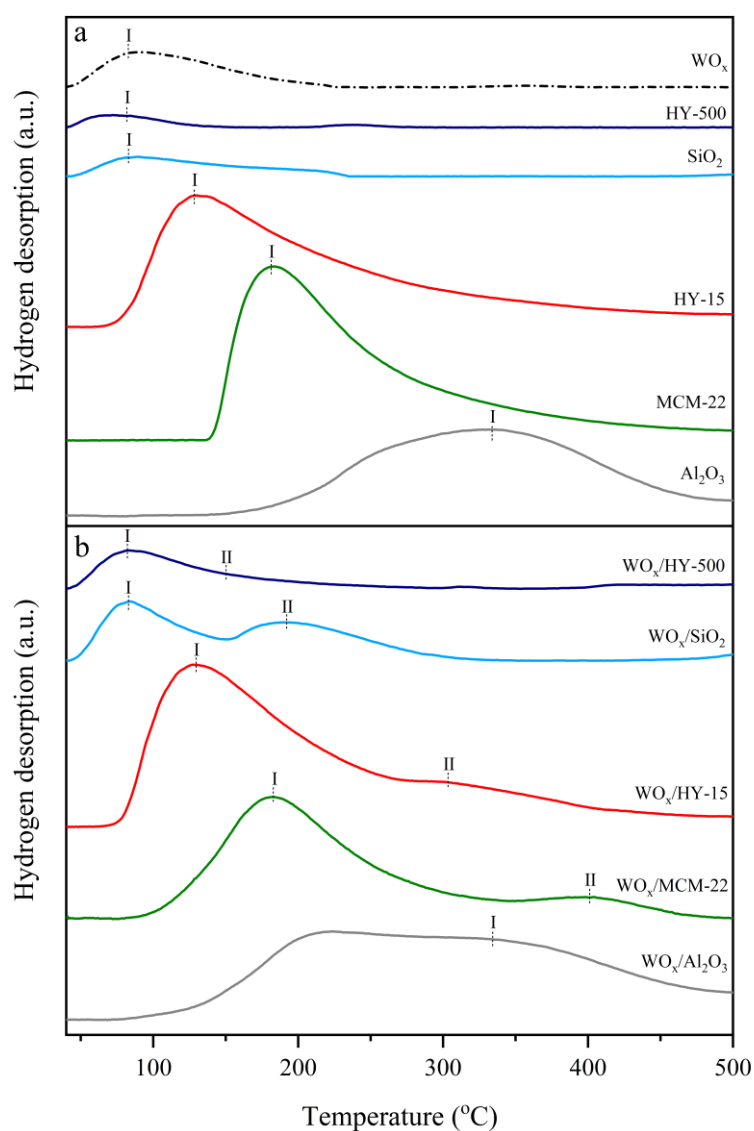
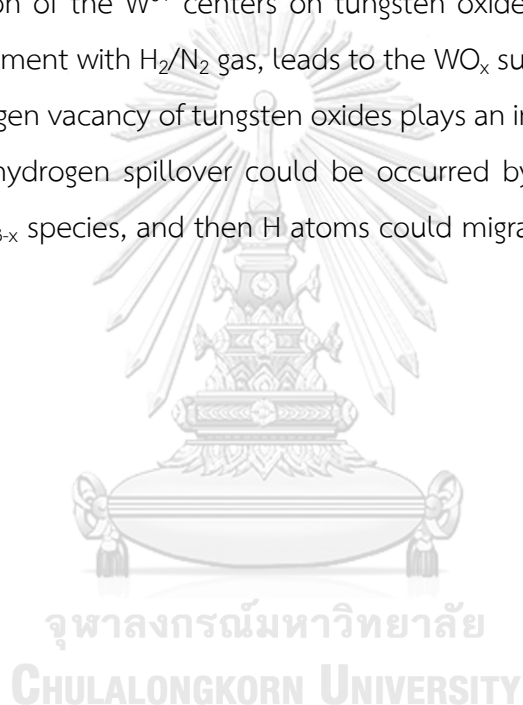


Figure 5.18 H₂-TPD profiles of the catalysts; Supported W catalysts (a) and only supports (b).

To further investigate the oxygen vacancies, the O₂-TPD was used to determine the nature of adsorbed and activated oxygen species. The O₂-TPD profiles of the Supported W catalysts are shown in **Figure 5.7**. In the temperature range studied (40-500 °C), the desorption peaks were appeared. Normally, the first peak about 100-210 °C can be assigned to adsorbed molecular oxygen species (O²⁻_{ad}) on oxygen vacancies, and the second peak at 300-460 °C can be attributed to atomic oxygen species (O⁻_{ad}) caused by charge imbalance from amorphous WO_x [102, 103]. Generally, surface density of oxygen vacancy was estimated based on the weakness of O²⁻_{ad} peak. There are almost no oxygen desorption peaks below 210 °C on the W/Al₂O₃, indicating that the surface oxygen vacancy is difficult to occur on W/Al₂O₃. The W/MCM-22 presents O²⁻_{ad} peak at 173 °C, while the W/HY-15 shows O²⁻_{ad} peak that is shifted to lower temperature around 137 °C. Moreover, the W/HY-500 and W/SiO₂ show the O²⁻_{ad} peak lower temperature than others around 75-85 °C. Comparing the O₂-TPD profiles of Supported W, it can be seen that the desorption temperature peak of O²⁻_{ad} weakens in the order of W/HY-500 > W/SiO₂ > W/HY-15 > W/MCM-22 > W/Al₂O₃, indicating that the highest oxygen vacancy was found in W/HY-500 catalyst and the lowest oxygen vacancy was observed in W/Al₂O₃ catalyst. This trend correlates to the reducibility of Supported W catalysts, which was consistent with the O 1s spectrum results.

The surface hydrogen of the catalysts was studied by H₂-TPD. The Supported W catalysts and their corresponding supports were carried out. The H₂-TPD profiles of the Supported W catalysts are shown in **Figure 5.8b**, while the H₂-TPD profiles of their corresponding supports are shown in **Figure 5.8a**. In the temperature range studied (40-500 °C), it was found that all catalysts showed hydrogen desorption peaks. As shown in **Figure 5.8a**, there is only one hydrogen desorption peak (peak I) appeared on all the supports. The weaker hydrogen adsorption was found in the HY-500 and SiO₂ supports. Comparing the H₂-TPD profiles of the support, it can be seen that the desorption temperature peak I weakens in the order of HY-500 < SiO₂ < HY-15 < MCM-22 < Al₂O₃. When the WO_x was added to the supports as Supported W catalysts and they were investigated by H₂-TPD as shown in **Figure 5.8b**, the second hydrogen desorption peak (peak II) was appeared on all the Supported W catalysts, while the WO_x showed only peak I as the dash line in **Figure 5.8b**. It indicated that the hydrogen

spillover from the WO_x to supports occurred. Generally, the hydrogen desorption peaks at low temperature ($< 200\text{ }^\circ\text{C}$) were assigned to hydrogen on metal particles, while the hydrogen desorption peaks at high temperature ($200\text{-}500\text{ }^\circ\text{C}$) correspond to hydrogen spillover to the support [104, 105]. The hydrogen desorption on Al_2O_3 was starting at high temperature around $340\text{ }^\circ\text{C}$, however amounts of hydrogen adsorbed over the W/Al_2O_3 catalyst, which was integrated from peak areas, was higher than Al_2O_3 catalyst. The WO_x surface with oxygen vacancy can activate hydrogen molecules easily in kinetics and thermodynamics [99]. These are consistent with the results in this study. The slight reduction of the W^{6+} centers on tungsten oxide catalysts, which occurred during the pretreatment with H_2/N_2 gas, leads to the WO_x surface with oxygen vacancy. Therefore, the oxygen vacancy of tungsten oxides plays an important role for hydrogen dissociation. The hydrogen spillover could be occurred by dissociation of hydrogen molecules on WO_{3-x} species, and then H atoms could migrate on to the supports.



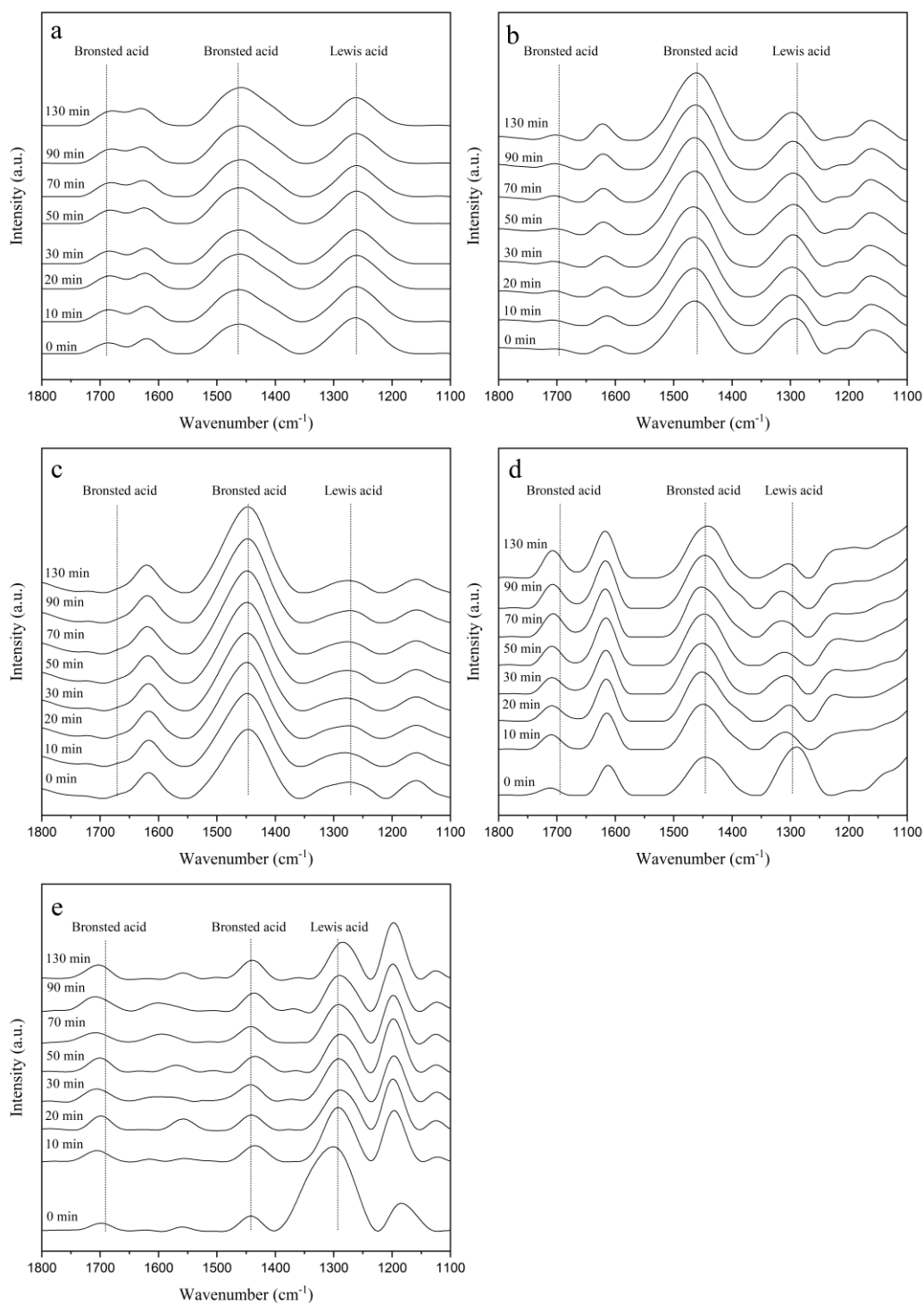


Figure 19 FTIR spectra of ammonia adsorbed during the introduction of hydrogen at 100 °C for 130 min over the Supported W catalysts; W/ Al_2O_3 (a), W/MCM-22 (b), W/HY-15 (c), W/ SiO_2 (d), W/HY-500 (e).

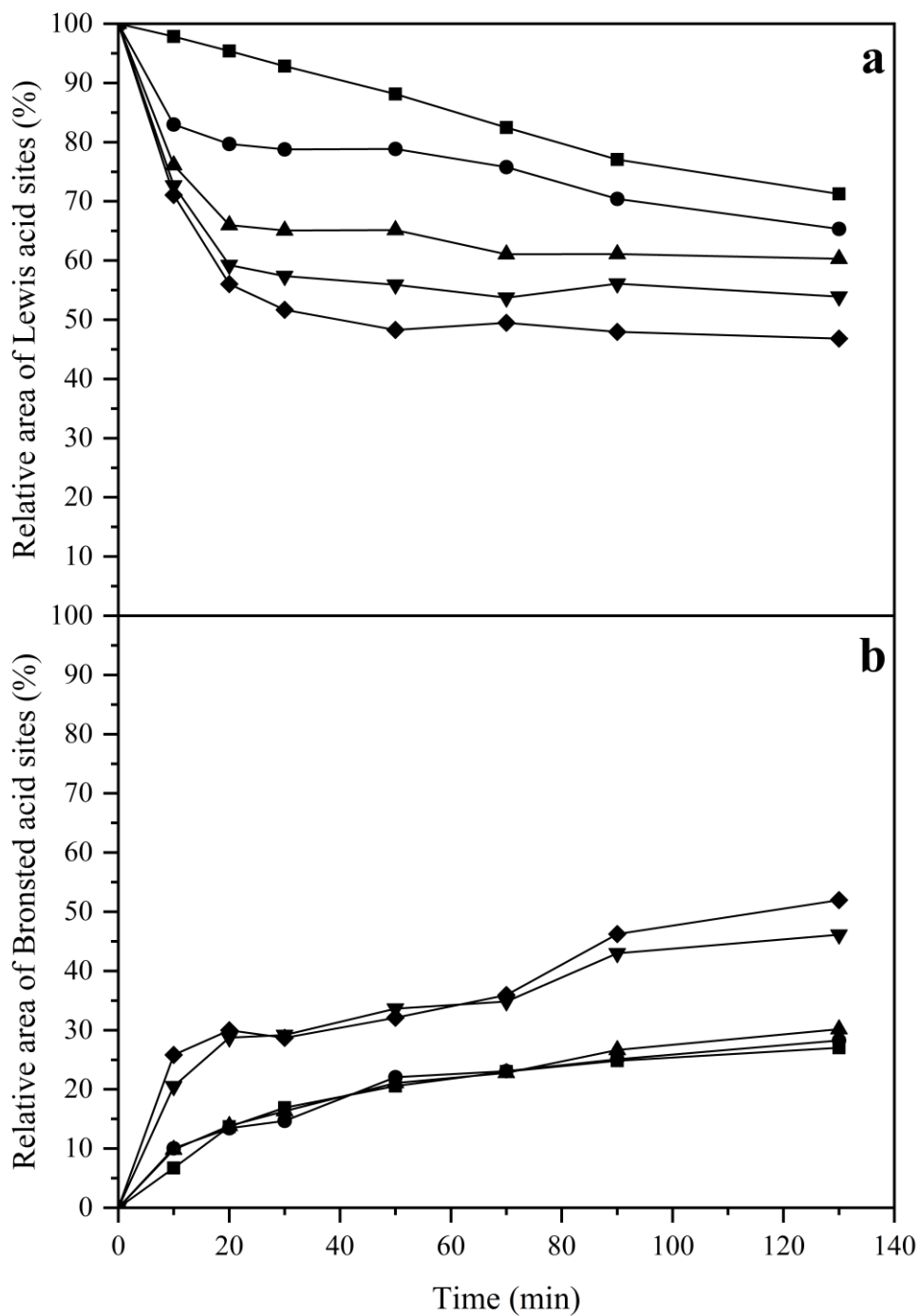


Figure 20 Percentages of remaining Lewis acid sites (a), and percentages of generated Brønsted acid sites (b) on Supported W catalysts; W/Al₂O₃ (■), W/MCM-22 (●), W/HY-15 (▲), W/SiO₂ (▼), W/HY-500 (◆).

Table 5.3 Percentage of loss of Lewis acid sites over Supported W catalysts for 130 min

Catalysts	Amount of Lewis acid at initial (a.u.)	Amount of Lewis acid at final (a.u.)	Loss of Lewis acid sites (%) ^a
W/HY-500	1.16	0.54	53.2
W/SiO ₂	0.25	0.13	46.1
W/HY-15	2.64	1.59	39.7
W/MCM-22	3.19	2.08	34.7
W/Al ₂ O ₃	16.82	11.98	28.8

^aPercentage of loss of Lewis acid sites = $[(\text{Lewis acid}_{\text{initial}} - \text{Lewis acid}_{\text{final}})/\text{Lewis acid}_{\text{initial}}] \times 100$

5.1.2 Effect of support of the Supported W catalysts on the Lewis acid transformation

The Lewis acid transformation on the Supported W catalysts was investigated by *in situ* diffuse reflectance infrared Fourier transform spectroscopy (DRIFTS) of adsorbed NH₃ at 100 °C under atmospheric pressure for 130 min. **Figure 5.9** shows FTIR spectra of ammonia adsorbed during the introduction of H₂ gas at 100 °C for 130 min on Supported W catalysts. The surface acidity was appeared and the band at around 1260-1325 cm⁻¹ were assigned to adsorbed NH₃ on Lewis acid sites. The bands around 1430-1473 and 1665-1680 cm⁻¹ were assigned NH₄⁺ on Brønsted acid sites [106-108]. According to the results of *in situ* DRIFTS as shown in **Figure 5.9**, the observed FTIR spectra were changed by introduction of H₂ gas with time on stream on all Supported W catalysts. It was found that the amounts of ammonia adsorbed on Lewis acid sites were decreased, while the amounts of ammonium ions on Brønsted acid sites were increased by the introduction of H₂ gas. It is proposed that ammonia migration from Lewis acid sites to Brønsted acid sites occurred over the WO_x catalysts supported on all different supports in the presence of WO_x surface with oxygen vacancy. To confirm the change of these surface acidity, the amounts of ammonia adsorbed on surface acidity were balanced by calculation of Eq. (1) and Eq. (2). These were summarized to

the percentages of remaining Lewis acid sites and the percentages of generated Brønsted acid sites as shown in **Figure 5.10a** and **Figure 5.10b**, respectively. The percentage of remaining Lewis acid sites was decreased from 100% by time on stream, while the percentage of generated Brønsted acid sites was increased from 0% by time on stream as well. This indicates that the Lewis acid transformation were occurred and some Lewis acid sites were transformed to Brønsted acid sites. All Supported W catalysts show a rapid decrease in the percentage of remaining Lewis acid sites at initial and show a steady in the percentage of remaining Lewis acid sites at final, excepting for W/Al_2O_3 catalyst. The W/Al_2O_3 catalyst shows slow and steady in the percentage of remaining Lewis acid sites. **Table 5.3** also summarizes the percentages of loss of Lewis acid sites over Supported W catalysts, which indicate the Lewis acid transformation. It can be seen that the order of Lewis acid transformation over Supported W catalysts is in the following order; $W/HY-500 > W/SiO_2 > W/HY-15 > W/MCM-22 > W/Al_2O_3$, indicating that the selected support is the crucial factor for Lewis acid transformation performances.

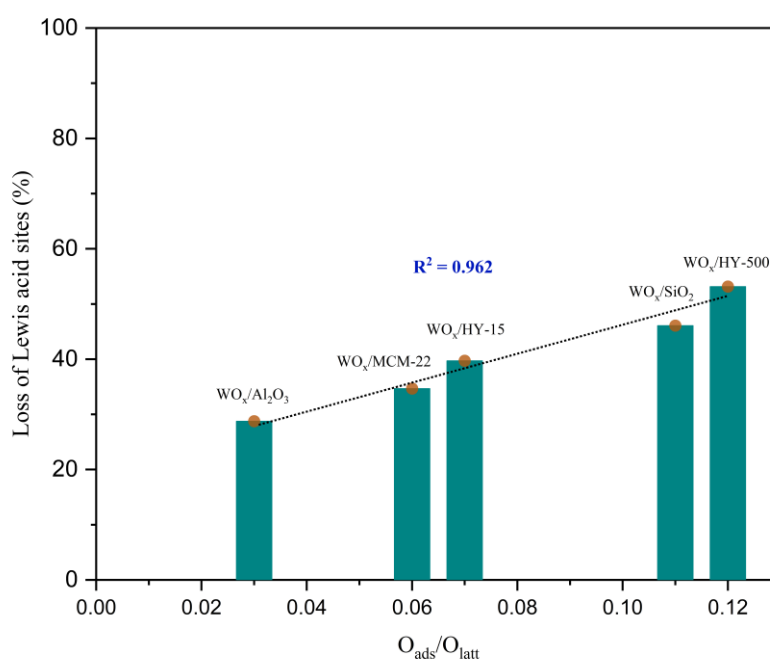


Figure 21 The effect of the amount of oxygen vacancy on the loss of Lewis acid sites over the Supported W catalysts.

In this research, we found that the order of Lewis acid transformations over Supported W catalysts is consistent with the amount of WO_x surface with oxygen vacancy on the catalysts. The characteristics of the WO_x catalysts supported on all different supports that were investigated by O_2 -TPD and XPS confirm that the order of surface oxygen vacancy concentration is $W/HY-500 > W/SiO_2 > W/HY > W/MCM > W/Al_2O_3$, which was consistent with the order of Lewis acid transformations. Therefore, the WO_x surface with oxygen vacancy plays an important role for Lewis acid transformation performances. According to the literature, the WO_x surface with oxygen vacancy on the Supported W catalysts could dissociate hydrogen molecules [99], indicating that the generated oxygen vacancies of the supported WO_x catalysts play an important role for activating the hydrogen spillover, leading to Lewis acid transformation to Brønsted acid. The results of H_2 -TPD also confirm the presence of hydrogen spillover from the WO_x to supports due to hydrogen dissociation by WO_x surface with oxygen vacancy. The WO_x surface with oxygen vacancy on the Supported W catalysts was occurred by the partial reduction of WO_3 [83]. According to the XRD and UV-vis results, the partial reduction of WO_3 could occur during the pretreatment under mixed H_2/N_2 gas due to reducibility of catalysts. The reduction peaks of H_2 -TPR results of W species confirmed that the Supported W catalysts can be reduced by hydrogen gas. The low intensities of hydrogen reduction peaks of H_2 -TPR results indicate that the order of reducibility of the Supported W catalysts is: $W/Al_2O_3 < W/MCM-22 < W/HY-15 < W/SiO_2 < W/HY-500$. This order is consistent with the tungsten dispersion, which was confirmed by XRD, TEM images, and TEM-EDS results. The amounts of W^{5+} species on Supported W catalysts that were investigated by XPS and UV-vis are also correlated with the reducibility and the amount of oxygen vacancy on the catalysts. As shown in the **Figure 5.11**, the percentages of the loss of Lewis acid sites, which were obtained from the data in **Table 5.3**, were directly proportional to the amounts of oxygen vacancies on the Supported W catalysts, which were obtained from the data in **Table 5.2**. The more oxygen vacancy on WO_x catalyst results in more efficient catalyst for hydrogen activation [99]. The behavior of surface hydrogen apparently affects the Lewis acid transformation. Therefore, it indicates that the

enhancement of oxygen vacancy improved the rate of Lewis acid transformation to Brønsted acid sites.

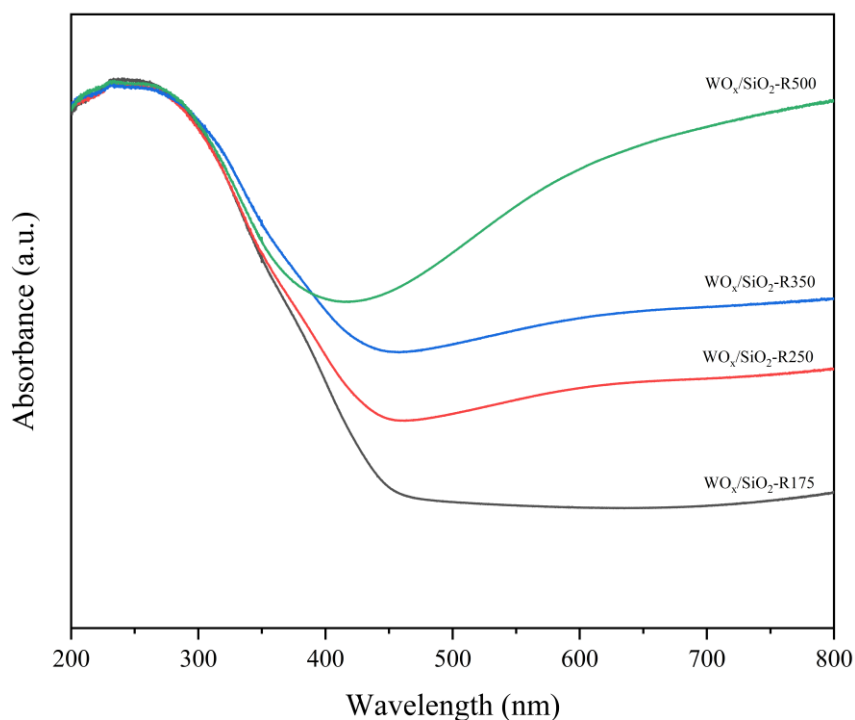


Figure 22 UV-Vis DRS patterns of the Supported W catalysts with H_2/N_2 gas pretreatments at different temperature (175, 250, 350, and 500 °C).

5.1.3 Effect of oxygen vacancy of the W/SiO_2 catalyst on the Lewis acid transformation

According to the results of in situ DRIFTS as shown in the **Figure 5.9**, it was found that the ammonia migration from Lewis acid sites to Brønsted acid sites occurred over the WO_x catalysts supported on all different supports. The order of Lewis acid transformations over Supported W catalysts is $W/HY-500 > W/SiO_2 > W/HY-15 > W/MCM-22 > W/Al_2O_3$, which is consistent with the amount of WO_x surface with oxygen vacancy on the catalysts. Therefore, the objective of this part is to confirm that the WO_x surface with oxygen vacancy can play an important role for Lewis acid transformation performances. The effect of oxygen vacancy on the Lewis acid transformation was studied on only the W/SiO_2 catalyst. According to the literature,

the nonstoichiometric property of tungsten oxides (WO_{3-x}), which consist of the WO_x surface with oxygen vacancy, could be generated by controlling the H_2 reduction conditions [99, 109]. The four W/SiO_2 catalysts with different amounts of oxygen vacancies were prepared by the pretreatment using H_2/N_2 flow at different temperature. In this section, the Lewis acid transformation to Brønsted acid was investigated over the four prepared W/SiO_2 catalysts with a different amount of oxygen vacancies by the pretreatment using H_2/N_2 flow at 175, 250, 350, and 500 °C for 1 h. After the pretreatment, the samples were carried out by the same step as done for the in situ DRIFTS of NH_3 adsorption and the introduction of H_2 gas as the previous section. The percentages of remaining Lewis acid sites over catalysts were also calculated by Eq. (1). The four prepared W/SiO_2 catalysts were denoted as W/SiO_2 -R175, W/SiO_2 -R250, W/SiO_2 -R350, and W/SiO_2 -R500 for W/SiO_2 catalysts, which were pretreated under H_2/N_2 gas flow at 175, 250, 350, and 500 °C for 1 h, respectively. Moreover, the samples were also investigated by UV-Vis DRS to confirm the structure of tungsten species of the W/SiO_2 catalysts with H_2/N_2 gas pretreatments at different temperature. The samples were pretreated with H_2/N_2 gas at 175, 250, 350, and 500 °C for 1 h, and then were analyzed by UV-Vis DRS. According to **Figure 5.12**, when the W/SiO_2 catalysts were pretreated with H_2/N_2 gas at a temperature higher than 175 °C, the adsorption bands at 400 nm were converted to broad bands between 400 and 800 nm, which were described to oxygen vacancies due to the reduction of WO_x and the W^{5+} in sub stoichiometric WO_{3-x} [94]. It can be obviously seen that the intensities of broad bands between 400 and 800 nm are consistent with the increasing of pretreatment temperature using H_2/N_2 flow. As shown in **Figure 5.12**, the order of intensities of broad bands between 400 and 800 nm is W/SiO_2 -R500 > W/SiO_2 -R350 > W/SiO_2 -R250 > W/SiO_2 -R175, indicating that the more generation of oxygen vacancies was occurred on W/SiO_2 catalysts by the increasing of pretreatment temperature using H_2/N_2 flow. The highest W^{4+} and W^{5+} species and oxygen vacancy appeared on the W/SiO_2 -R500 catalyst.

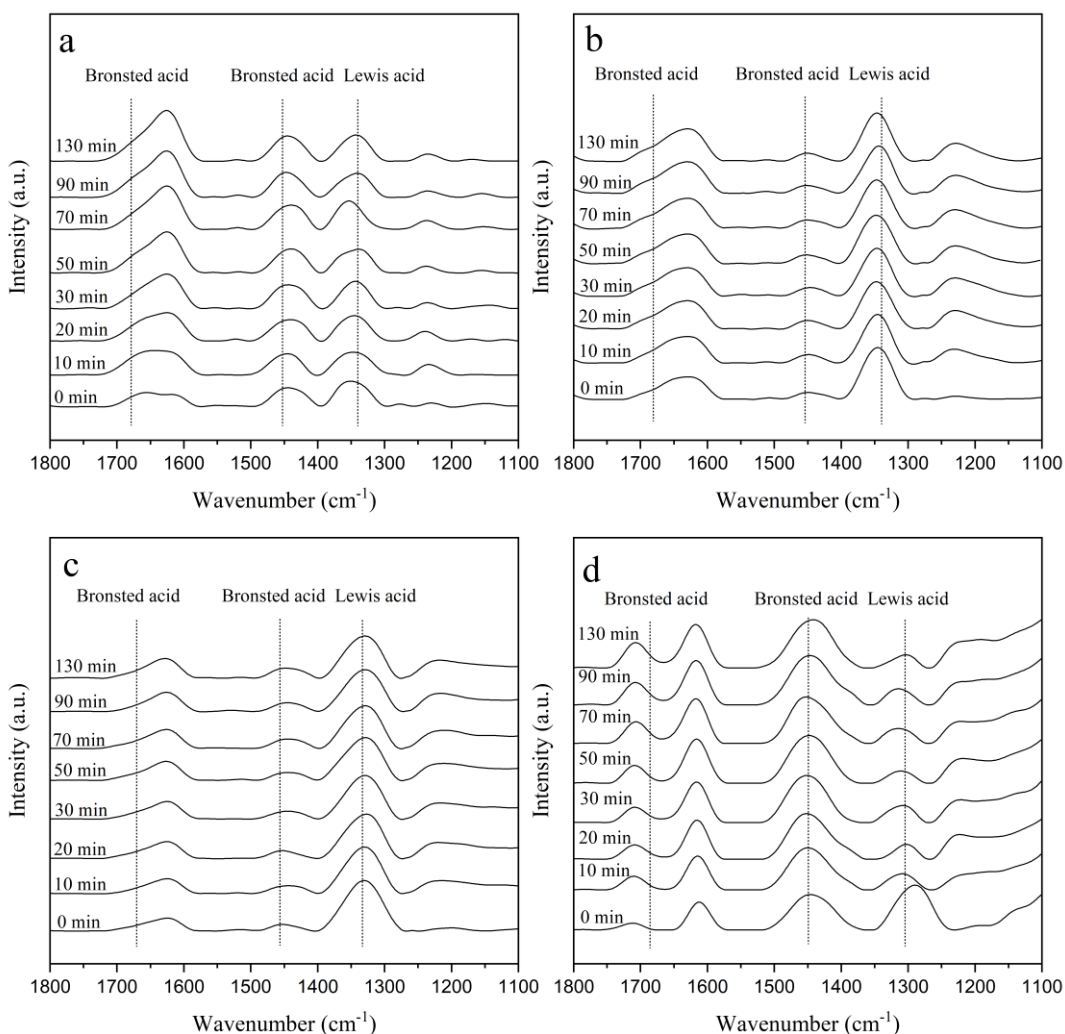


Figure 23 IR spectra of ammonia adsorbed during the introduction of hydrogen at 100 °C for 130 min over the W/SiO₂ catalysts with H₂/N₂ gas pretreatments at different temperature; (a) 175 °C, (b) 250 °C, (c) 350 °C, (d) 500 °C.

To investigate the effect of oxygen vacancy of the W/SiO₂ catalyst on the Lewis acid transformation, the W/SiO₂ catalysts were conducted with pretreatment using H₂/N₂ gas flow at different temperature for 1 h by the same investigation of in situ DRIFTS of adsorbed ammonia over the Supported W catalysts as mentioned in previous section. **Figure 5.13** shows FTIR spectra of ammonia adsorbed during the introduction of H₂ gas at 100 °C for 130 min on W/SiO₂ catalysts with pretreatment using H₂/N₂ gas flow at different temperature. Comparing the bands at the initial, it

was found that all samples showed stronger Lewis acid sites than Brønsted acid sites. However, the W/SiO₂-R175 catalyst showed stronger Brønsted acid bands than the W/SiO₂-R250, W/SiO₂-R350, and W/SiO₂-R500 catalysts, which the Brønsted acid bands may be disturbed by adsorbed water or hydroxyl groups at around 1410 cm⁻¹ [110]. Thus, these bands at the initial were disappeared after pretreatment at high temperatures of 250, 350, and 500 °C. In addition, when the W/SiO₂ was pretreated at low temperature, the bands at around 1637 cm⁻¹ of the W/SiO₂-R175 catalyst seems to be disturbed by adsorption of water as well due to the presence of O-H bending vibration [111]. The Brønsted and Lewis acid sites at the initial (0 min) were increased by increasing pretreatment temperature in the range of 250-500 °C due to the formation of Si-O-W-OH species through the reaction of terminal silanols and surface WO₃ [112]. According to the **Figure 5.13**, it is also found that the observed FTIR spectra were changed by introduction of H₂ gas with time on stream on all W/SiO₂ catalysts with H₂/N₂ gas pretreatments at different temperature. The amounts of ammonia adsorbed on Lewis acid sites were decreased, while amounts of ammonium ions on Brønsted acid sites were increased by the introduction of H₂ gas as well. The summarized percentages of remaining Lewis acid sites and percentages of generated Brønsted acid sites, which were calculated by calculation of Eq. (1) and Eq. (2), are shown in **Figure 5.14a** and **Figure 5.14b**, respectively. It was found that all the samples showed a decreased percentage of remaining Lewis acid sites and showed an increased percentage of generated Brønsted acid sites by time on stream. This indicates that the Lewis acid transformation was occurred and some Lewis acid sites were transformed to Brønsted acid sites. As shown in **Figure 5.14**, the W/SiO₂-R500 showed abrupt change in the percentages of remaining Lewis acid sites and the percentages of generated Brønsted acid sites than the others, while the W/SiO₂-R350, W/SiO₂-R250, and W/SiO₂-R175 showed slower change in the percentages of these acidity. It can be seen that the order of Lewis acid transformations over W/SiO₂ catalysts is W/SiO₂-R500 > W/SiO₂-R350 > W/SiO₂-R250 > W/SiO₂-R175, which was consistent with the results of UV-Vis DRS as shown in **Figure 5.12**. This indicates that the oxygen vacancy is the main factor for Lewis acid transformation performances on W/SiO₂ catalysts. The Lewis acid transformation performances over the W/SiO₂ catalyst depend on the

amount of generated oxygen vacancies. Thus, the large amount of oxygen vacancies leads to high Lewis acid transformation.

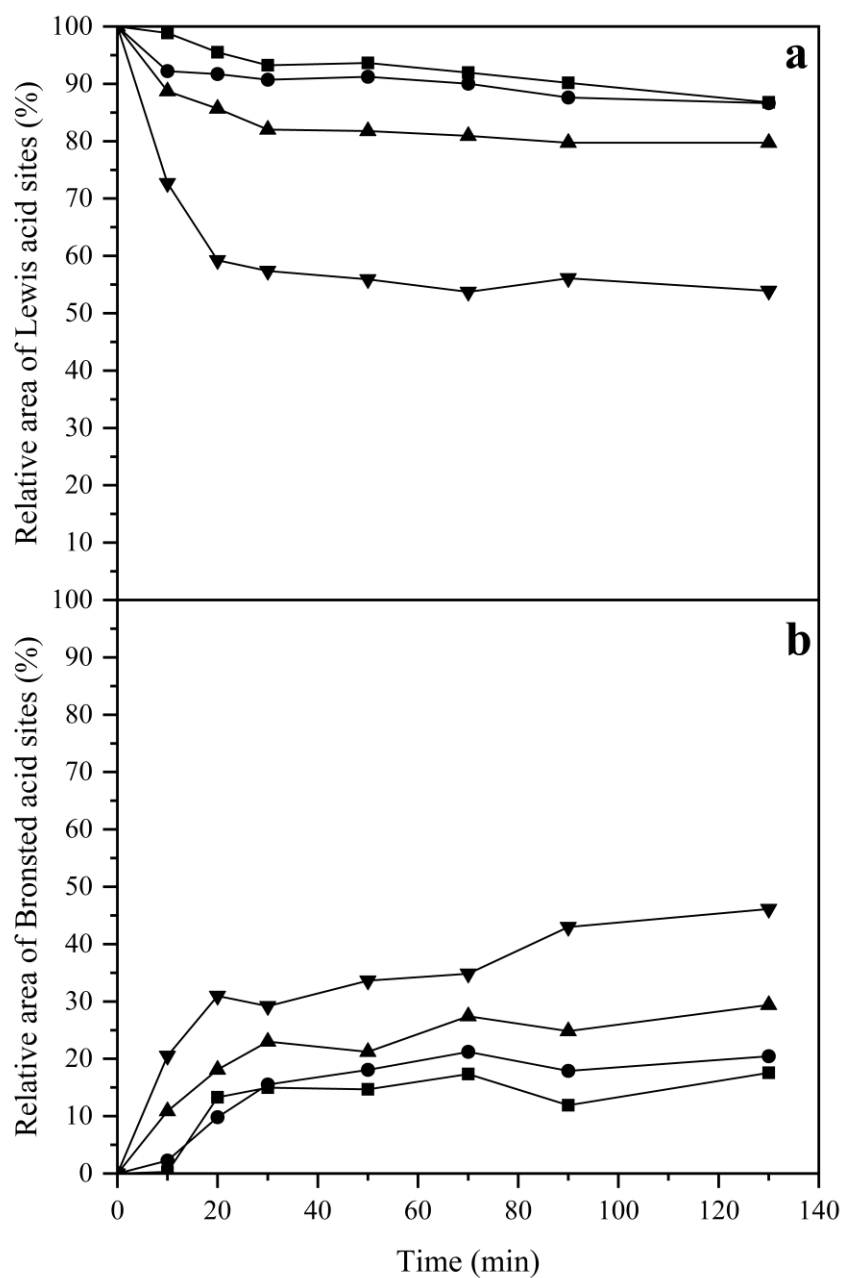
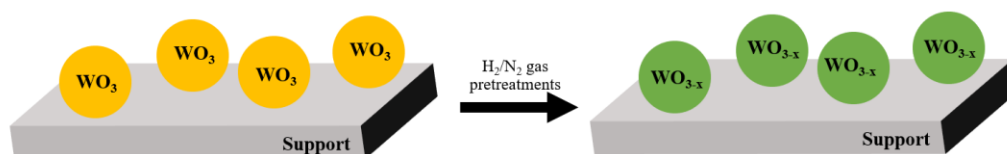


Figure 24 Percentages of remaining Lewis acid sites (a), and percentages of generated Brønsted acid sites (b) on W/SiO₂ catalysts with H₂/N₂ gas pretreatments at different temperature; 175 °C (■), 250 °C (●), 350 °C (▲), 500 °C (▼).

The concept of the summarized Lewis acid transformation over Supported W catalysts is demonstrated in Scheme 1. Firstly, the partial reduction of WO_x occurred under the H_2/N_2 pretreatment, and then the catalysts exhibited the WO_x surface with oxygen vacancy. From hydrogen dissociation, hydrogen atoms occurred on the WO_x surface with oxygen vacancy during the introduction of hydrogen. The hydrogen molecules, which are dissociated on the generated oxygen vacancies of the supported WO_x catalysts to form hydrogen atoms migrates on the catalyst surface to Lewis acid sites. The hydrogen atoms decompose into electrons, which are trapped on the Lewis acid site, and protons, which can be stabilized on the oxygen anions near the Lewis acid sites. Finally, the Lewis acid site converts into a Brønsted acid site. Moreover, ammonium ions are formed on the Brønsted acid sites by the migration of ammonia adsorbed on Lewis acid sites to adjacent Brønsted acid sites.

a) WO_x -supported catalysts with H_2/N_2 gas pretreatments



b) Ammonia migration on Lewis acid sites to Brønsted acid sites

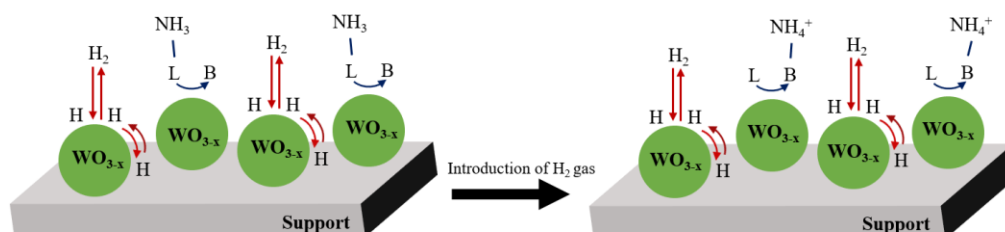


Figure 25 The summarized Lewis acid transformation over the Supported W catalysts.

5.2 Active Site Formation in WO_x Supported on Spherical Silica Catalysts for Lewis Acid Transformation to Brønsted Acid Activity.

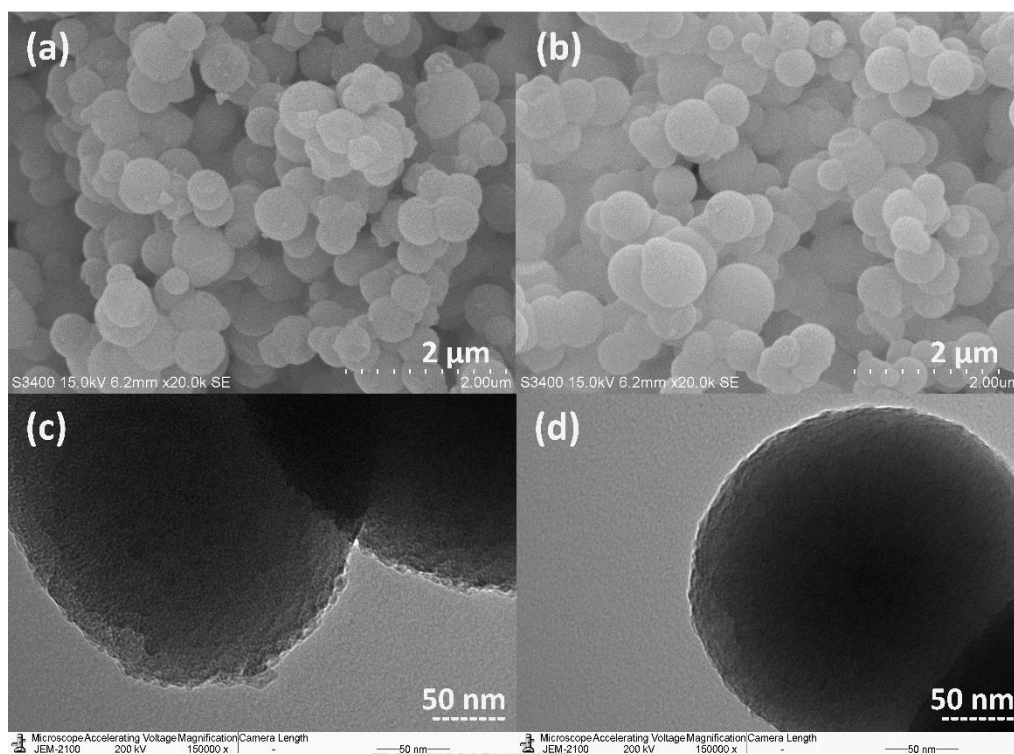


Figure 5.26 SEM images (a, b), TEM images (c, d): (a,c) W/SSP, (b, d) W-SSP.

5.2.1 Textural properties of the catalysts.

SEM and TEM images as shown in **Figure 5.16** demonstrate the spherical nanoparticles shape indicating the uniform of SSP support. The impregnated W/SSP exhibits crystalline phase of WO_3 around the support surface obviously compared with incorporated W-SSP in the TEM image in **Figure 5.16c**. This is also evident with the XRD patterns in **Figure 5.17a**. Wide-angle XRD patterns of SSP-supported W catalysts show the distinct diffraction peaks corresponding to monoclinic WO_3 as standard data reference in JCPDS[113]. Most crystalline phases appear on the impregnated W/SSP catalyst. Raman spectra in **Figure A1** also demonstrate more crystalline phase of WO_3 vibrations on W/SSP than W-SSP, in which the major Raman bands at 706-715 and 805 cm^{-1} are assigned to the stretching mode of W-O-W [114, 115]. This result indicates that, W species are highly dispersed over the incorporated W-SSP catalyst.

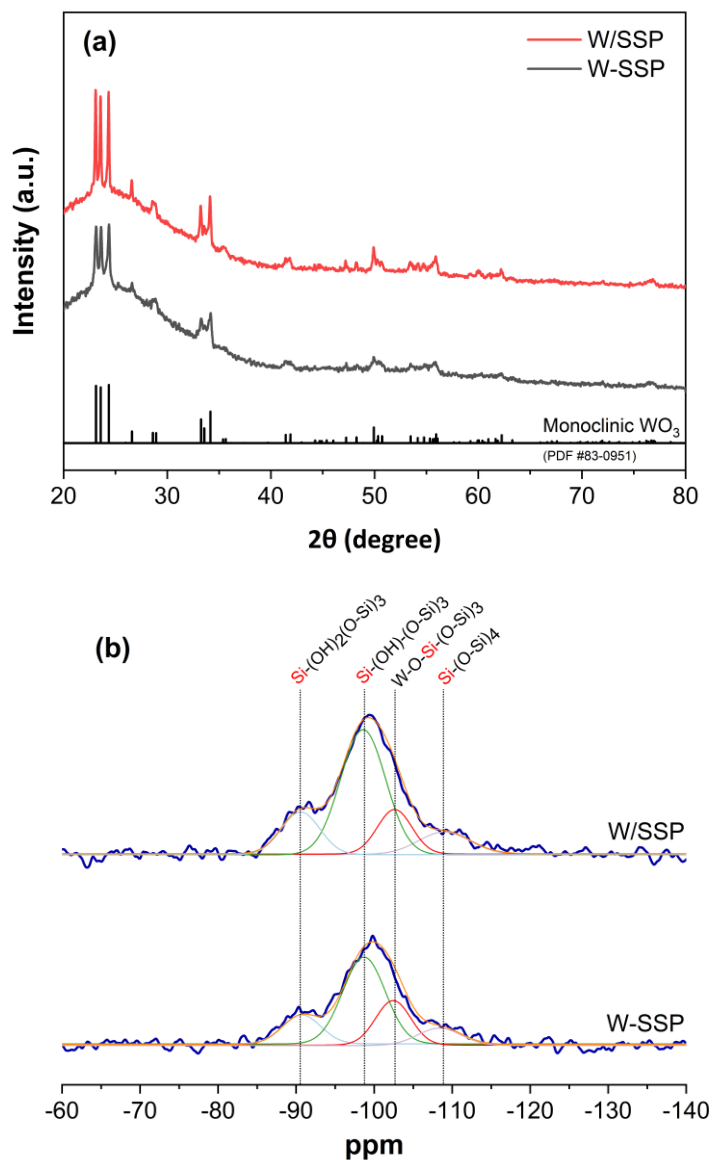


Figure 5.27 Wide-angle XRD patterns (a) and ²⁹Si NMR spectra (b) of SSP-supported W catalysts.

Textural properties of catalysts in **Table A1** show the outstanding average BET surface area of materials around 834 m²/g. The obtained materials from two preparation methods are not significantly different in the morphology, BET surface area, pore volume, and pore size. Energy-dispersive X-ray spectroscopy (EDS) measurement allowed to investigate the element surface concentration on the sample. The amount of W surface concentration on incorporated W-SSP is slightly higher than that on

impregnated W/SSP catalyst. This result indicated the uniformly dispersed W-SSP catalyst that agreed with the results of XRD and Raman. The structure of tungsten species was investigated by UV-vis DRS as shown in **Figure A2** indicating three absorption bands. The band at 225 nm attributed to isolated tetrahedral ($[\text{WO}_4]^{2-}$) species involved the ligand-to-metal charge transfer, while the band at 262 nm referred to octahedral polytungstate ($[\text{WO}_6]^{n-}$) species involved $\text{O}^{2-} \rightarrow \text{W}^{6+}$ charge transfer[14, 116]. The absorption band up to 480 nm was assigned to bulk WO_3 species[117]. The impregnated W/SSP shows higher band intensities of octahedral polytungstate at 262 nm and bulk WO_3 at 400 nm compared with incorporated W-SSP, which is consistent with TEM, XRD, and Raman results. Thus, these indicate that impregnated W/SSP has higher concentrations of W^{6+} species than incorporated W-SSP.

Table 5.4 Relative area of X-ray photoelectron spectroscopy (XPS) of SSP-supported W catalysts with gas pretreatment.

Sample	Relative area of XPS (%)	
	% W^{5+}	% W^{6+}
W-SSP- H_2	64.2	35.8
W/SSP- H_2	53.2	46.8
W-SSP- N_2	51.1	48.9
W/SSP- N_2	18.3	81.7

To further probe the structure of W species, ^{29}Si NMR was employed. The NMR spectra are shown in **Figure 5.17b** (the deconvoluted results are shown in **Table A2**). The shoulder peak around -103.7 ppm assigned to W-O-Si-(O-Si)_3 species is observed[118]. This peak involved the $\text{Si}(3\text{Si},\text{W})$ structure, in which the silicon is flanked by three Si atoms and one W atom in tungsten-incorporated W-MCM-41 as reported by Klepel et al.[119]. Moreover, the different three peaks are also observed at around -91.3 ppm for $\text{Si-(OH)}_2(\text{O-Si})_2$ species, -99.2 ppm for Si-(OH)(O-Si)_3 , and -108.1 ppm for Si-(O-Si)_4 species[118, 120]. As shown in **Table A2**, peaks area (%) of incorporated W-SSP in W-O-Si-(O-Si)_3 species is higher, while Si-(O-Si)_4 species is lower than impregnated W/SSP. The decrease of Si-(O-Si)_4 species in incorporated W-SSP

indicates that they are converted into $W-O-Si-(O-Si)_3$ species, which was also reported by Hu et al.[120]. In addition, the hydroxyl groups of $Si-(OH)_2(O-Si)_2$ and $Si-(OH)(O-Si)_3$ species relatively decrease, compared to that of the $Si-(O-Si)_4$ species indicating the formation of $Si-O-W$ bonds on the silica support by the combination of tungsten and hydroxyl groups during the preparations[121]. These results reveal that W species in incorporated W-SSP could be embedded into the lattice of bulk SSP support, instead of aggregating together to form structure characteristic of W^{6+} species such as crystalline WO_3 , which is well consistent with XRD, Raman, and UV-vis results.

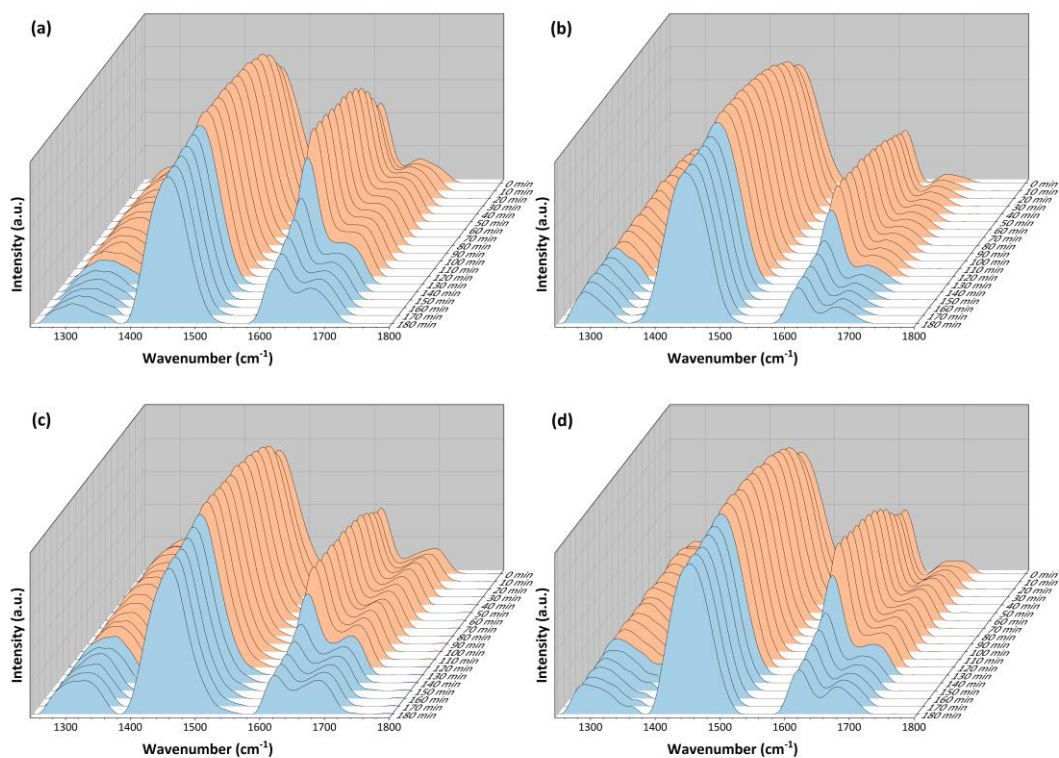


Figure 28 In situ DRIFTS spectra of adsorbed NH_3 upon hydrogen exposure for 0-120 min (orange region) and nitrogen purging for 120-180 min (blue region) at 100 °C over catalysts; W-SSP- H_2 (a), W/SSP- H_2 (b), W-SSP- N_2 (c), and W/SSP- N_2 (d).

5.2.2 Lewis acid transformation to Brønsted acid over SSP-supported W catalysts.

The Lewis acid transformation over SSP-supported W catalysts was investigated by *in situ* DRIFTS of adsorbed NH_3 at 100 °C under atmospheric pressure. To explore

the activating processes involved in the formation of catalytically active sites, the samples were pretreated with N₂ pretreatment (W-SSP-N₂, W/SSP-N₂) as seen in **Figure 5.18c,d** compared with H₂ pretreatment (W-SSP-H₂, W/SSP-H₂) as seen in **Figure 5.18a,b**. IR spectra of all sample adsorbed NH₃ in **Figure 5.18** exhibit the surface acidity bands at 1622 cm⁻¹ assigned to adsorbed NH₃ on Lewis acid sites, while 1448 and 1680 cm⁻¹ referred to NH₄⁺ on Brønsted acid sites[122-124]. The sample was investigated regarding to the effect of hydrogen gas on Lewis acid transformation to Brønsted acid by hydrogen exposure for 120 min (orange region of 0-120 min). To eliminate the effects of moisture and hydrogen-bonded OH groups at around 1410, 1609, and 1700 cm⁻¹ [110, 125], which may occur under the process, the sample was then purged with nitrogen gas for 60 min (blue region of 120-180 min). Comparing between initial (0 min) and final (180 min) of IR spectra in **Figure 5.18**, it is clearly seen that the Lewis acid at the band of 1622 cm⁻¹ was decreased, while the Brønsted acid at the bands of 1448 and 1680 cm⁻¹ were increased under the process (see **Figure A3**). These results clearly indicate that the adsorbed ammonia on Lewis acid site migrated to Brønsted acid site by the introduction of hydrogen gas. It can be said that Lewis acid transformation to Brønsted acid could be occurred over SSP-supported W catalysts in the presence of hydrogen. The H₂-TPD in **Figure A4** was used to investigate the surface hydrogen on catalysts. It was found that molecular H₂ can access on all the surface of SSP-supported W catalysts, in which the desorption peaks at low temperature (< 200 °C) assigned to hydrogen on metal particles, while the desorption peaks at high temperature (200-500 °C) assigned to hydrogen spillover to the silica support[105]. These results indicate that the activated tungsten oxide in SSP-supported W catalysts can dissociate molecular H₂ that agreed with the literatures[23, 99]. The summarized change in percentages of surface acidity was calculated by Eq. (5) and Eq. (6) as shown in **Figure 5.19**. The decreased percentages for Lewis acid of all sample were found to correlate with increased percentages of Brønsted acid. Therefore, the decreased percentages of Lewis acid can be used to consider the transformation performance. The ability of Lewis acid transformation over SSP-supported W catalysts is in the following order; W-SSP-H₂ > W/SSP-H₂ > W-SSP-N₂ > W/SSP-N₂. According to **Figure 5.19**, the W-SSP catalyst exhibits high performance of Lewis acid transformation in both

of activation process with H₂ and N₂, while the W/SSP catalyst seems to be low active in N₂ pretreatment. However, the performance is not much different between W-SSP-N₂ and W/SSP-H₂, indicating that the W/SSP catalyst needs H₂ pretreatment for activating active site formation, whereas this is not necessary for W-SSP catalyst. Therefore, it is proposed that W-SSP has demonstrated well performance for Lewis acid transformation.

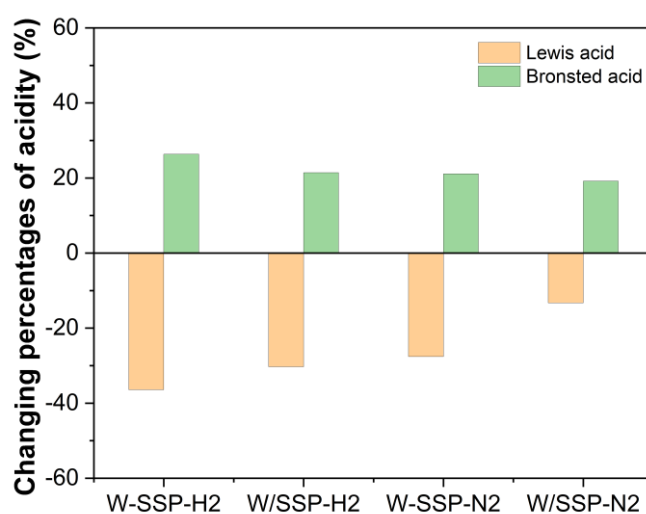


Figure 29 Percentages of decreased Lewis acid sites (yellow), and increased Brønsted acid sites (green) over SSP-supported W catalysts.

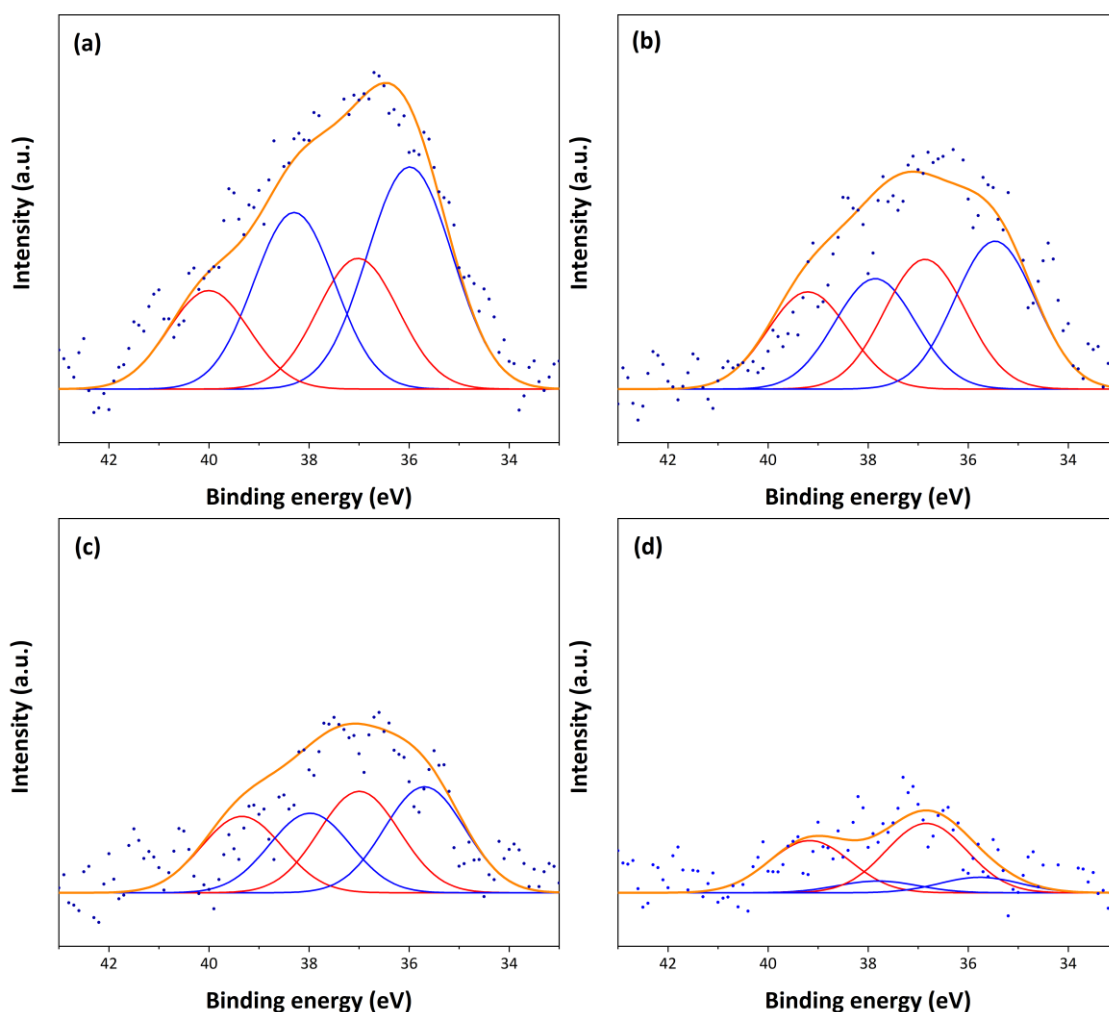


Figure 30 XPS spectra of W $4f_{7/2}$ and W $4f_{5/2}$ for SSP-supported W catalysts with gas pretreatment; W-SSP- H_2 (a), W/SSP- H_2 (b), W-SSP- N_2 (c), and W/SSP- N_2 (d).

5.2.3 Active site formation for Lewis acid transformation to Brønsted acid over SSP-supported W catalysts.

The activating processes, which involve in the formation of catalytically active sites on SSP-supported W catalysts, were investigated to explore the formation of catalytically active sites by N_2 pretreatment compared with H_2 pretreatment. The previous section has found that the W/SSP catalyst needs H_2 pretreatment to activate catalysts for Lewis acid transformation to Brønsted acid. Surprisingly, not only the H_2 pretreatment can be potentially applied for active site activation in the W-SSP catalyst, but also the N_2 pretreatment. H_2 -TPR characterization was used to investigate the

reducibility over SSP-supported W catalysts, which is shown in **Figure A5**. There are two appeared peaks at 757-789 and 862-897 °C assigned to reduction of the surface WO_3 species[82, 91]. The reduction peaks of surface WO_3 species on the incorporated W-SSP catalyst shift to lower temperature than the impregnated W/SSP, indicating that WO_3 surface reduction is easily occurred on the incorporated W-SSP catalyst. These results are agreeable that the activated W-SSP- H_2 demonstrated the highest Lewis acid transformation on SSP-supported W catalysts. The XPS spectra in **Figure 5.20** were obtained to analyze the surface chemical states of tungsten on the surface of SSP-supported W catalysts with gas pretreatment. The binding energies at around 35.2–35.7 and 37.9–38.5 eV (Blue line) could be assigned to $\text{W}^{5+} 4f_{7/2}$ and $\text{W}^{5+} 4f_{5/2}$ [96-98], while 36.6-37 and 39.8-40.4 eV (Red line) could be assigned to $\text{W}^{6+} 4f_{7/2}$ and $\text{W}^{6+} 4f_{5/2}$ [94, 95], respectively. The exhibition of different amount of W^{5+} and W^{6+} phases in this experiment indicated that the activating processes of H_2 and N_2 pretreatment is important for the generated surface chemical states. The peak-fitting results were summarized in Table 1. The low W^{5+} content of 18.3 % was detected on W/SSP- N_2 with the absence of reduction under activating process, while the high W^{5+} contents of 64.2% and 53.2% were obtained on the activating process of H_2 pretreatment of W-SSP- H_2 and W/SSP- H_2 , respectively. Moreover, the high W^{5+} content of 51.1% was also found on the activating process of N_2 pretreatment of W-SSP- N_2 . These results indicated that incorporated W-SSP catalyst revealed the presence of tungstate W^{5+} species under activating process of N_2 pretreatment without H_2 reduction. Basrur et al. reported the possible loss of lattice oxygen from WO_3 leading to formation of tungsten oxides of nonstoichiometric oxidation states under N_2 pretreatment at high temperature[126]. Choung and Weller also reported that some loss of oxygen to nonstoichiometric tungsten oxide over WO_3/SiO_2 catalyst could be occurred from the gas pretreatments by N_2 [127]. In addition, the formation of W^{5+} species can be generated by partially reduced WO_3 with reactants or products including controlling the H_2 reduction conditions. However, the W^{5+} species appeared on the top layer of as-prepared W-doped spherical silica catalysts, which is active for catalyzing the propene metathesis as reported by Watmanee *et. al.*[81]. In our results, we found that the incorporated W-SSP catalyst rendered the abundance of surface tungstate W^{5+}

species, which can be more generated under both of H₂ and N₂ pretreatment. These results are agreeable with XRD, Raman, UV-vis, and ²⁹Si NMR results indicating that the W species in incorporated W-SSP are highly dispersed and embedded into the SSP support, instead of aggregating together to form structure characteristic of W⁶⁺. In addition, these were further confirmed by XRD results in **Figure 5.21a**. The XRD patterns of two samples having abundance of tungstate W⁵⁺ species obtained from XPS results (i.e. W-SSP-H₂ and W/SSP-H₂), were changed from bulk crystal structure WO₃ to WO_{2.92} pattern as seen in **Figure 5.21a**. The change of this bulk crystal to WO_{2.92} pattern indicated that the tungsten oxides on SSP-supported W catalysts were transformed to oxygen-deficient tungsten oxide and formation of W⁵⁺ species under the activation process[99]. Those of the W-SSP-N₂ and W/SSP-N₂ were less changed in XRD patterns, which indicated that nitrogen activation was less effected bulk crystal structure. However, the W-SSP-N₂ can still generate tungstate W⁵⁺ species as XPS results. This evidence that the tungstate W⁵⁺ species in the incorporated W-SSP can be formed without the reduction agreed with Watmanee *et. al.*[81]. In addition, X-ray absorption near-edge structure (XANES) spectroscopy was also used to investigate the oxidation state of W in SSP-supported W catalysts with gas pretreatment. The normalized W L₁ edge XANES spectra are shown in **Figure 5.21b**. The standard compound of WO₃ exhibits the pre-edge shoulder features characteristic of W⁶⁺ at around 12105 eV[118, 128]. When SSP-supported W catalysts were activated under H₂ and N₂ pretreatment, the pre-edge shoulder seemed to disappear, which is corresponding to the tungsten compounds of WO_{3-x} with a different valence state of tungsten from W⁶⁺ (WO₃) to W⁴⁺ (WO₂)[128]. The disappearance of these pre-edge features is similar with the formed W⁵⁺ species in SSP-supported W catalysts as shown in XPS and XRD results. In addition, the W/SSP-N₂ showing the abundant of W⁶⁺ species, demonstrated nearly similar shape as WO₃ standard. Therefore, it is further confirmed that W⁵⁺ species were formed on SSP-supported W catalysts during the activating by H₂ and N₂. This suggested that some loss of lattice oxygen from tungsten oxide led to the formation of nonstoichiometric oxidation states.

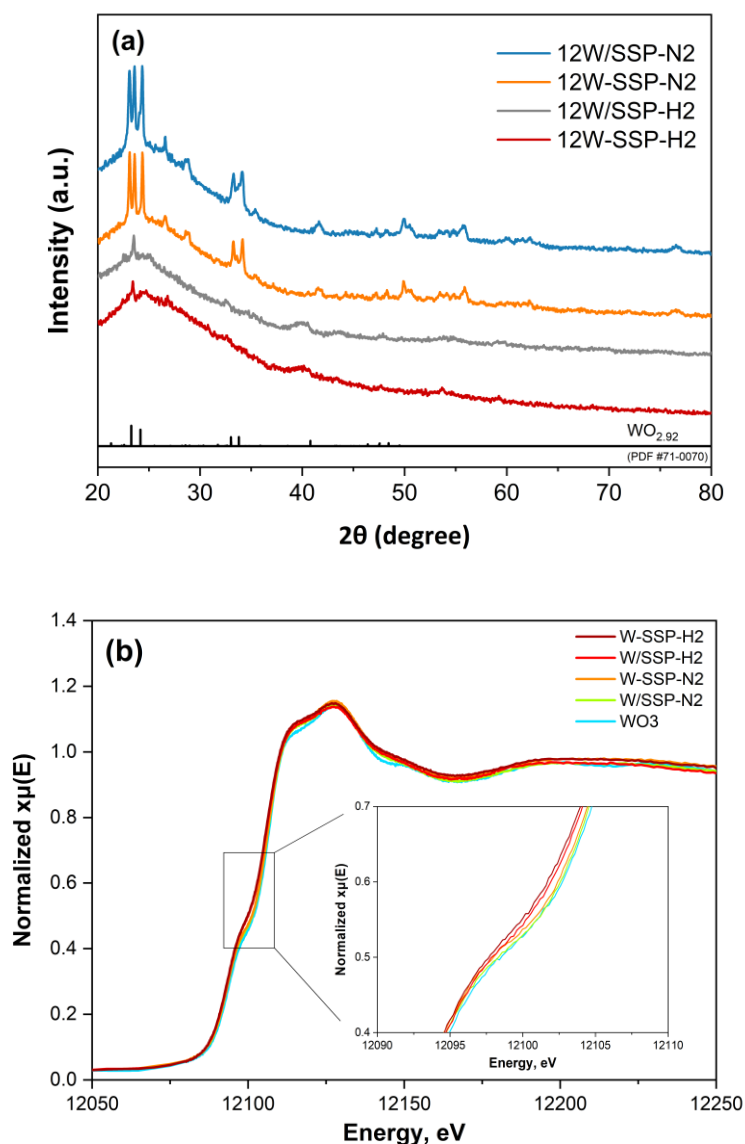


Figure 31 Wide-angle XRD patterns (a) and W L_1 edge XANES spectra (b) for SSP-supported W catalysts with gas pretreatment.

In our analysis of SSP-supported W catalysts, the impregnated W/SSP exhibits more W surface structure such as tetrahedral, octahedral, and crystalline WO_3 , which demonstrates the characteristic of W^{6+} species than the incorporated W-SSP as confirmed by UV-vis, Raman, TEM, and XRD results. Although the incorporated W-SSP exhibits high dispersion of tungsten oxide on the SSP support, this catalyst prefers the formed feature characteristic of tungstate W^{5+} species. ^{29}Si NMR and XPS proved that

W species in the incorporated W-SSP could be embedded into SSP support and formed tungstate W^{5+} species rather than the W dispersed on SSP surface to form W surface structure characteristic of W^{6+} species. However, the performance of Lewis acid transformation to Brønsted acid was found to correlate with tungstate W^{5+} species, which could be more generated by activating process of H_2 and N_2 pretreatments as confirmed by XRD and XANES results. These W^{5+} species offer the oxygen-deficient tungsten oxide property, which can facilitate the activation of molecular H_2 [99]. Therefore, these are agreeable with our work that the W^{5+} species is active site in SSP-supported W catalysts for Lewis acid transformation, which could activate molecular H_2 to form H atoms, then migrated onto Lewis acid site leading to the change of acidity. The impregnated W/SSP needs H_2 pretreatment to activate active site formation. However, the active site in the incorporated W-SSP could be formed in both of H_2 and N_2 pretreatments due to this preparation method offers the formation of tungstate W^{5+} species in catalyst. Therefore, the W-SSP catalyst shows high performance of Lewis acid transformation in both of activation process with H_2 and N_2 pretreatment, while the W/SSP catalyst seems to be low active in N_2 pretreatment. In general, the reaction/pathway mechanism essentially employs on acid sites (i.e. Brønsted and Lewis acidity) of solid acid catalysts. Thus, the changing of Lewis acid to new Brønsted acid can also readily affect the reaction pathway including the activity and selectivity of a catalytic reaction. Baertsch *et. al.* reported that a high turnover rate of 2-Butanol dehydration in WO_x-ZrO_2 catalysts required Brønsted acid sites, which were formed during the reaction by activation of 2-butanol to form hydrogen atoms[129]. In these processes, several W-atoms could be stabilized by electron density to form active $H^{\delta+}(WO_3)^{\delta-}$ sites on polytungstate domains. Although the tungsten carbide with Brønsted acid sites in $WO_x-Al_2O_3$ and WO_x-SiO_2 catalysts can catalyze many reactions (i.e. methanol dehydration and propylene oligomerization and cracking reactions), low propylene metathesis selectivity, which requires Lewis acid site, shows that the converted Lewis acid sites into Brønsted acid sites occurred on the tungsten carbide by the interactions of WO_x with hydrogen atoms formed during hydrogen/hydrocarbons dissociation[56, 130].

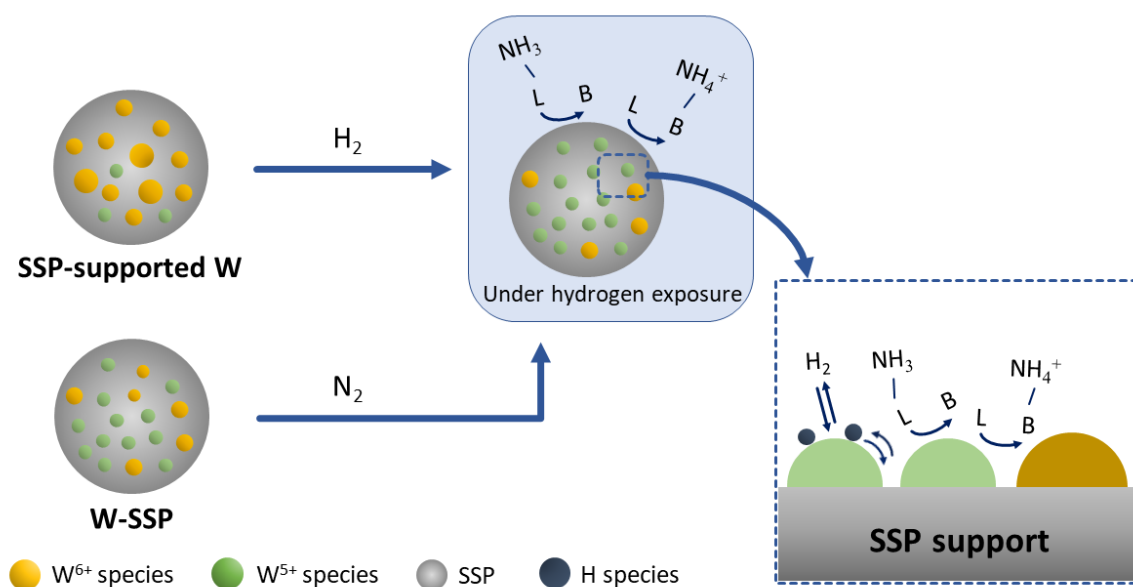
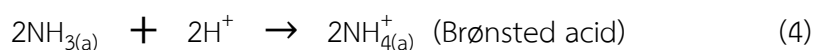


Figure 32 Activation of active site and Lewis acid transformation to Brønsted acid over SSP-supported W catalysts.

The conceptual model mechanism is demonstrated in Scheme 1. The W⁵⁺ active species can be formed on all SSP-supported W catalysts (W/SSP and W-SSP) by activating process of H₂ pretreatment. In addition, W-SSP catalyst showing the abundance of W⁵⁺ species can further generate active species by activating process of N₂ pretreatment. When the process is under hydrogen exposure, the molecular H₂ is dissociated to form hydrogen atoms via oxygen-deficient surface of tungstate W⁵⁺ species in activated catalysts leading to transformation of Lewis acid site. This is clearly confirmed by the correlation plot of increased Brønsted acid sites and tungstate W⁵⁺ species (see **Figure A6**). The possibly proposed mechanism of Lewis acid transformation to Brønsted acid upon hydrogen exposure with adsorbed NH₃ is shown in Eq. (1)-(4) as follows:



The spillover hydrogen atoms migrate to the Lewis acid site, which can be stabilized and trapped the electrons decomposed from hydrogen atoms to become a proton on the oxygen anions around its site. After that, the Lewis acid site (L) can be changed to the new Brønsted acid site (B). Finally, ammonia (NH_3) adsorbed on Lewis acid site migrates to adjacent Brønsted acid site to form ammonium ion (NH_4^+). This is a strong evidence and useful information to give better understanding of the influence of W species on the support and their transformation of ammonia adsorbed on Lewis and Brønsted acid site.

5.3 Influence of isolated tungstate sites on surface Si-OH formation with hydrogen-bonded clusters over spherical silica-supported WO_x catalysts.

5.3.1 Characterization of catalysts.

The content of W surface concentration was measured by Energy-dispersive X-ray spectroscopy (EDS) as shown in **Table A3**. The results show the same W content with an average of 0.45 at% (i.e. 4W-SSP and 4W/SSP) and 0.94 at% (i.e. 8W-SSP and 8W/SSP), indicating that the prepared sample is well uniformly dispersed during the synthesis, in which pore size, pore-volume, and surface area are not significantly changed. This indicates that the preparation methods (i.e. impregnation and incorporation) and W content are not significantly caused the morphology of catalysts. TEM and SEM images were also applied to investigate the morphology as shown in **Figure 5.23** and **Figure A7**, respectively. All samples show the spherical shape of SSP materials, in which the impregnated 8W/SSP presents more crystalline WO_3 surrounding on their surface than the others. It was further confirmed by XRD and Raman analysis as shown in **Figure 5.24**. The impregnated 8W/SSP catalyst presents the highest peaks of monoclinic WO_3 patterns on XRD [131, 132]. Additionally, Raman spectra of 8W/SSP and 8W-SSP show the high intensity of stretching mode of W–O–W at 718 and 808 cm^{-1} [114, 115], while the 4W/SSP show the O=W=O band of isolated tetrahedral at 970 cm^{-1} instead of their crystalline [133]. The results are agreeable with the Wachs group that the crystalline WO_3 nanoparticles will present on W/SiO₂ at W loading ≥ 8 wt% [134]. However, the isolated tetrahedral ($[\text{WO}_4]^{2-}$) and octahedral polytungstate ($[\text{WO}_6]^{n-}$) species are also formed with increasing W content, which is

shown in UV-vis DRS (see **Figure A8**) at the band 225 and 262 nm [133, 135], respectively.

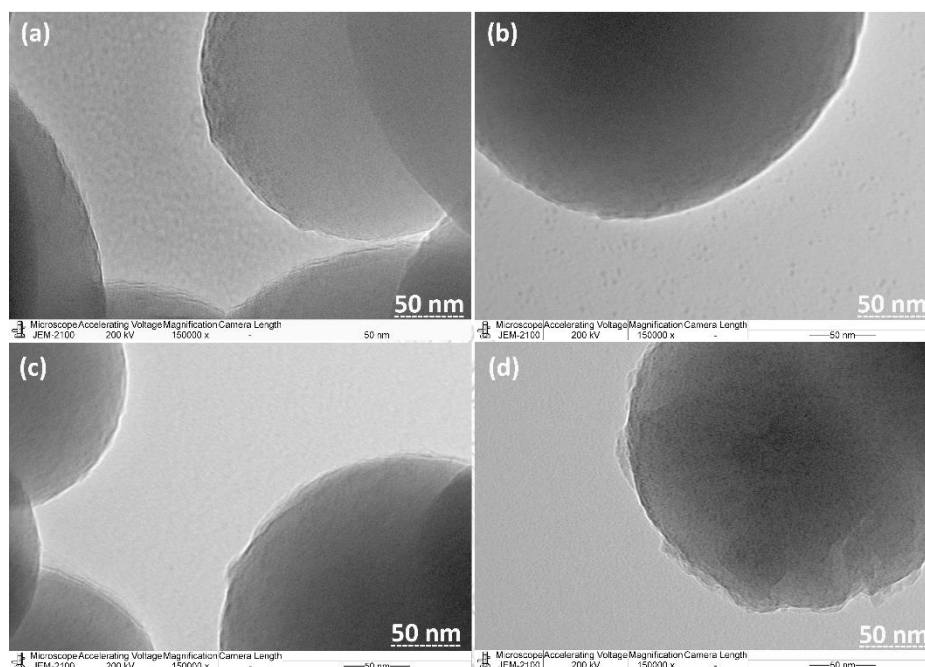


Figure 33 TEM images of catalysts (a) 4W-SSP, (b) 4W/SSP, (c) 8W-SSP, (d) 8W/SSP.

X-ray absorption near-edge structure (XANES) spectroscopy was applied to investigate the oxide structure, in which the W L_1 edge XANES spectra and Fitting pre-edge peaks are shown in **Figure 5.25a** and **Figure A9**, respectively. The observed XANES pre-edge peaks indicate the pre-edge feature for WO_4 coordinated structures and isolated tungstate oxo species (mono-oxo $O=WO_4$ and di-oxo $(O=)_2WO_2$), which absorbing W atom is displaced from the inversion symmetry center [21, 134, 136]. The results reveal that SSP-supported W catalysts present both dioxo and mono-oxo tungstate species as similar pre-edge features characteristic of standard compound $Ce_2(WO_4)_3$, which contains only isolated WO_4 sites [118, 134]. High intensity of XANES pre-edge peaks is observed on incorporated W-SSP catalyst, indicating the isolated tungstate oxo species is mostly presented on their surface (see **Figure A9**). The FT-IR spectra result in **Figure S10** encourages that the major two bands of 921-970 and 855 cm^{-1} assigned to Si-O-W species and the formation of dodecatungstosilicic acid units on the surface are presented on the catalysts [21, 121, 137, 138], respectively. The incorporated W-

SSP catalyst show a higher intensity band of Si–O–W species than those of impregnated W/SSP catalyst. This Si–O–W species is involved in the tungsten oxide structure types of mono-oxo $O=WO_4$ and di-oxo $(O=)_2WO_2$ species, in which W atoms flanked by either two/four –O–Si moieties) [21, 118]. Additionally, the formed Si–O–W species are further evidenced by the ^{29}Si MAS NMR in **Figure 5.25b**, in which their peaks fitting results are shown in a 1. There are four peaks at the chemical shift -91.3 , -99.2 , -103.7 , and -108.1 ppm, assigned to species of $Si-(OH)_2(O-Si)_2$, $Si-(OH)(O-Si)_3$, $W-O-Si-(O-Si)_3$, and $-Si-(O-Si)_4$, respectively [118-120]. According to **Table 5.5**, the percentage of $W-O-Si-(O-Si)_3$ structure more occurs in the incorporated W-SSP catalysts than the impregnated W/SSP catalysts as agree with FT-IR result. Klepel et al. [119] reported that this structure indicated the silicon is flanked by one W atom and three Si atoms in W-incorporated silicate catalysts. The percentage of $W-O-Si-(O-Si)_3$ structure follows the trend $8W-SSP > 4W-SSP > 8W/SSP > 4W/SSP$, while three species of $Si-(O-Si)_4$, $Si-(OH)(O-Si)_3$, and $Si-(OH)_2(O-Si)_2$ are relatively decreased. The results reveal that these three species are commuted to $W-O-Si-(O-Si)_3$ by the combining of W species and –OH groups as reported by literatures [120, 121]. This indicates that W species can be mostly embedded into their bulk silica support to form Si–O–W species over the incorporated W-SSP instead of aggregating together to form the crystalline phase, which well agrees with TEM, Raman, FT-IR, and W L_1 edge XANES results.

จุฬาลงกรณ์มหาวิทยาลัย
CHULALONGKORN UNIVERSITY

Table 5.5 Deconvoluted results of relative peaks ^{29}Si NMR analysis of catalysts.

Sample	Deconvoluted results of relative peaks ^{29}Si NMR (%)			
	$Si-(OH)_2(O-Si)_2$	$Si-(OH)(O-Si)_3$	$W-O-Si-(O-Si)_3$	$Si-(O-Si)_4$
8W-SSP	16.9	57.5	13.4	12.2
4W-SSP	17.0	57.9	11.4	13.6
8W/SSP	17.2	58.2	10.5	14.1
4W/SSP	18.2	58.7	8.2	14.9

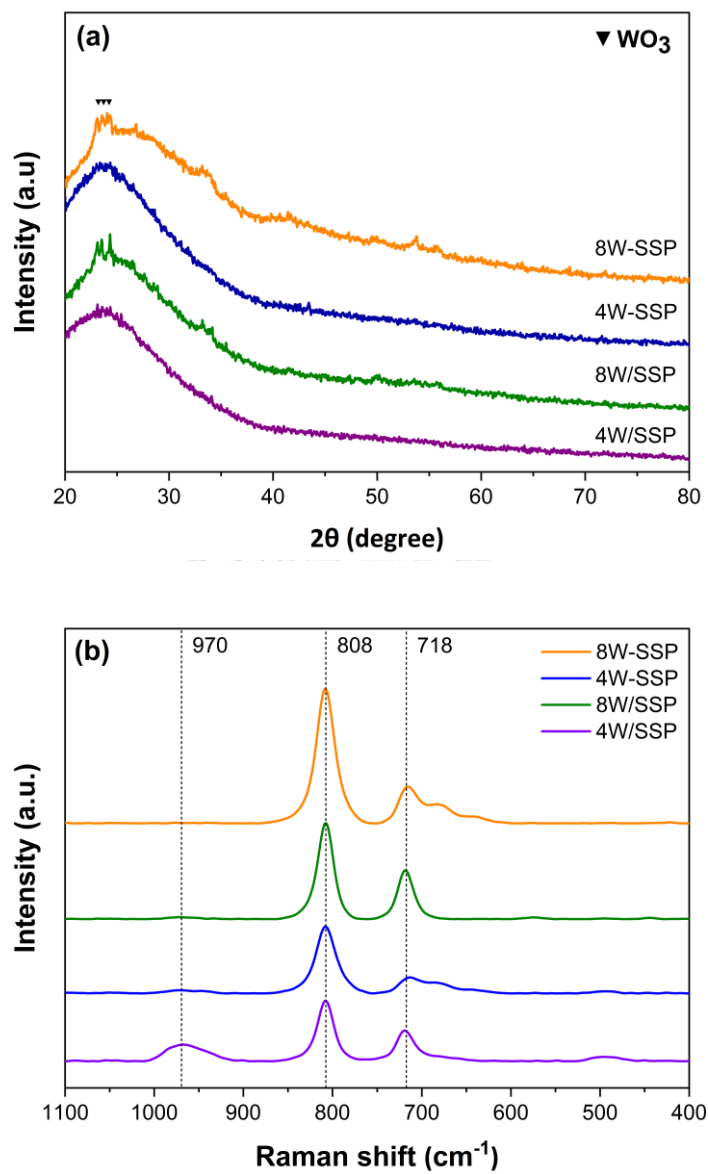


Figure 34 (a) XRD patterns and (b) Raman spectra of catalysts.

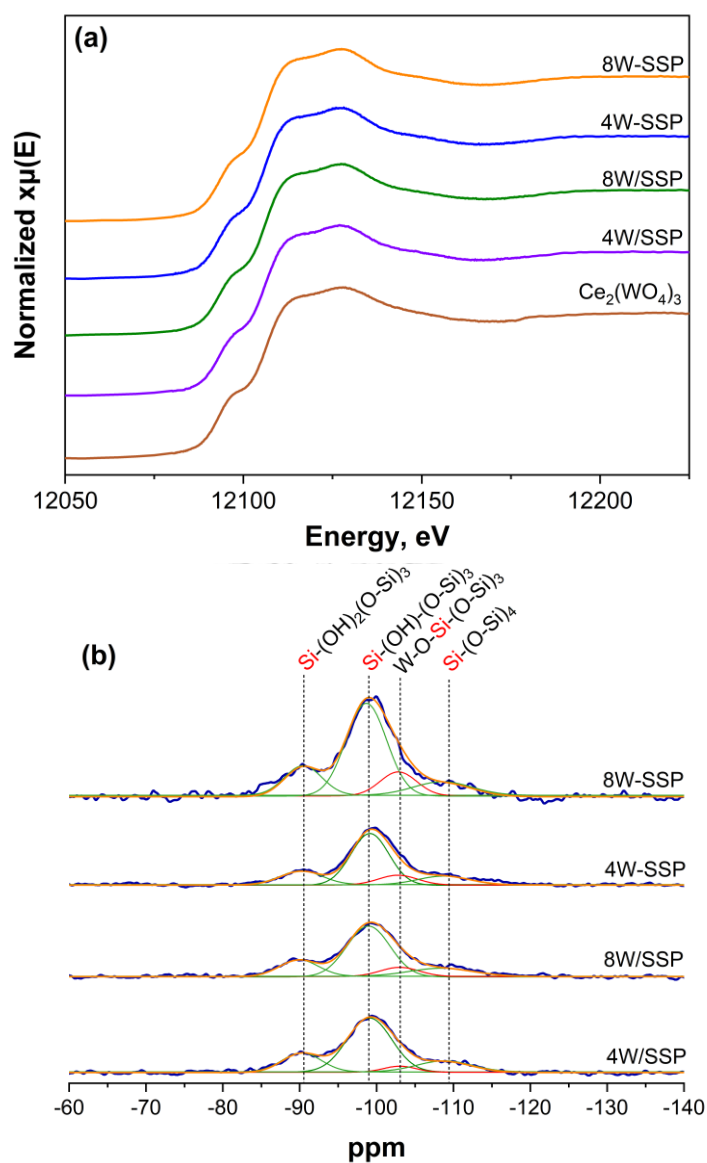


Figure 35 (a) Normalized W L_1 edge XANES spectra and (b) ^{29}Si NMR of catalysts.

5.3.2 Hydrogen surface behavior over silica-supported WO_x catalysts.

The hydrogen surface behavior on WO_x supported on SSP catalysts was analyzed using *in situ* DRIFTS with hydrogen exposure at 40 °C and atmospheric pressure. The IR spectra were automatically recorded every 2 min. As shown in Figure 5.26, the intensities of all spectra were increased during hydrogen exposure, indicating the hydrogen-bonded interactions on their surface catalysts. The major band at 3455 and 3646 cm^{-1} are related to the isolated silanol Si-OH groups on the surface, which

provides opportunities to form hydrogen bonds [45, 139]. Besides, the sharp band was increased at 3741 cm^{-1} assigned to surface silanols Si-OH vibration [140, 141]. The results reveal that the hydroxyl (-OH) groups were generated onto the surface catalyst during hydrogen exposure. The bands intensity of the formed Si-OH species (i.e. 3455, 3646, and 3741 cm^{-1}) are relatively increased with the order: 8W-SSP > 4W-SSP > 8W/SSP > 4W/SSP as seen in **Figure 5.26**. These results imply that the OH groups prefer to generate over silica surface of incorporated W-SSP catalysts than the impregnated W/SSP catalysts.

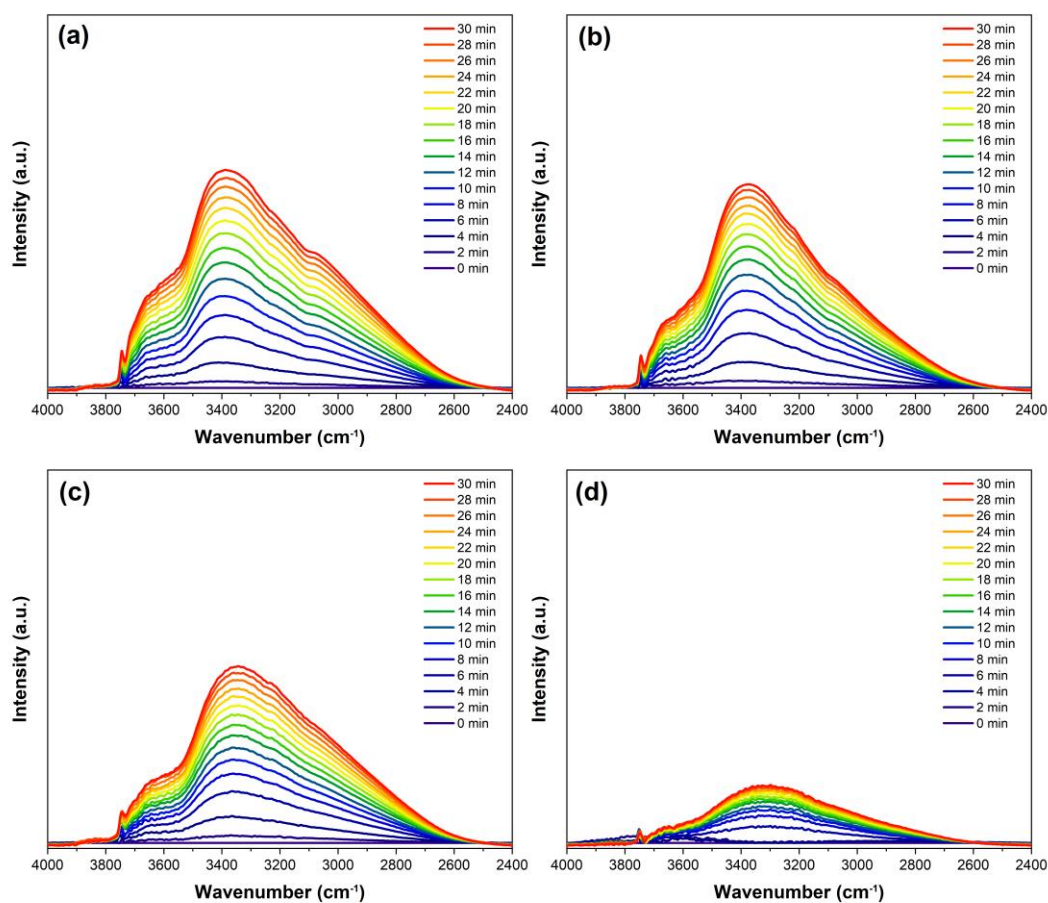


Figure 36 In situ DRIFTS spectra with hydrogen exposure of catalysts; 8W-SSP (a), 4W-SSP (b), 8W/SSP (c), and 4W/SSP (d).

Additionally, the major band at 921-970 cm^{-1} in **Figure 5.27** assigned to Si-O-W species of the incorporated catalysts (i.e. 8W-SSP and 4W-SSP) were decreased during the hydrogen exposure. Meanwhile, these peaks seem to stable in the impregnated catalysts, especially in 4W/SSP catalysts. Surprisingly, these results indicate that the Si-O-W species could be consumed, while the Si-OH species were simultaneously generated during this process. Thus, the Si-O-W species should be a key role in the adsorbed atomic hydrogen to form Si-OH formation. Shen et. al. reported that the molecular hydrogen was hydrogenated on Ru/SBA-15 catalysts to form H atoms, in which the H species were adsorbed on the residing along with Ru-SiO₂ interface. The suggested H species were active in hydrogenation[48]. Also, the surface coverage of new hydroxyl (OH) groups were formed at the vicinity of the Pt particles under the hydrogen atmosphere, in which the interface of Pt-silica is a major importance for the OH groups formation [45]. In this process, the electron-transfer process of dissociated H species also occurred at the Pt-SiO₂ interface [45]. Moreover, Qian et al. also suggested the process of CH₄ reforming with CO₂ over Rh/MCF catalysts, in which the spillover hydrogen atoms from CH₄ decomposition on rhodium surface were found to adsorb on Si-O-Si bridged oxygen sites of MCF and to form surface Si-OH groups[47]. Therefore, the results of Si-OH formation can indicate the activation/dissociation of molecular hydrogen to form the adsorbed atomic hydrogen on the silica surface. In our results, the Si-OH species were generated on WO_x supported on SSP catalysts during hydrogen exposure, indicating that the migration of atomic hydrogen onto silica surface has occurred. Our results reveal that atomic hydrogen should be adsorbed at Si-O-W species, and then the new Si-OH species were formed surrounding its sites.

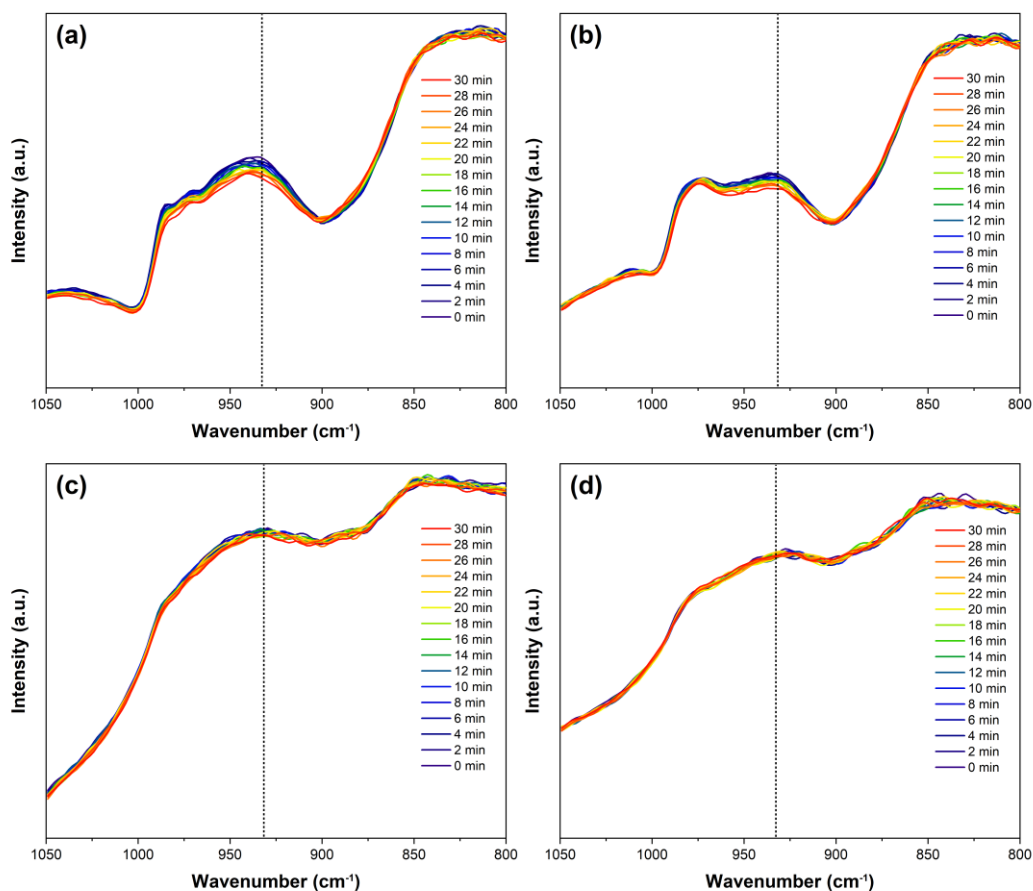


Figure 37 In situ DRIFTS spectra with hydrogen exposure of catalysts; 8W-SSP (a), 4W-SSP (b), 8W/SSP (c), and 4W/SSP (d).

5.3.3 Influence of W species on hydrogen surface behavior over WO_x supported on SSP catalysts.

The hydrogen adsorption was investigated by H_2 -TPD analysis as shown in Figure 5.28. All samples show two hydrogen desorption peaks. The first peaks (I) at temperatures range < 200 °C were attributed to hydrogen desorption on the metal site, while the second peaks (II) at temperatures range 200-400 °C were related to spillover hydrogen onto the silica support [105]. It is clear that the molecular hydrogen was adsorbed and dissociated on the catalyst to form spillover hydrogen onto the silica support, which is well agreeable with the *in situ* DRIFTS results. Song et al. reported that the oxygen-deficient surface of tungsten oxide can activate hydrogen very easily in kinetics and thermodynamics [99]. The atomic hydrogen was generated

and migrated to the silica support as seen in peaks II of **Figure 5.28**. The incorporated 8W-SSP and 4W-SSP show lower desorption peak (II) at around 235 °C and 246 °C, respectively, while the impregnated 8W/SSP and 4W/SSP show higher desorption peak (II) at around 264 °C and 280°C, respectively. These results indicate the accessibility of hydrogen to the catalyst surface in the following order: 8W-SSP > 4W-SSP > 8W/SSP > 4W/SSP. The results are agreed with the formed Si-OH species during hydrogen exposure. Additionally, the final state of spillover hydrogen is involved in the -OH groups generation, in which the oxygen ions can accept the atomic hydrogen or ions[31]. Therefore, this confirmed that the spillover hydrogen from tungsten oxide to SSP support and Si-OH formation has essentially occurred.

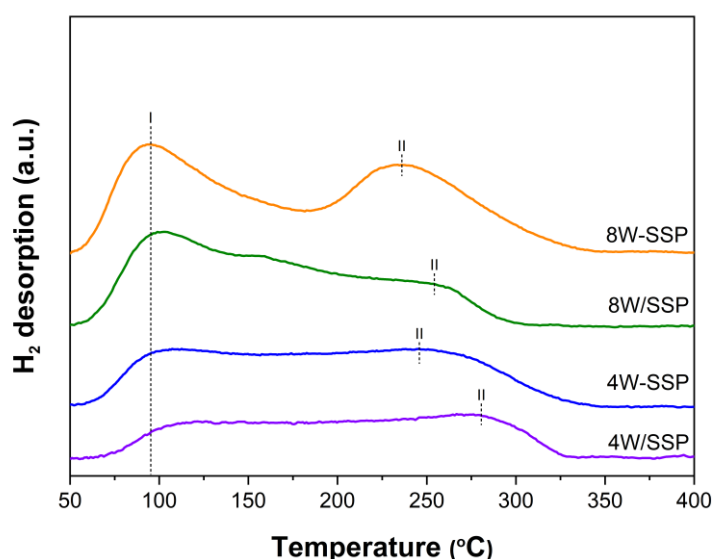
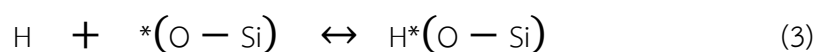


Figure 38 H₂-TPD profiles of catalysts.

The ²⁹Si MAS NMR and FT-IR results indicated the W species were dispersed on catalysts, which the Si-O-W species mostly formed on the incorporated W-SSP catalysts (i.e. 4W-SSP and 8W-SSP). Meanwhile, the impregnated W/SSP (i.e. 4W/SSP and 8W/SSP) presented a higher crystalline WO₃ phase confirmed by XRD, Raman, and TEM results. Thus, W species prefer to aggregate together to form crystalline WO₃ on the impregnated W/SSP catalysts, while W species prefer to embed into the lattice of bulk SSP support over the incorporated W-SSP catalysts. Our results show that the order of Si-O-W species follows the trend 8W-SSP > 4W-SSP > 8W/SSP > 4W/SSP,

which is correlated with Si–OH formation during hydrogen exposure. The surface Si–O–W species is involved in the tungsten oxide structure types of mono-oxo $O=WO_4$ and di-oxo $(O=)_2WO_2$ species (W atoms flanked by either two/four –O–Si moieties) [21, 118], which was detected in SSP-supported W catalysts. The isolated di-oxo and mono-oxo types are presented on W/SiO_2 catalyst when the W loading is below 8 wt% as reported by Wachs group [134]. More recently, Subramaniam group reported that the W–O–Si species in di-oxo $(O=)_2WO_2$ and mono-oxo $O=WO_4$ are active site precursors for olefins metathesis with W-Incorporated Silicates [118]. These are agreed with our results that the Si–O–W species, in which the existence of isolated tungstate oxo species was supported by the W L_1 edge XANES technique, is a key role for the adsorbed atomic hydrogen subsequent formation of Si–OH species as confirmed in **Figure 5.26** and **Figure 5.27**. It is clearly confirmed the Si–O–W species is a major importance for adsorbed hydrogen, in which atomic hydrogen can be adsorbed at around Si–O–W interface, then migrates onto the Si–O–Si bridged oxygen sites leads to Si–OH formation as well agreed with the *in situ* DRIFTS and H_2 -TPD results.

The schematic model of Si–OH formation surrounding their Si–O–W site over WO_x supported on SSP catalysts is shown in **Figure 5.29**. Additionally, the possible mechanism is proposed as follows:[47, 142]



where $*(O - Si)$ and $*(Si - O - Si)$ are different oxygen sites on a silica support. In this process, molecular hydrogen was dissociated on the WO_x sites to form the adsorbed atomic hydrogen at Si–O–W interface of mono-oxo $O=WO_4$ and di-oxo $(O=)_2WO_2$ species. After that, the spillover hydrogen migrates onto the surface catalyst, which the atomic hydrogen adsorbed and reacted around Si–O–W species and Si–O–Si species conducts to the Si–OH formation. The results can provide useful information, in which the formed OH groups on the catalyst surface are usually active precursors for adsorbed substances[38-41, 143]. Therefore, the Si–OH species, which can be

formed under the hydrogen atmosphere, can definitely affect the pathway of the reaction involving hydrogen. However, this hypothesis should be testified by further systematic investigations.

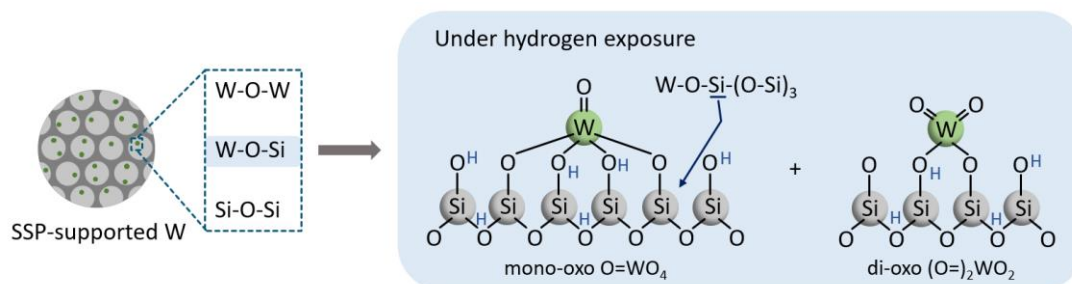


Figure 39 Schematic model of Si–OH formation under hydrogen exposure over SSP-supported WO_x catalysts.

5.4 Influence of surface Sn species and hydrogen interactions on the OH group formation over spherical silica-supported tin oxide catalysts.

5.4.1 Textural properties.

SEM and TEM images were used to characterize the particle morphology and the elemental distribution. As seen in **Figure 5.30**, all catalysts show spherical particles representative of the SSP material. When tin oxide was impregnated onto SSP support, Sn species were observed on the SSP support as shown in **Figure 5.30b,c,e,f**. The IW1-10Sn catalyst presented notable (about 20 nm) Sn nanoparticles on the surface of SSP support, indicating that the high Sn loading of this catalyst led to Sn aggregation into clusters on the silica surface[144]. For the incorporated catalysts, no aggregated particles of Sn were observed on Inc-5Sn as shown in **Figure 5.30h,i**. However, the Sn species were detected using TEM-EDS mapping analysis as shown in **Figure 5.30m**. It confirmed that the Sn species were incorporated into SSP support, indicating the uniform dispersion of Sn species over the substrate, and not observable agglomeration [145]. The results clearly indicate that the incorporation of Sn with the SSP support exhibits higher dispersion than when Sn is introduced by impregnation of the support.

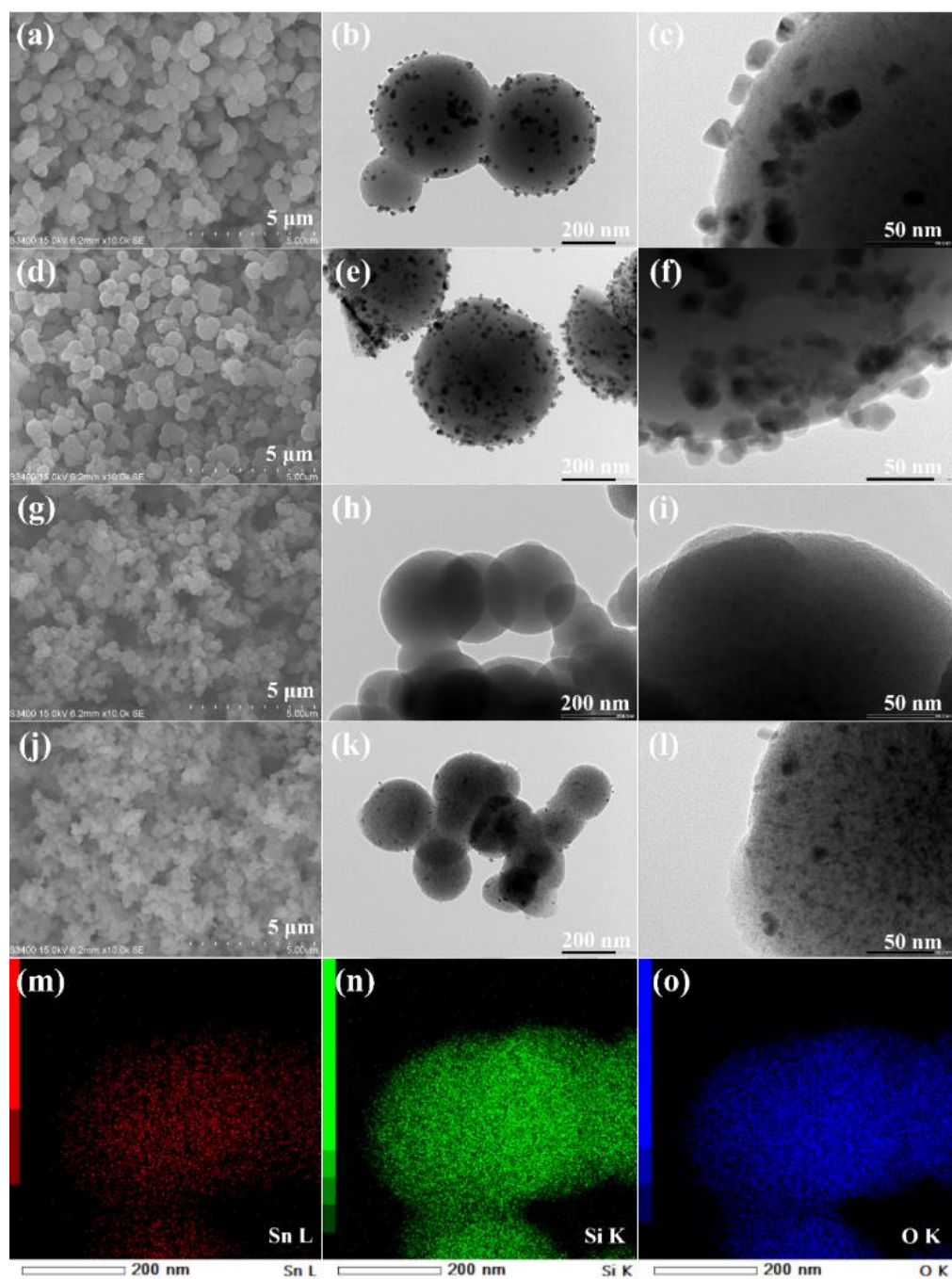


Figure 40 SEM images (a, d, g, j), TEM images (b, c, e, f, h, i, k, l), and EDS elemental mapping analysis (m-o): (a-c) IWI-5Sn, (d-f) IWI-10Sn, (g-i) Inc-5Sn, (j-l) Inc-10Sn, (m-o) Inc-5Sn.

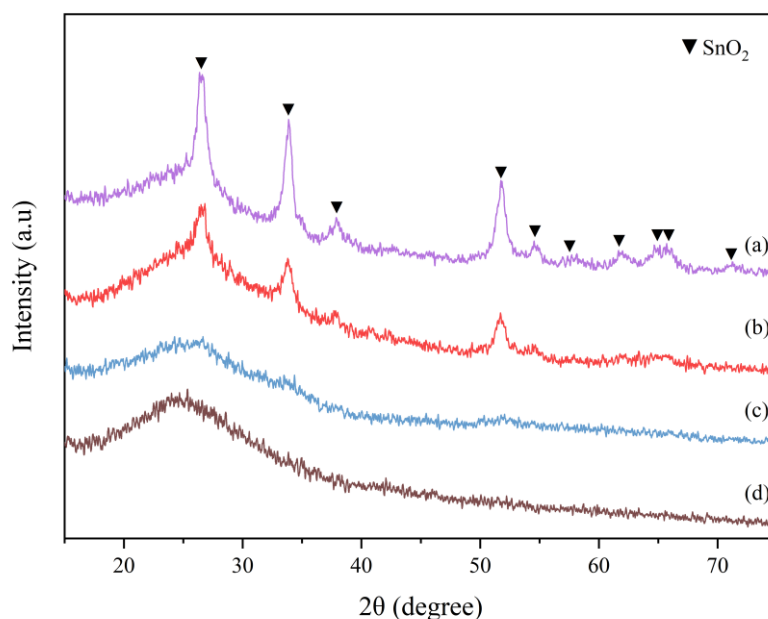


Figure 41 Wide-angle XRD patterns of SSP-supported Sn catalysts; IWI-10Sn (a), IWI-5Sn (b), Inc-10Sn (c), and Inc-5Sn (d).

Table 5.6 Textural properties of SSP-supported Sn catalysts.

Sample	Relative area of XPS (%)			Relative area of ^{29}Si NMR (%)		
	$S_{\text{BET}}^{\text{[a]}}$ (m^2/g)	$V^{\text{[b]}}$ (cm^3/g)	$P^{\text{[c]}}$ (nm)	Sn	O	Si
SSP	990	0.52	2	-	-	-
IWI-5Sn	939	0.57	2	5.3	22.8	72.0
IWI-10Sn	950	0.58	2	7.1	22.0	70.8
Inc-5Sn	840	0.40	2	6.7	22.8	70.6
Inc-10Sn	688	0.32	2	11.4	21.4	67.2

^[a] Specific surface area

^[b] Total pore volume ($P/P_0 = 0.990$)

^[c] Average pore size

^[d] TEM-EDS elemental analysis

The wide-angle XRD pattern of IWI-5Sn and IWI-10Sn catalysts show sharp peaks corresponding to crystalline SnO_2 , as seen in **Figure 5.31**, while Inc-5Sn and Inc-10Sn

catalysts seem to exhibit only one broad peak at around 20° to 40° corresponding to amorphous silica [146-148]. These results also agree with TEM image and H_2 -TPR (see **Figure A11**). This indicates that Sn species are highly dispersed on Inc-5Sn and Inc-10Sn catalysts [149], meaning the incorporation of Sn species onto silica support leads to a higher dispersion of Sn species over the silica substrate, or even embedding them into the lattice of bulk silica, instead of aggregating together to form crystalline SnO_2 [145]. A summary of the textural properties of the catalysts is presented in **Table 5.6**. All catalyst samples showed high surface area with average pore size around 2 nm, while the SSP support material showed an especially high surface area of around $990\text{ m}^2/\text{g}$. When tin oxide was impregnated onto the SSP support, the IWI-5Sn and IWI-10Sn catalysts retained the large surface area and pore volume. However, the incorporated catalysts led to a decrease in the BET surface area and pore volume, especially for the Inc-10Sn catalyst. TEM-EDS measurements were used to investigate the element surface concentration on the samples as shown in **Table 5.6**, which indicates that surface concentration of Sn increases with increasing Sn loading. Comparing the incorporated and impregnated catalysts, it was found that Inc-5Sn and Inc-10Sn showed a higher concentration of surface Sn than IWI-5Sn and IWI-10Sn, respectively. These results demonstrate the better dispersion of incorporated tin oxide.

5.4.2 Structural properties of the catalysts.

To investigate the structure of the SSP-supported Sn catalysts, the samples were analyzed by UV-Vis DRS as shown in **Figure 5.32**. All samples display the absorption band (208 nm) typical for Sn^{4+} species in tetrahedral coordination [149, 150]. The increase in Sn content led to increased intensity of this band. Moreover, the impregnated catalysts (IWI-Sn) exhibited another absorption band at around 280 nm convoluted with the main absorption band, assigned to hexacoordinated polymeric Sn–O–Sn [150, 151]. This absorption features also increased with increasing of Sn content on IWI-Sn. However, this absorption band was almost unobservable on the incorporated catalysts (Inc-Sn), indicating that the incorporation of Sn species to SSP preferred to form tetrahedral coordination, rather than hexacoordinated polymeric structures. The broader character of this band observed on Inc-Sn suggests the

occupancy of Sn atoms in site isolated positions in the silica framework on incorporated catalysts inhibits this 280 nm band [150].

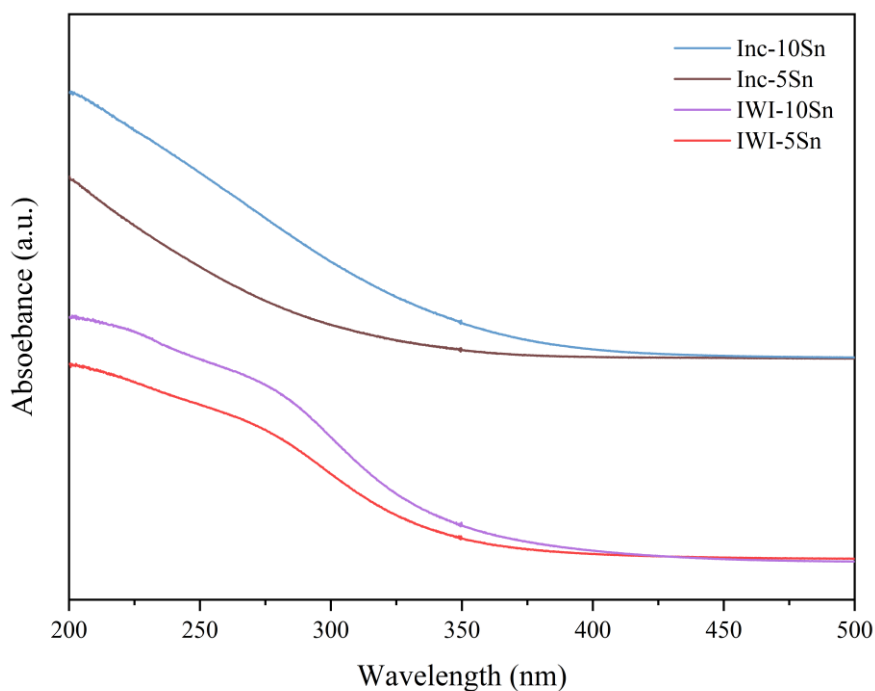


Figure 42 UV-vis DRS spectra of SSP-supported Sn catalysts.

XPS analysis was employed to investigate the surface chemical states of catalysts Sn_{3d} . XPS spectra and deconvoluted peaks are shown in **Figure 5.33a**. All samples present two groups of peaks located at around 496 and 487.6 eV attributed to Sn $3d_{3/2}$ and Sn $3d_{5/2}$ core levels, respectively [152]. The Sn $3d_{5/2}$ peak can be separated into three peaks at around 488.5, 487.6, and 484.5 eV, which were assigned to Sn species bound to the support (Sn-support), oxidized $\text{Sn}^{2+,4+}$, and Sn^0 , respectively [153-155]. The results of deconvolution are summarized in **Table 5.7**. Generally, XPS cannot discriminate between Sn^{2+} and Sn^{4+} oxidized states due to the small difference between the binding energy of the Sn $3d$ peak of both species. According to **Table 5.7**, the percentage of the Sn^0 peak was higher for species on the impregnated catalysts (IWI-Sn) than those on the incorporated catalysts (Inc-Sn). It also indicates that the Sn species on impregnated IWI-Sn catalysts can be reduced more easily than on Inc-Sn catalysts, which is consistent with the H_2 -TPR results. Besides, the Inc-Sn catalysts

exhibited a higher amount of Sn-support and a lower amount of Sn^0 , which indicates the greater interaction between Sn species and silica (Sn–O–Si) [153]. The percentage of this species on the catalyst surface follows the trend Inc-10Sn > Inc-5Sn > IWI-10Sn > IWI-5Sn. It is seen that the incorporating Sn species onto SSP leads to high dispersion of Sn species over SSP and surface Sn–O–Si bonds. The results of Sn_{3d} XPS are consistent with the O 1s XPS spectra as shown in **Figure 5.33b**. All catalysts exhibited only one peak located at a binding energy around 532.7 eV, which was assigned to the characteristic of SiO_2 in metal-incorporated mesoporous silica [145, 156]. The intensity of O 1s XPS peaks decreased when the surface Sn–O–Si species XPS signal increased. These results further suggest that the Sn species are probably embedded into the framework of SSP, which contributes to a high concentration of surface Sn–O–Si bonds. These results are consistent with the FT-IR characterization results as shown in **Figure A12**. The addition of Sn species onto SSP shows a significant change on the IR bands at 810 cm^{-1} and 962 cm^{-1} , with exhibit lower intensity, indicating the existence of the surface Sn–O–Si species. This intensity decrease can be easily observed on the Inc-10Sn catalyst. Moreover, these results also agree with a decrease on silanol groups signal at around 3740 cm^{-1} as shown in **Figure A12b** [21, 157]. Thus, the incorporation of Sn species onto SSP and high Sn content have a strong effect on the silica mesoporous structure.

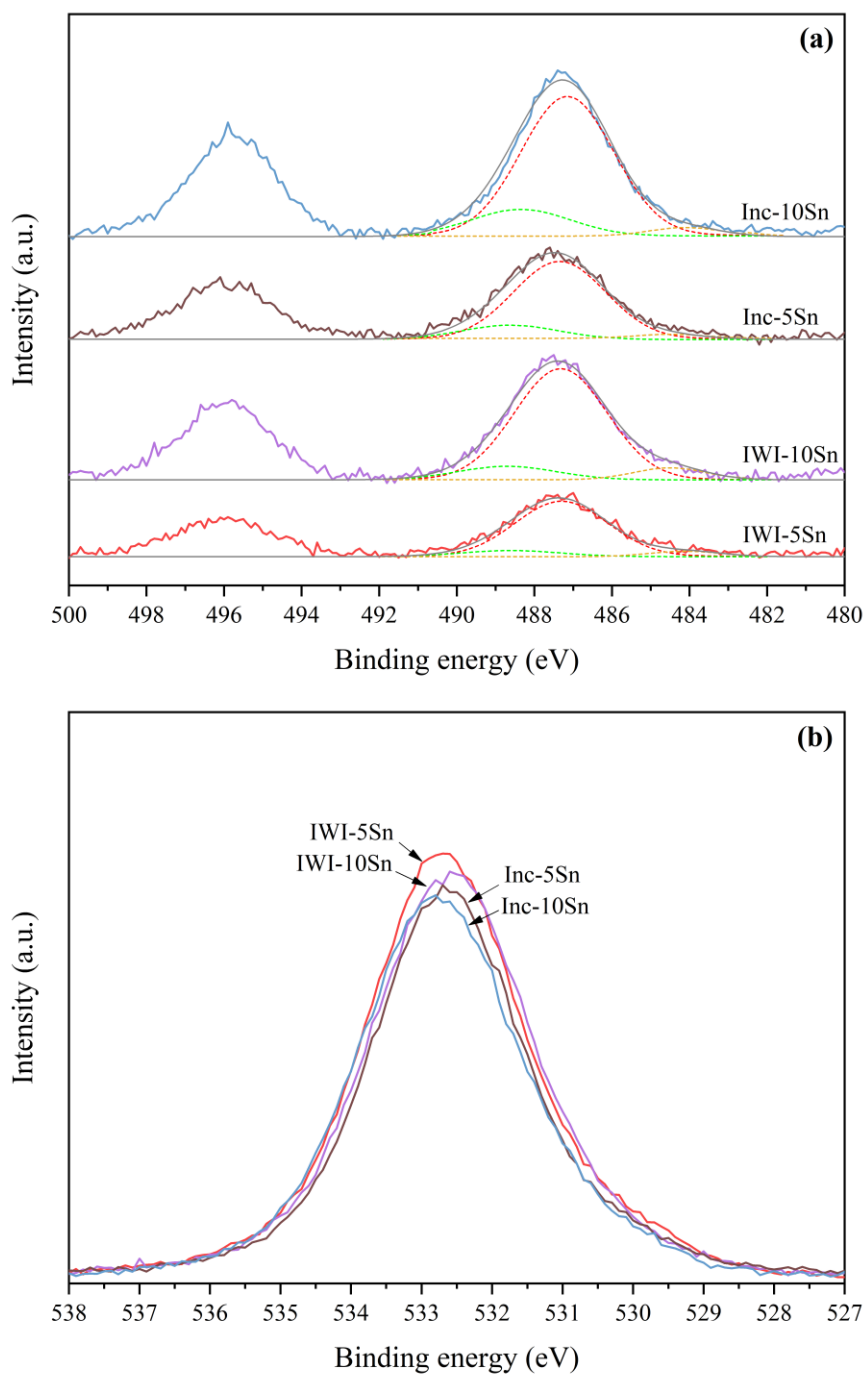


Figure 43 (a) Sn3d XPS spectra and deconvoluted peak results (b) O1s XPS spectra of SSP-supported Sn catalysts.

The existence of surface Sn–O–Si species of catalysts was further confirmed by the solid state ^{29}Si MAS NMR, shown in **Figure 5.34**. This technique was used for a more in-depth study of the Si species on catalysts, and the effects of Sn species. All

samples displayed three peaks at around -90, -100, and -110 ppm assigned to germinal silanol (Q^2 : $\text{Si}(\text{OSi})_2(\text{OH})_2$), free silanol (Q^3 : $\text{Si}(\text{OSi})_3\text{OH}$), and siloxanes (Q^4 : $\text{Si}(\text{OSi})_4$), respectively [158]. The relative areas of these three peaks are summarized in Table 5.7. The impregnated catalysts (IWI-Sn) exhibited more silanol groups than the incorporated catalysts (Inc-Sn), and the silanol concentration followed the trend IWI-5Sn > IWI-10Sn > Inc-5Sn > Inc-10Sn, which is consistent with the FT-IR results. Comparison of silanol group concentrations reveals that the Inc-Sn catalysts presented a decreasing **percentage of** silanol group characteristic signal. Previous research has reported that the incorporation of Sn atoms requires consumption of four Si-OH groups for the full framework connectivity[159]. Moreover, These catalysts show more siloxanes $\text{Si}(\text{OSi})_4$ species than impregnated catalysts (IWI-Sn) due to silica framework-connected Sn atoms, the relative area of siloxanes follows the trend Inc-10Sn > Inc-5Sn > IWI-10Sn > IWI-5Sn. These results agree with the XPS and FT-IR results.

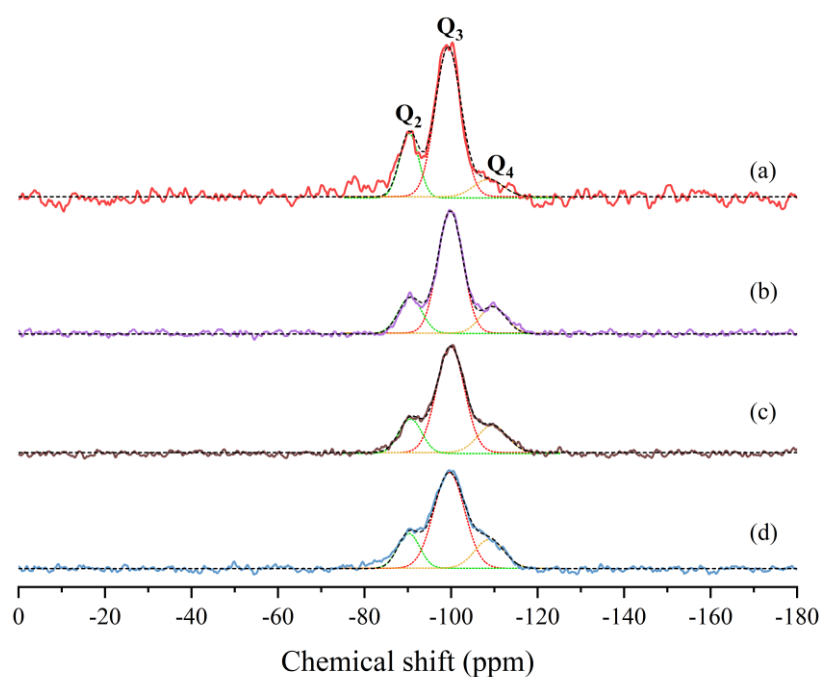


Figure 44 Solid state ^{29}Si NMR spectra and deconvoluted peak results of SSP-supported Sn catalysts; IWI-5Sn (a), IWI-10Sn (b), Inc-5Sn (c), and Inc-10Sn (d).

5.4.3 Formation of new OH groups on ssp-supported Sn catalysts.

The *in situ* DRIFTS spectra of catalysts during hydrogen adsorption condition are shown in **Figure 5.35**. It shows that bands for OH species, between 2600 cm^{-1} and 3800 cm^{-1} , increase in intensity with exposure time. The three absorption bands at 3752 cm^{-1} , 3678 cm^{-1} , and 3544 cm^{-1} are attributed to the vibration of the hydroxyl group (OH) on the tin oxide [147, 160]. The results indicate that hydrogen molecules can access the surface oxygen species of tin oxide, which are well known to be reducible [161]. Additionally, the sharp peak that appeared at 3740 cm^{-1} was assigned to the characteristic OH stretching vibration of isolated silanol groups [21, 157]. The low-intensity band at 2245 cm^{-1} , was assigned to Si-H stretching [162], which was observed only on Inc-5Sn and Inc-10Sn catalysts. The broader band at 3200 cm^{-1} , was assigned to OH groups (hydrogen-bonded to oxygen) on the silica surface [45, 163, 164]. It is remarkable that these new OH groups can form on silica surfaces of SSP-supported Sn, without the presence of any noble metal, due to the interaction of molecular hydrogen directly with the catalysts. Wallin *et al.* [45] found that the isolated OH groups formed on the silica surface of Pt/SiO₂ catalyst by the DRIFTS measurements at the broad band around 3270 cm^{-1} . These new hydroxyl groups are formed on silica during exposure of H₂ in the presence of Pt particles. It was suggested that hydrogen molecules adsorbed dissociatively on the metal particles to produce atomic hydrogen, resulting in hydrogen spillover, migration of H atoms to the silica surface, and formation of new OH groups [45]. Mériaudeau *et al.* [163] reported a band centered at 3200 cm^{-1} after exposing Pt/silicalite catalyst to hydrogen, which they assigned to H bonded to Pt interacting with the silicalite framework. In this work, the broad band at 3200 cm^{-1} , was deconvoluted and assigned to the newly generated OH groups on the silica surfaces. The calculated area of this band is summarized as a function of the exposure time in **Figure 5.36**. All SSP-supported Sn catalyst showed a rapid increase in OH groups band intensity at the initial stage slowing down until reaching a steady value at the final stage (30 min). The amount of new OH species followed the decreasing trend Inc-10Sn > Inc-5Sn > IWI-10Sn > IWI-5Sn. Incorporated catalysts (Inc-Sn) showed better performance on new OH formation than impregnated

catalysts (IWI-Sn). Thus, the influence of Sn species on the incorporated catalysts (Inc-Sn) is a crucial factor for this phenomenon.

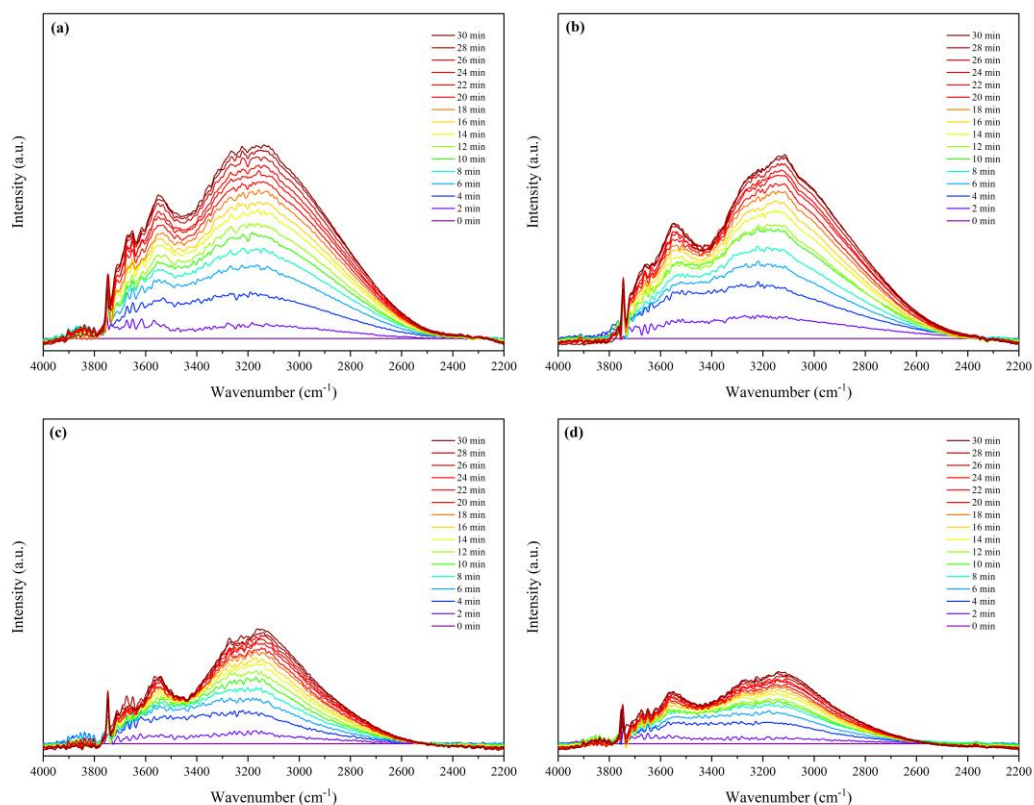


Figure 45 In situ DRIFT spectra during the introduction of hydrogen at 40 °C for 30 min over the SnO_x supported on SSP catalysts; Inc-10Sn (a), Inc-5Sn (b), IWI-10Sn (c), and IWI-5Sn (d).

The behavior of surface hydrogen was investigated by H₂ TPD as shown in **Figure 5.37**. All catalysts showed only one hydrogen desorption peak, the desorption temperature (200-500 °C) was assigned to hydrogen spillover on the silica support [104, 105]. The results confirmed that hydrogen spillover to the support can occur on the catalyst surface. Thus, tin oxide plays a major role in hydrogen dissociation, leading to hydrogen spillover to SSP support. Inc-5Sn and Inc-10Sn catalysts showed lower desorption temperature peak (T I ≈ 226 °C) than IWI-5Sn and IWI-10Sn catalysts temperature peak (T II ≈ 277 °C). However, high Sn loading was related to high desorption intensity. Therefore, the accessibility of hydrogen follows the trend Inc-10Sn > Inc-5Sn > IWI-10Sn > IWI-5Sn. These results correlate with the formation of

new OH groups. In addition, hydrogen spillover also influences the formation of these new OH groups. This is also evidenced by the ^1H MAS NMR results shown in **Figure A13**. All samples showed a peak around 2.8 ppm, related to the hydrogen spillover on Si–O–Si of the support [47, 165]. Therefore, this further confirms the occurrence of hydrogen spillover. In addition, all samples showed a peak at 4.0 ppm assigned to the hydroxyls Si–OH group. Thus, the results further confirm that the interaction between H spillover and Si–O–Si groups leads to the formation of Si–OH group [47].

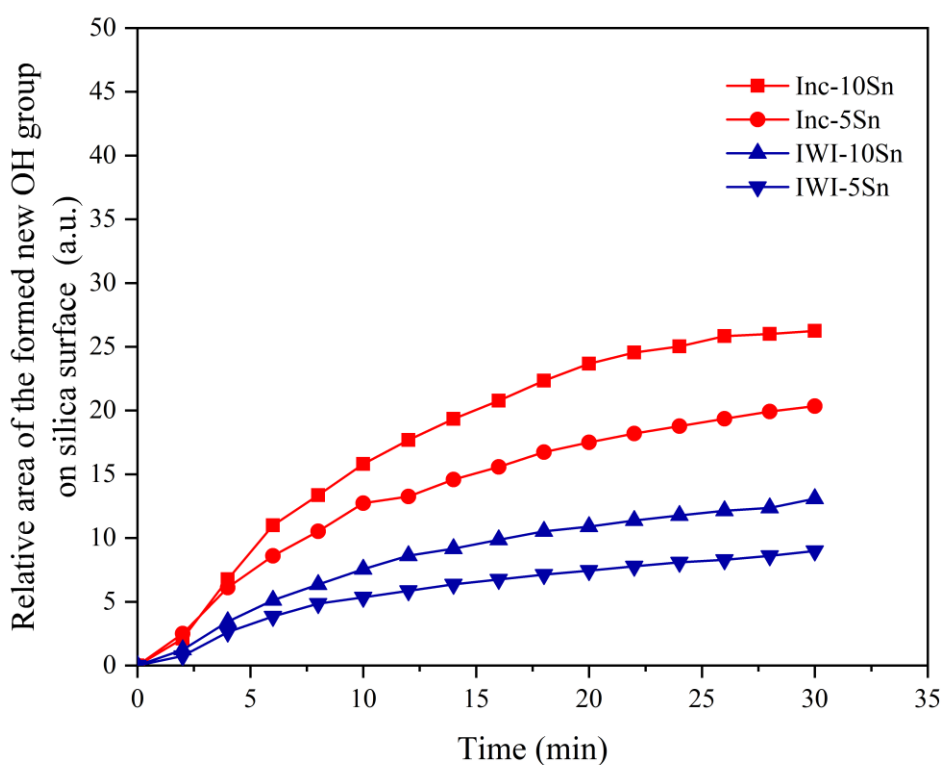


Figure 46 Relative area (IR band at 3200 cm^{-1}) of formation of new OH groups on silica surface over the SSP-supported Sn catalysts.

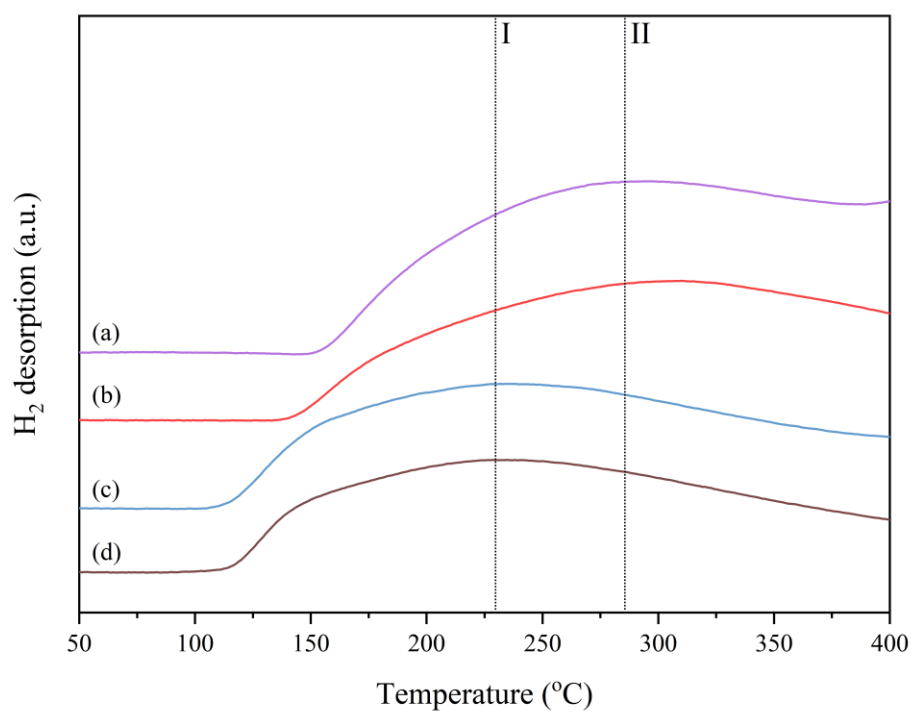


Figure 47 H₂-TPD profiles of SSP-supported Sn catalysts; IWI-10Sn (a), IWI-5Sn (b), Inc-10Sn (c), and Inc-5Sn (d).

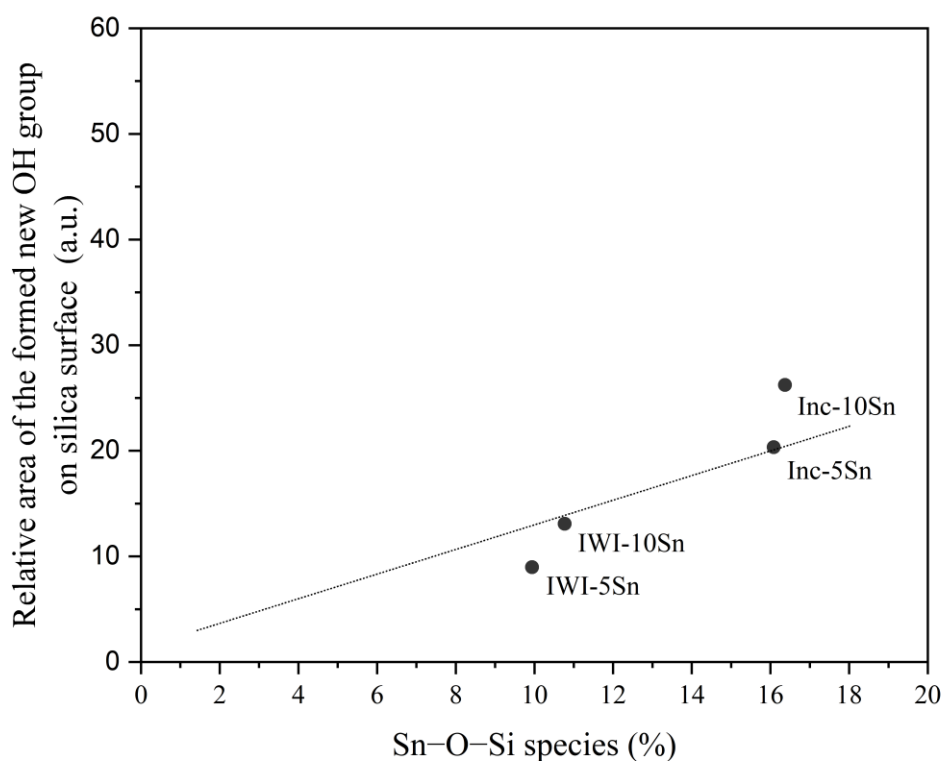


Figure 48 Correlation of the amount of Sn-O-Si species^[a] on the formation of new OH groups^[b] on silica surface over SSP-supported Sn catalysts. ^[a] XPS analysis, ^[b] Area of IR band 3200 cm⁻¹ at final

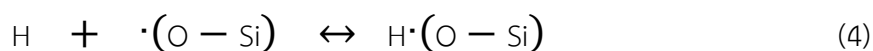
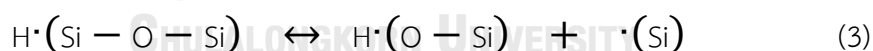
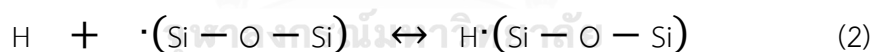
Table 5.7 Normalized relative area of XPS and ²⁹Si NMR analysis of SnO_x supported on SSP catalysts.

Sample	Relative area of XPS (%)			Relative area of ²⁹ Si NMR (%)		
	Sn-O-Si	SnII, IV	Sn0	Q2 line	Q3 line	Q4 line
IWI-5Sn	9.9	83.6	6.5	22.0	68.9	9.2
IWI-10Sn	10.8	82.3	6.9	18.4	66.5	15.1
Inc-5Sn	16.1	80.5	3.4	17.3	65.1	17.6
Inc-10Sn	16.4	79.8	3.9	16.8	64.7	18.5

5.4.4 Influence of Sn species on silica-supported Sn catalysts for the formation of new OH groups.

The Sn_{3d} XPS indicates that Sn–O–Si species mostly appeared in the incorporated catalysts (Inc-Sn). The results of ^{29}Si MAS NMR, O 1s XPS, and FT-IR further confirmed the existence of surface Sn–O–Si species on the catalysts. It is suggested that the incorporation of Sn species onto SSP leads to surface Sn–O–Si bonds due to the embedding of Sn species into the framework of SSP. The increased Sn contents on the incorporated catalysts (Inc-Sn) led to a decreased BET surface area. At the same time, the impregnated catalysts (IWI-Sn) presented various types of Sn species. High crystalline SnO_2 phase presence on impregnated catalysts (IWI-Sn) was confirmed by XRD and TEM results. Also, the polymeric Sn–O–Sn species were detected on these catalysts by UV–vis DRS results. However, those species were not detected on incorporated catalysts (Inc-Sn), indicating that the incorporation method induced the generation of Sn–O–Si species. Besides, the Sn–O–Si species increased with the increasing of Sn contents in both preparation methods. The formation of new OH groups on the silica surface correlates with the concentration of Sn–O–Si species as shown in **Figure 5.38**. This clearly indicates that the Sn–O–Si species on the catalyst surface play a key role in the new OH groups generation. The hydrogen surface behavior from H_2 TPD indicates that the molecular hydrogen can be dissociated on tin oxide to form H atoms via spillover onto SSP support. The newly generated OH groups indicate an electron-transfer process, between H and Si–O–Si, to produce charged adsorbed species reported by Wallin *et al.*[45] IN MANY CASES OF HYDROGEN SPILLOVER, THE FINAL STATE IS THE FORMATION OF NEW HYDROXY GROUPS, WHERE THE OXYGEN IONS CAN SERVE AS ACCEPTORS OF H ATOMS OR IONS [31]. Generally, the OH groups on the surface of silica-based catalysts can provide some information on nature (i.e. the acid strength) of hydroxyl groups, these species usually act as effective adsorptive/reactive sites for adsorbed substances[38-41]. Therefore, the formed OH groups also certainly affect the reaction pathway including the selectivity and activity. Qian *et al.*[47] reported that hydroxyl Si–OH groups were formed in CH_4 dry reforming reaction over Rh/MCF. The CH_4 was decomposed into CH_3^* and H^* , then H species adsorbed on bridged oxygen sites (Si–O–Si) of the support to form Si–OH groups, which can improve the rate of dry

reforming reaction[47]. When the process depends on this step (e.g. hydrogenation, dehydrogenation, reforming, and partial oxidation of methane to syngas), the reaction can be improved by the formed OH species[46, 47, 166-168]. The addition of noble metals, including Pt, Ru, Rh, and Ir, was used to modify the silica surface and the active centers [44-46, 48]. Dissociative adsorption of H₂ on the metal surface is followed by diffusion of H atoms to form new OH groups on the metal-silica interface. For SSP-supported Sn catalysts, tin oxide was embedded into the framework of SSP to produce surface Sn–O–Si bonds. In the hydrogen exposure, the dissociated H atoms adsorbed on the Si–O–Si species led to the formation of Si–OH groups, which agrees with previous reports [46, 169]. It is remarkable that incorporated catalysts (Inc-Sn) exhibited higher new OH groups production on the silica surface than impregnated catalysts (IWI-Sn), indicating a strong influence of Sn–O–Si species concentration of catalysts on the amount of new generated OH groups. In addition, this surface coverage of new OH groups increased with increasing Sn loading in both incorporated and impregnated catalysts. Therefore, the analytical results indicate that the newly generated OH groups appeared mostly on the silica surface surrounding the Sn–O–Si species. The proposed mechanism follows Eq. (1)-(4):[47]



where $\cdot(\text{Si} - \text{O} - \text{Si})$ and $\cdot(\text{O} - \text{Si})$ represent the support with different oxygen sites, while $\cdot(\text{Si})$ refers to the silica with oxygen vacancy sites, respectively. First, the adsorption/dissociation of molecular hydrogen occurs on the tin oxide species to form H atoms. After that hydrogen spillover occurs, in which the H atoms migrate to the catalyst surface. H atoms adsorb and react with Si–O–Si species leading to the formation of H \cdot (O – Si) species. This concept was summarized in **Figure 5.39**. atoms. The Sn–O–Si species were predominant on the incorporated catalysts (Inc-Sn), while the impregnated catalysts (IWI-Sn) presented various types of Sn species on the

support such as crystalline SnO_2 , polymeric Sn-O-Sn , and Sn-O-Si species. Additionally, the Sn-O-Si species increased with the increasing of Sn contents in all samples. After the pre-treatment, the catalysts were exposed to hydrogen. Then, the dissociated H atoms adsorbed on the Si-O-Si species, leading to the formation of Si-OH groups surrounding the Sn-O-Si species.

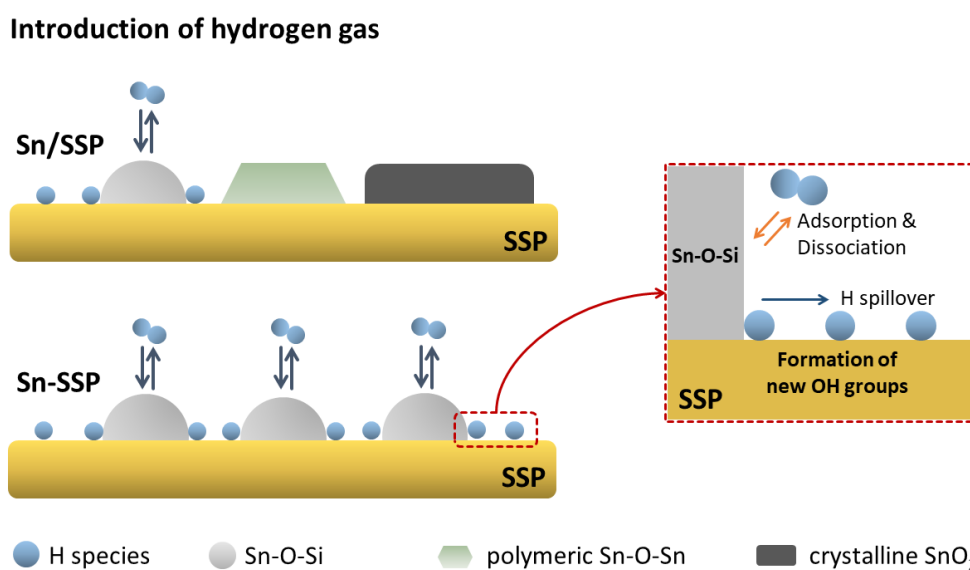


Figure 49 Summarized the formation of new OH groups on silica surface over SnO_x supported on SSP catalysts.

5.5 Model mechanism of hydrogen spillover on acidic properties

The effect of hydrogen spillover on acidic properties of silica-supported tungsten oxide catalysts was summarized in this section. As shown in **Figure 5.40**, molecular hydrogen is dissociated at oxygen vacancy and tungstate W^{5+} active species to form hydrogen spillover, in which it can migrate onto two parts on surface catalyst. Firstly, H atoms can spillover to adsorb surrounding the oxygen sites of catalysts (e.g., M-O-Si , Sn-O-Si , and O-Si species), leading to the formation of new Si-OH groups. Therefore, the *in situ* DRIFTS with hydrogen exposure experiments detected the increasing of Si-OH groups. However, this formed hydroxyl groups should provide a new Brønsted acid site. Secondly, H atoms can migrate to adsorb at Lewis acid sites, leading to the transformation of Lewis acid. The H atoms can release an electron to

Lewis acid, then it can lose its property and can desorb an NH_3 that is adsorbed on its sites. However, this NH_3 should be migrated to adsorb at new Brønsted acid sites or new hydroxyl groups, then Brønsted acid sites donate protons to form NH_4^+ . Therefore, the *in situ* DRIFTS with adsorbed ammonia experiments detected the increasing of NH_4^+ .

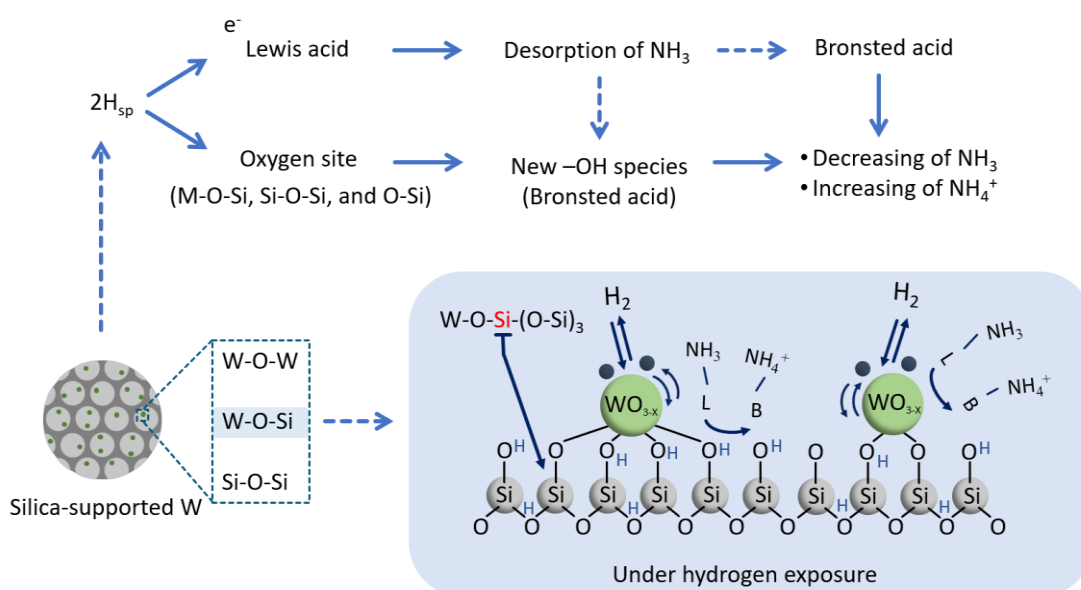


Figure 50 Model mechanism of hydrogen spillover on acidic properties of silica-supported tungsten oxide catalysts.

CHAPTER VI CONCLUSION AND RECOMMENDATION

6.1 Conclusions

The acidic property of silica-supported W catalysts was affected by hydrogen spillover. During the hydrogen exposure, molecular hydrogen can be dissociated to form hydrogen spillover onto surface catalysts. The results of *in situ* DRIFTS experiments have indicated that the Lewis acid site can be transformed to the Brønsted acid site upon hydrogen exposure of activated catalysts (i.e., W/HY-500, W/SiO₂, W/HY-15, W/MCM-22, W/Al₂O₃, W/SSP, and W-SSP). The Lewis acid transformation performance correlates with oxygen vacancy and tungstate W⁵⁺ active species. This active site could be generated by catalyst preparations and activating a process of H₂ and N₂ pretreatments. Additionally, the Si–OH species are formed, while the Si–O–W species are relatively decreased. It was postulated that the Si–O–W species is a major importance for adsorbed hydrogen, in which the atomic hydrogen can be adsorbed surrounding the Si–O–W species. Some atomic hydrogen should be adsorbed around the Lewis acid site of Si–O–W species leads to the Si–OH formation. Besides, this is agreeable on the other metal oxide that the Si–OH formation could be also occurred surrounding the Sn–O–Si species. During this process, molecular hydrogen is dissociated to form hydrogen spillover, in which it can migrate onto two parts on surface catalyst. Firstly, H atoms can spillover to adsorb surrounding the oxygen sites of catalysts (e.g., M–O–Si, Sn–O–Si, and O–Si species), leading to the formation of new Si–OH groups. Therefore, the *in situ* DRIFTS with hydrogen exposure experiments detected the increasing of Si–OH groups. However, this formed hydroxyl groups should provide a new Brønsted acid site. Secondly, H atoms can migrate to adsorb at Lewis acid sites, leading to the transformation of Lewis acid. The H atoms can release an electron to Lewis acid, then it can lose its property and can desorb an NH₃ that is adsorbed on its sites. However, this NH₃ should be migrated to adsorb at new Brønsted acid sites or new hydroxyl groups, then Brønsted acid sites donate protons to form NH₄⁺. Therefore, the *in situ* DRIFTS with adsorbed ammonia experiments detected the increasing of NH₄⁺.

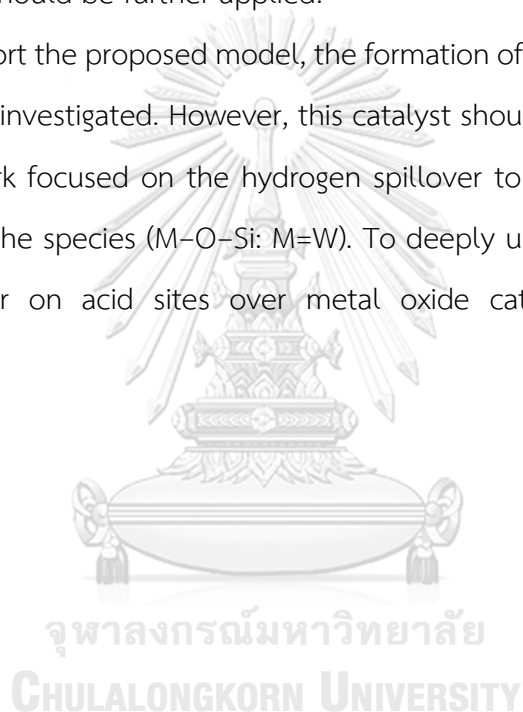
6.2 Recommendations

1) This work focused on the oxidation state of W and the interaction of metal-support catalysts for hydrogen spillover activation. However, its structure should be further studied to deeply understand.

2) The new species formation was mostly considered by in situ DRIFTS technique, which the results may contain some needed information. However, in situ characterizations should be further applied.

3) To support the proposed model, the formation of new OH groups over silica-supported Sn was investigated. However, this catalyst should be further studied.

4) This work focused on the hydrogen spillover to support and formation of acid sites around the species (M–O–Si: M=W). To deeply understanding, the effect of hydrogen spillover on acid sites over metal oxide catalysts should be further investigated.



APPENDIX A

Supporting information

A.1) Active Site Formation in WO_x Supported on Spherical Silica Catalysts for Lewis Acid Transformation to Brønsted Acid Activity**Table A1.** Textural properties for SSP-supported W catalysts.

Samples	Porous texture			Element ^[d] (at%)		
	$S_{\text{BET}}^{\text{[a]}}$ (m^2/g)	$V^{\text{[b]}}$ (cm^3/g)	$P^{\text{[c]}}$ (nm)	W	O	Si
W/SSP	848	0.52	2.4	1.46	61.58	36.96
W-SSP	820	0.56	2.7	1.56	62.69	35.79

^[a] Specific surface area

^[b] Total pore volume ($P/P_0 = 0.980$)

^[c] Average pore size

^[d] EDS elemental analysis

จุฬาลงกรณ์มหาวิทยาลัย
CHULALONGKORN UNIVERSITY

Table A2. Peak-fitting results of ^{29}Si NMR Spectra for SSP-supported W catalysts.

Samples	Peak area (%)			
	$\text{Si}-(\text{OH})_2(\text{O}-\text{Si})_2$	$\text{Si}-(\text{OH})(\text{O}-\text{Si})_3$	$\text{W}-\text{O}-\text{Si}-(\text{O}-\text{Si})_3$	$\text{Si}-(\text{O}-\text{Si})_4$
W/SSP	16.5	56.5	15.4	11.6
W-SSP	15.6	51.7	22.0	10.7

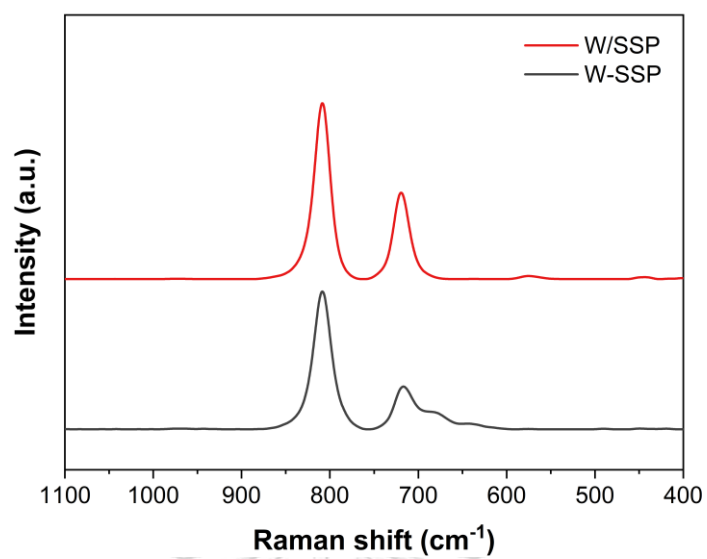


Figure A1. Raman spectra of SSP-supported W catalysts.

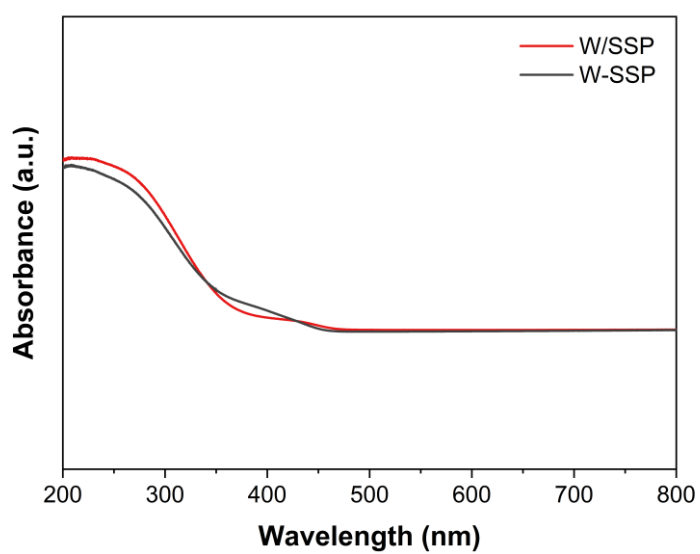


Figure A2. UV-vis DRS spectra of SSP-supported W catalysts.

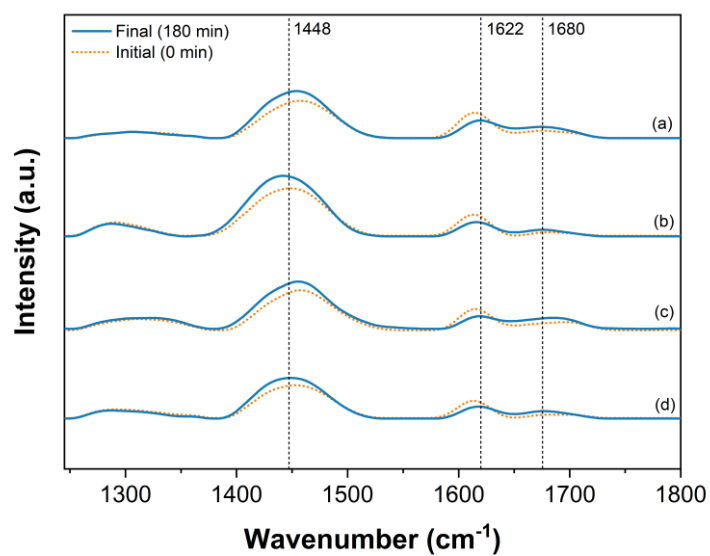


Figure A3. *In situ* DRIFTS spectra of adsorbed NH_3 upon hydrogen exposure at initial (orange line) and final (blue line) over catalysts; W-SSP- H_2 (a), W/SSP- H_2 (b), W-SSP- N_2 (c), and W/SSP- N_2 (d).

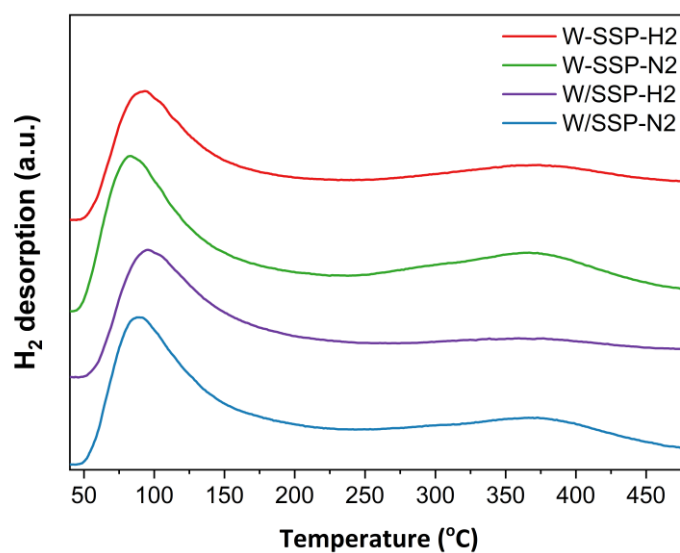


Figure A4. H_2 -TPD profiles of SSP-supported W catalysts with gas pretreatment.

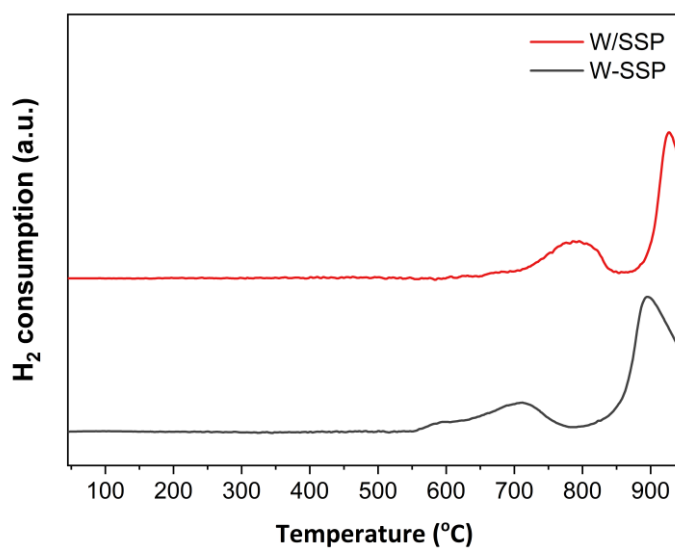


Figure A5. H₂-TPR profiles of SSP-supported W catalysts.

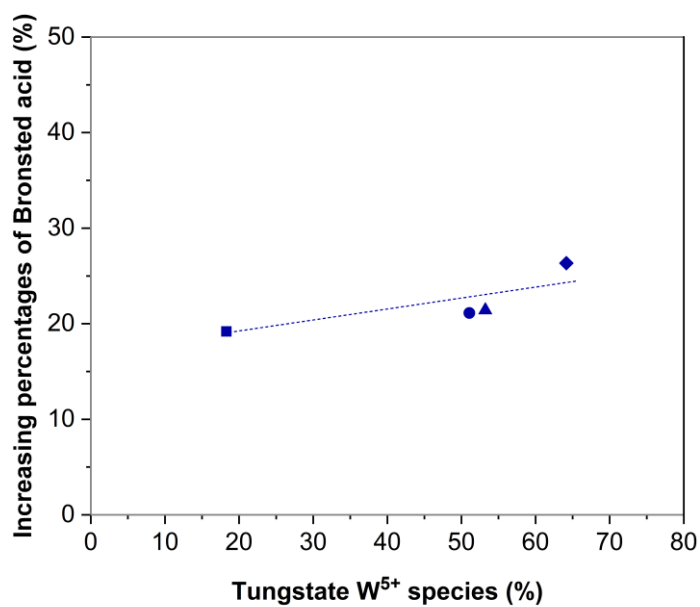


Figure A6. Correlation of increased Bronsted acid and tungstate W⁵⁺ species of SSP-supported W catalysts: W/SSP-N₂ (■), W-SSP-N₂ (●), W/SSP-H₂ (▲), W-SSP-H₂ (◆)

A.2) Influence of isolated tungstate sites on surface Si-OH formation with hydrogen-bonded clusters over spherical silica-supported WO_x catalysts

Table A3. Porous texture and element surface concentration of SSP-supported WO_x catalysts.

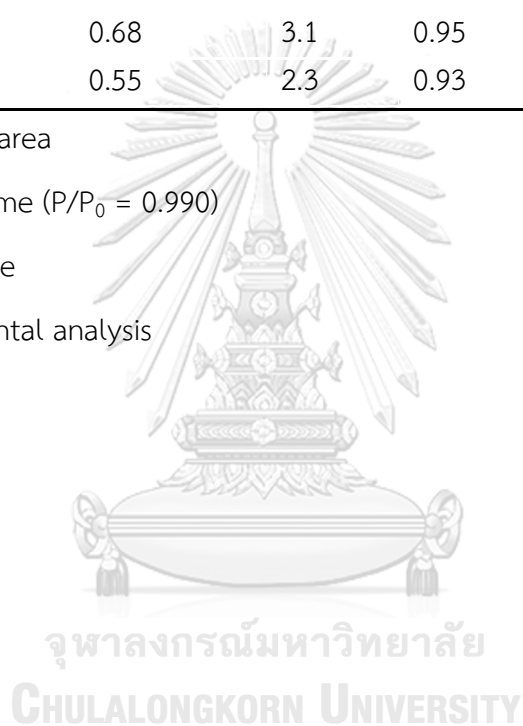
Sample	Porous texture			Element ^d		
	S _{BET} ^a (m ² /g)	V ^b (cm ³ /g)	P ^c (nm)	W (at%)	O (at%)	Si (at%)
4W-SSP	975	0.74	3.0	0.47	62.35	37.18
4W/SSP	942	0.61	2.6	0.43	57.96	41.62
8W-SSP	892	0.68	3.1	0.95	62.68	36.37
8W/SSP	944	0.55	2.3	0.93	58.20	40.87

^[a] Specific surface area

^[b] Total pore volume (P/P₀ = 0.990)

^[c] Average pore size

^[d] SEM-EDS elemental analysis



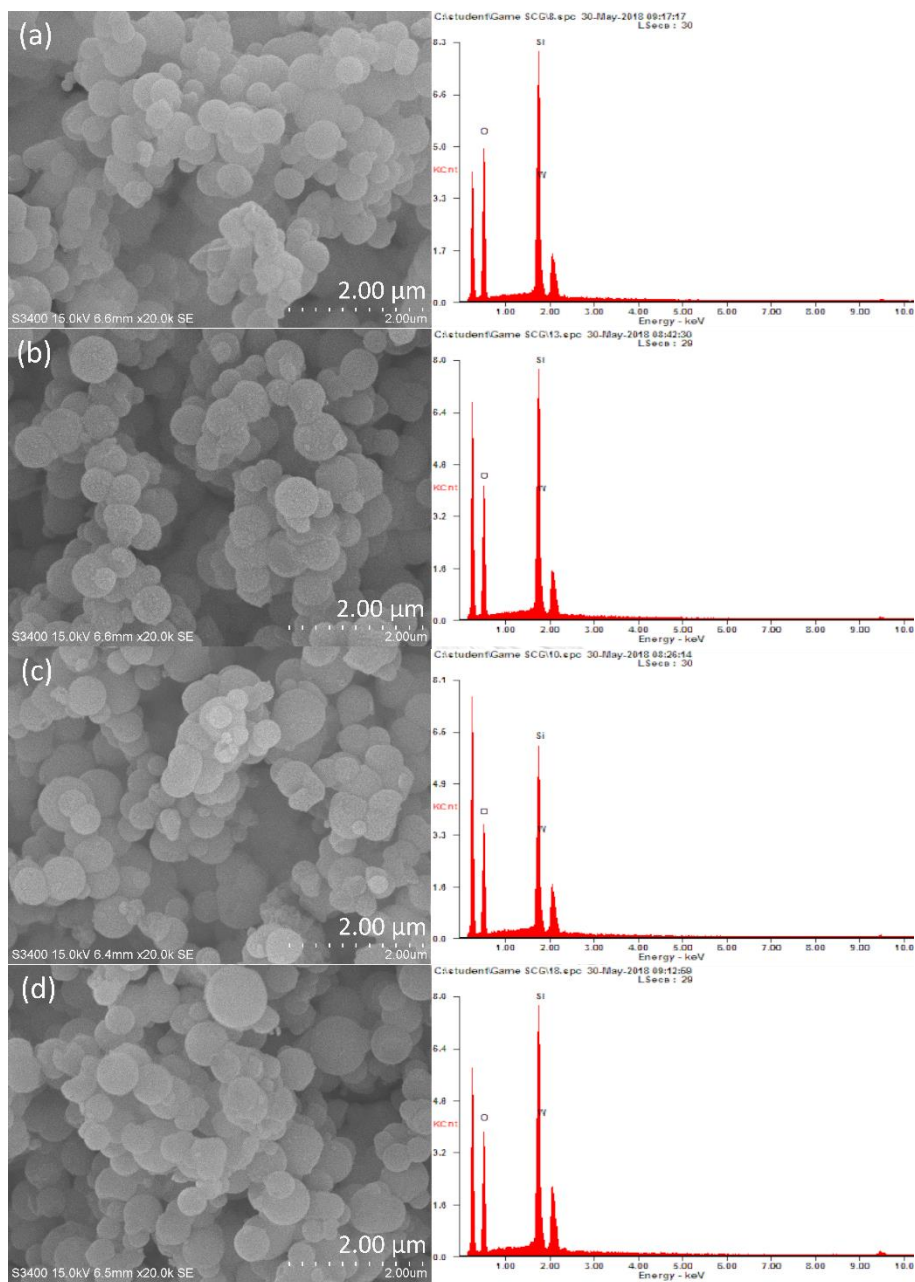


Figure A7. SEM image and SEM-EDS analysis of catalysts: 4W-SSP (a), 4W-SSP (b), 8W-SSP (c), 8W-SSP (d).

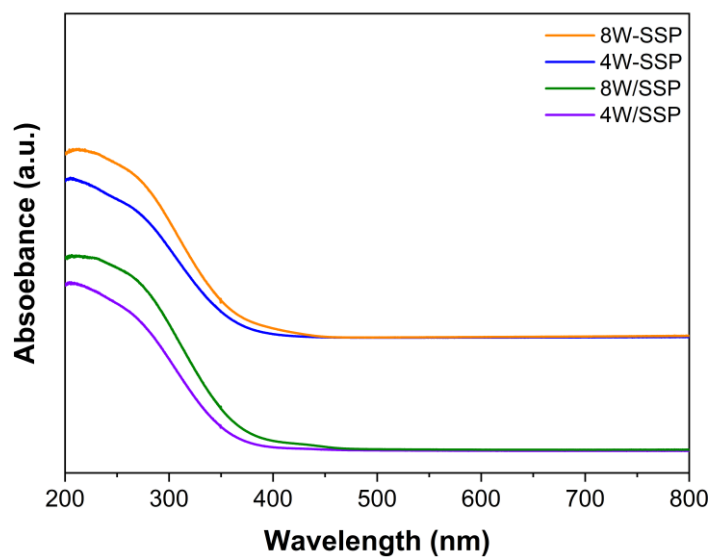


Figure A8. UV-vis spectra of SSP-supported WO_x catalysts.

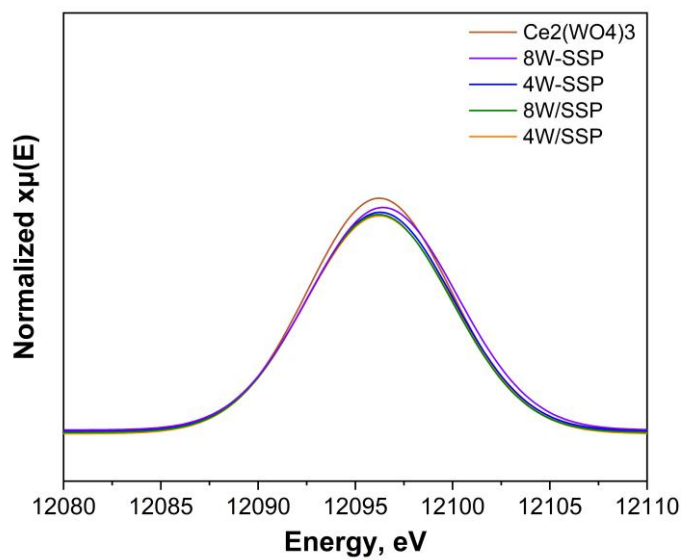


Figure A9. Fitting W L1 edge XANES pre-edge peaks of SSP-supported WO_x catalysts.

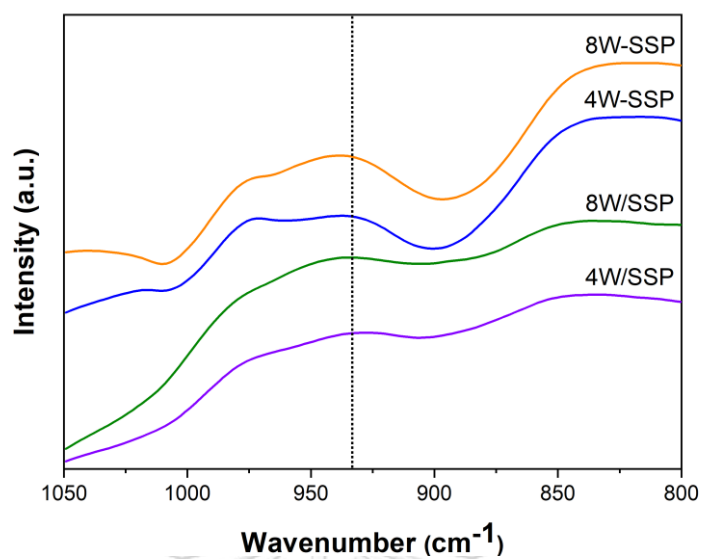


Figure A10. FT-IR spectra of SSP-supported WO_x catalysts.



A.3) Influence of surface Sn species and hydrogen interactions on the OH group formation over spherical silica-supported tin oxide catalysts.

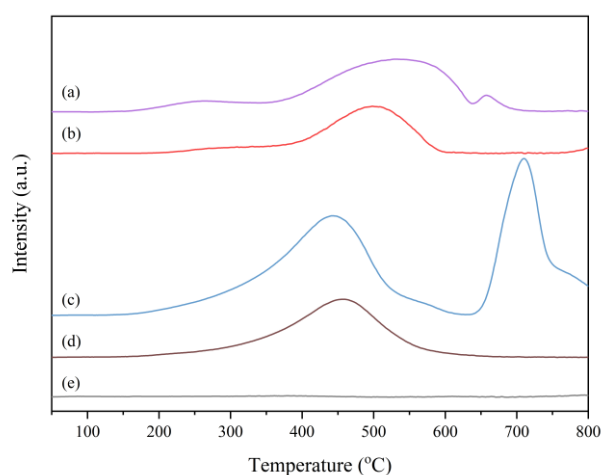


Figure A11. H₂-TPR profiles of SSP-supported Sn catalysts; IWI-10Sn (a), IWI-5Sn (b), Inc-10Sn (c), Inc-5Sn (d), SSP (e).

The reducibility of the SSP-supported Sn was investigated by the H₂-TPR as shown in Figure S1. In the temperature range studied (40-800 °C), all samples show the reduction peaks of Sn species on SSP support, excepting for the SSP support. There is no reduction peak below 800 °C on the SSP due to its nonreducible support property. In the low temperature range of 100-500 °C, there are two reduction peaks of Sn species on the impregnated catalysts (IWI-Sn) at around 250 °C and 480 °C, which is assigned to the reduction of small nano-sized SnO₂ species [149, 159]. Nevertheless, there are only one reduction peak of Sn species at around 440 °C on the incorporated catalysts (Inc-Sn) observed in the same temperature range of 100-500 °C. This indicates that the incorporation of Sn species into SSP are strongly interacted with support and are difficultly reduced to metallic Sn than those of the impregnated sample. In the high temperature range of 600-800 °C, the 10Sn/SSP and 10Sn-SSP show a high temperature reduction peak at around 640 and 725 °C, respectively, which is assigned to the reduction of crystalline SnO₂ [170]. These results indicate that the crystalline

SnO₂ species appear on high Sn content loading of IWI-10Sn and Inc-10Sn. The reduction peak of crystalline SnO₂ of Inc-10Sn is shifted to higher temperature than IWI-10Sn, indicating that Sn species are highly dispersed on catalyst surface Inc-Sn. These results are well consistent with the TEM and XRD results

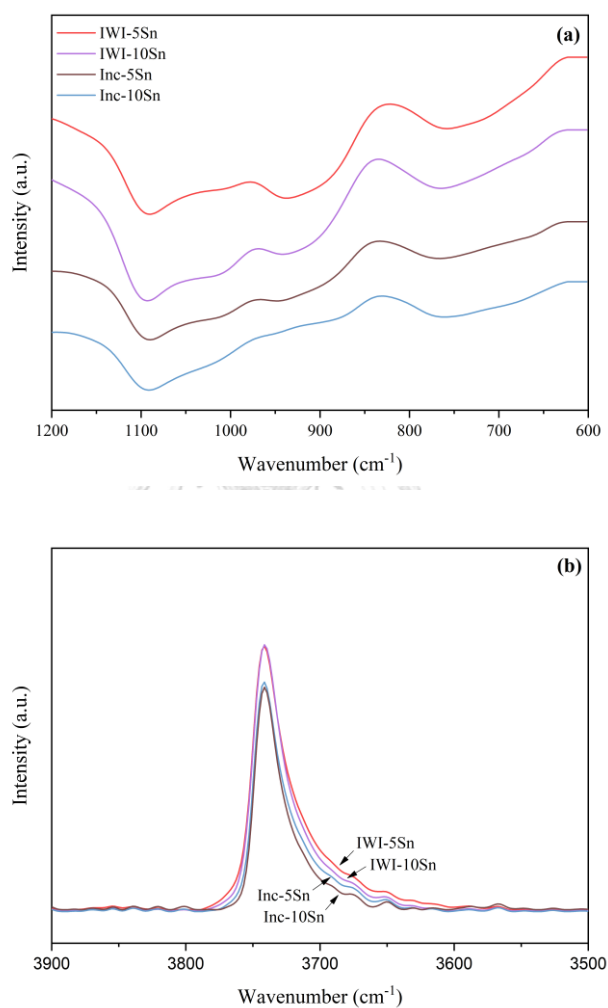


Figure A12. FT-IR spectra of SSP-supported Sn catalysts.

The FT-IR characterization was also used to analyze the existence of Sn species onto SSP framework as shown in Figure S2. The IR band at around 810 cm⁻¹, which is corresponded to the symmetric vibration modes of tetrahedral SiO₄ structure unit [171], can be obviously observed on all samples. In addition, all samples also show

the vibration peak at around 962 cm^{-1} corresponded to surface Sn–O–Si, suggesting the incorporation of Sn into the framework of pore walls in the silica support [153, 172]. The previous studies reported that the direct evidence for the isomorphous substitution could be observed on the IR band at around $950\text{--}970\text{ cm}^{-1}$ [173, 174]. Comparing the intensity of all IR bands, it was found that the incorporated catalysts (Inc-Sn) exhibit lower intensity of all bands than the impregnated catalysts (IWI-Sn) due to the partial destruction of the ordered mesoporous structure on the incorporating of Sn species onto SSP. Moreover, it was also found that the intensity was decreased with increasing Sn content in both catalysts.

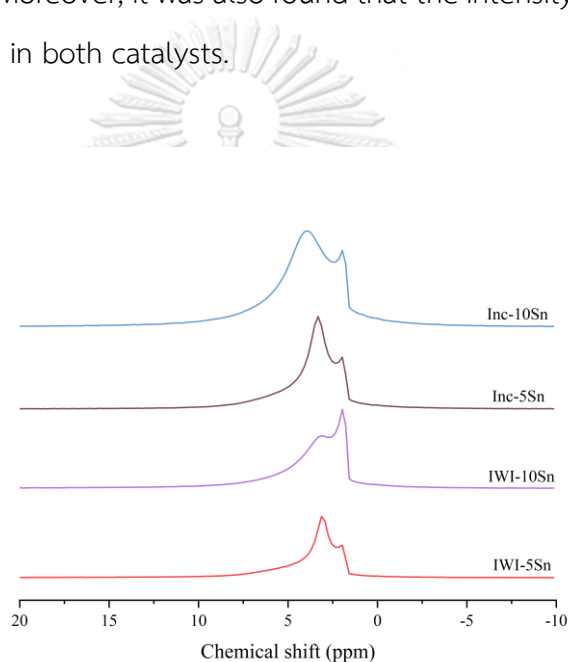


Figure A13. Solid state ^1H NMR spectra of SSP-supported Sn catalysts.

To obtain more information of the surface hydrogen on the SSP-supported Sn catalysts, the samples were investigated by ^1H MAS NMR as shown in Figure S3. Prior to investigation, the samples were pretreated with H_2/N_2 gas by the same step as done for the *in situ* DRIFTS experiments. The sharp signal at around 2.0 ppm was assigned to the terminal silanols on SiO_2 bulk and silica support appeared on all samples [175]. It is interesting that all samples exhibited the peak around 2.8 ppm, ascribing to the hydrogen spillover adsorbed on Si–O–Si of the support [47, 165]. Therefore, it is further confirmed that the hydrogen spillover from tin oxide onto SSP support was essentially

occurred. In addition, all samples also showed the peak at around 4.0 ppm, which ascribing to the hydroxyls Si-OH group. It is suggested that the further interaction between the adsorbed H species and Si-O-Si leads to the formation of Si-OH group [47]. The capacity of this peak was in the following order: Inc-10Sn > Inc-5Sn > IWI-10Sn > IWI-5Sn, which is well consistent with the *in situ* DRIFTS and H₂-TPD results.



APPENDIX B

List of Publications

- 1) Hydrogen activated WO_x -supported catalysts for Lewis acid transformation to Bronsted acid observed by *in situ* DRIFTS of adsorbed ammonia: Effect of different supports on the Lewis acid transformation, **Published in *Catalysis Today***
S. Boonpai, K. Suriye, B. Jongsomjit, J. Panpranot, P. Praserthdam, Catal. Today, 358 (2020) 370–386.
- 2) Active Site Formation in WO_x Supported on Spherical Silica Catalysts for Lewis Acid Transformation to Brønsted Acid Activity, **Published in *Journal of Physical Chemistry C***
S. Boonpai, S. Wannakao, J. Panpranot, B. Jongsomjit, P. Praserthdam, J. Phys. Chem. C, 124 (2020) 15935-15943.
- 3) Influence of surface Sn species and hydrogen interactions on the OH group formation over spherical silica-supported tin oxide catalysts, **Published in *Reaction Chemistry and Engineering***
S. Boonpai, S. Wannakao, K. Suriye, V. Márquez, J. Panpranot, B. Jongsomjit, P. Praserthdam, A.T. Bell, React. Chem. Eng., 5 (2020) 1814-1823.

REFERENCES



จุฬาลงกรณ์มหาวิทยาลัย
CHULALONGKORN UNIVERSITY

- [1] M. Sudhakar, V.V. Kumar, G. Naresh, M.L. Kantam, S.K. Bhargava, A. Venugopal, Vapor phase hydrogenation of aqueous levulinic acid over hydroxyapatite supported metal (M = Pd, Pt, Ru, Cu, Ni) catalysts, *Applied Catalysis B: Environmental*, 180 (2016) 113-120.
- [2] A. Romero, E. Alonso, Á. Sastre, A. Nieto-Márquez, Conversion of biomass into sorbitol: Cellulose hydrolysis on MCM-48 and d-Glucose hydrogenation on Ru/MCM-48, *Microporous Mesoporous Mater.*, 224 (2016) 1-8.
- [3] S. Kattel, B. Yan, J.G. Chen, P. Liu, CO₂ hydrogenation on Pt, Pt/SiO₂ and Pt/TiO₂: Importance of synergy between Pt and oxide support, *J. Catal.*, 343 (2016) 115-126.
- [4] J. Jia, C. Qian, Y. Dong, Y.F. Li, H. Wang, M. Ghoussoub, K.T. Butler, A. Walsh, G.A. Ozin, Heterogeneous catalytic hydrogenation of CO₂ by metal oxides: defect engineering - perfecting imperfection, *Chem. Soc. Rev.*, 46 (2017) 4631-4644.
- [5] Á. Prekob, V. Hajdu, G. Muránszky, B. Fiser, A. Sycheva, T. Ferenczi, B. Viskolcz, L. Vanyorek, Application of carbonized cellulose-based catalyst in nitrobenzene hydrogenation, *Materials Today Chemistry*, 17 (2020).
- [6] E.R. Mawarnis, A.A. Umar, Fibrous bimetallic silver palladium and ruthenium palladium nanocrystals exhibit an exceptionally high active catalytic process in acetone hydrogenation, *Materials Today Chemistry*, 14 (2019).
- [7] X. Kong, Y. Gong, S. Mao, Y. Wang, Selective Hydrogenation of Phenol, *ChemNanoMat*, 4 (2018) 432-450.
- [8] K. Yan, J. Liao, X. Wu, X. Xie, A noble-metal free Cu-catalyst derived from hydrotalcite for highly efficient hydrogenation of biomass-derived furfural and levulinic acid, *RSC Advances*, 3 (2013).
- [9] S.D. Senanayake, P.J. Ramirez, I. Waluyo, S. Kundu, K. Mudiyansele, Z. Liu, Z. Liu, S. Axnanda, D.J. Stacchiola, J. Evans, J.A. Rodriguez, Hydrogenation of CO₂ to Methanol on CeO_x/Cu(111) and ZnO/Cu(111) Catalysts: Role of the Metal–Oxide Interface and Importance of Ce³⁺ Sites, *The Journal of Physical Chemistry C*, 120 (2016) 1778-1784.
- [10] F.A. Westerhaus, R.V. Jagadeesh, G. Wienhofer, M.M. Pohl, J. Radnik, A.E. Surkus, J. Rabeah, K. Junge, H. Junge, M. Nielsen, A. Bruckner, M. Beller, Heterogenized cobalt

- oxide catalysts for nitroarene reduction by pyrolysis of molecularly defined complexes, *Nat Chem*, 5 (2013) 537-543.
- [11] R.M. Bullock, Abundant metals give precious hydrogenation performance, *Science*, 342 (2013) 1054-1055.
- [12] S. Zhang, D.F. Consoli, S.K. Shaikh, Y. Román-Leshkov, Effects of WO₃ nanoparticle size on ethylene-butene metathesis activity, *Applied Catalysis A: General*, 580 (2019) 53-58.
- [13] L. Zhang, H. Wang, J. Liu, Q. Zhang, H. Yan, Nonstoichiometric tungsten oxide: structure, synthesis, and applications, *Journal of Materials Science: Materials in Electronics*, 31 (2019) 861-873.
- [14] K. Gayapan, S. Sripinun, J. Panpranot, P. Praserttham, S. Assabumrungrat, Effects of calcination and pretreatment temperatures on the catalytic activity and stability of H₂-treated WO₃/SiO₂ catalysts in metathesis of ethylene and 2-butene, *RSC Advances*, 8 (2018) 28555-28568.
- [15] Q. Wang, A. Puntambekar, V. Chakrapani, Vacancy-Induced Semiconductor-Insulator-Metal Transitions in Nonstoichiometric Nickel and Tungsten Oxides, *Nano Lett.*, 16 (2016) 7067-7077.
- [16] Z.F. Huang, J. Song, L. Pan, X. Zhang, L. Wang, J.J. Zou, Tungsten Oxides for Photocatalysis, Electrochemistry, and Phototherapy, *Adv. Mater.*, 27 (2015) 5309-5327.
- [17] W.-L. Dai, J. Ding, Q. Zhu, R. Gao, X. Yang, Tungsten containing materials as heterogeneous catalysts for green catalytic oxidation process, *Catalysis2016*, pp. 1-27.
- [18] M. Kaur, S. Sharma, P.M.S. Bedi, Silica supported Brønsted acids as catalyst in organic transformations: A comprehensive review, *Chinese Journal of Catalysis*, 36 (2015) 520-549.
- [19] P. Gupta, S. Paul, Solid acids: Green alternatives for acid catalysis, *Catal. Today*, 236 (2014) 153-170.
- [20] X.Y. Chen, G. Clet, K. Thomas, M. Houalla, Correlation between structure, acidity and catalytic performance of WO_x/Al₂O₃ catalysts, *J. Catal.*, 273 (2010) 236-244.

- [21] S. Watmanee, K. Suriye, P. Praserttham, J. Panpranot, Formation of isolated tungstate sites on hierarchical structured SiO₂- and HY zeolite-supported WO_x catalysts for propene metathesis, *J. Catal.*, 376 (2019) 150-160.
- [22] D. Kiani, S. Sourav, J. Baltrusaitis, I.E. Wachs, Oxidative coupling of methane (OCM) by SiO₂-supported tungsten oxide catalysts promoted with Mn and Na, *ACS Catalysis*, 9 (2019) 5912-5928.
- [23] S. Boonpai, K. Suriye, B. Jongsomjit, J. Panpranot, P. Praserttham, Hydrogen activated WO_x-supported catalysts for Lewis acid transformation to Bronsted acid observed by in situ DRIFTS of adsorbed ammonia: Effect of different supports on the Lewis acid transformation, *Catal. Today*, (2019).
- [24] S. Sarish, B.M. Devassy, W. Bohringer, J. Fletcher, S.B. Halligudi, Liquid-phase alkylation of phenol with long-chain olefins over WO_x/ZrO₂ solid acid catalysts, *Journal of Molecular Catalysis a-Chemical*, 240 (2005) 123-131.
- [25] S. Watmanee, K. Suriye, P. Praserttham, J.J.T.i.C. Panpranot, Effect of Surface Tungstate W 5+ Species on the Metathesis Activity of W-Doped Spherical Silica Catalysts, 61 (2018) 1615-1623.
- [26] M. Scheithauer, T.K. Cheung, R.E. Jentoft, R.K. Grasselli, B.C. Gates, H. Knozinger, Characterization of WO_x/ZrO₂ by vibrational spectroscopy and n-pentane isomerization catalysis, *J. Catal.*, 180 (1998) 1-13.
- [27] R. Ladera, E. Finocchio, S. Rojas, G. Busca, J.L.G. Fierro, M. Ojeda, Supported WO_x-based catalysts for methanol dehydration to dimethyl ether, *Fuel*, 113 (2013) 1-9.
- [28] A. Corma, Inorganic Solid Acids and Their Use in Acid-Catalyzed Hydrocarbon Reactions, *Chem. Rev.*, 95 (1995) 559-614.
- [29] S.J. Huang, S.L. Liu, W.J. Xin, J. Bai, S.J. Xie, Q.X. Wang, L.Y. Xu, Metathesis of ethene and 2-butene to propene on W/Al₂O₃-HY catalysts with different HY contents, *Journal of Molecular Catalysis a-Chemical*, 226 (2005) 61-68.
- [30] J. Song, Z.-F. Huang, L. Pan, J.-J. Zou, X. Zhang, L.J.A.c. Wang, Oxygen-deficient tungsten oxide as versatile and efficient hydrogenation catalyst, 5 (2015) 6594-6599.
- [31] V.V. Rozanov, O.V. Krylov, Hydrogen spillover in heterogeneous catalysis, *Russian chemical reviews*, 66 (1997) 107.

- [32] W.C. Conner, J.L. Falconer, Spillover in Heterogeneous Catalysis, *Chem. Rev.*, 95 (1995) 759-788.
- [33] S.J.T.J.o.P.C. Khoobiar, Particle to particle migration of hydrogen atoms on platinum—alumina catalysts from particle to neighboring particles, 68 (1964) 411-412.
- [34] J. Sinfelt, P. Lucchesi, Kinetic evidence for the migration of reactive intermediates in surface catalysis, *J. Am. Chem. Soc.*, 85 (1963) 3365-3367.
- [35] T. Huizinga, R.J.T.J.o.P.C. Prins, Behavior of titanium (3+) centers in the low-and high-temperature reduction of platinum/titanium dioxide, studied by ESR, 85 (1981) 2156-2158.
- [36] R. Prins, Hydrogen Spillover. Facts and Fiction, *Chem. Rev.*, 112 (2012) 2714-2738.
- [37] W. Karim, C. Spreafico, A. Kleibert, J. Gobrecht, J. VandeVondele, Y. Ekinci, J.A. van Bokhoven, Catalyst support effects on hydrogen spillover, *Nature*, 541 (2017) 68-+.
- [38] M.B. Yue, L.B. Sun, Y. Cao, Z.J. Wang, Y. Wang, Q. Yu, J.H. Zhu, Promoting the CO₂ adsorption in the amine-containing SBA-15 by hydroxyl group, *Microporous Mesoporous Mater.*, 114 (2008) 74-81.
- [39] R. van Grieken, G. Calleja, D. Serrano, C. Martos, A. Melgares, I. Suarez, The Role of the Hydroxyl Groups on the Silica Surface When Supporting Metallocene/MAO Catalysts, *Polym. React. Eng.*, 11 (2007) 17-32.
- [40] Y. Inaki, H. Yoshida, T. Yoshida, T. Hattori, Active sites on mesoporous and amorphous silica materials and their photocatalytic activity: an investigation by FTIR, ESR, VUV- UV and photoluminescence spectroscopies, *The Journal of Physical Chemistry B*, 106 (2002) 9098-9106.
- [41] M.L. Hair, Hydroxyl groups on silica surface, *J. Non-Cryst. Solids*, 19 (1975) 299-309.
- [42] L. Zhuravlev, Concentration of hydroxyl groups on the surface of amorphous silicas, *Langmuir*, 3 (1987) 316-318.
- [43] R. Singh, N. Bayal, A. Maity, D.J. Pradeep, J. Trébosc, P.K. Madhu, O. Lafon, V. Polshettiwar, Probing the Interfaces in Nanosilica-Supported TiO₂ Photocatalysts by Solid-State NMR and In Situ FTIR, *ChemNanoMat*, 4 (2018) 1231-1239.

- [44] T. Miyao, A. Yoshida, H. Yamada, S. Naito, Mechanistic study of hydrogen occlusion in hollow silica nano-spheres encapsulating iridium metal clusters, *J. Mol. Catal. A: Chem.*, 378 (2013) 174-178.
- [45] M. Wallin, H. Grönbeck, A.L. Spetz, M. Eriksson, M. Skoglundh, Vibrational analysis of H₂ and D₂ adsorption on Pt/SiO₂, *The Journal of Physical Chemistry B*, 109 (2005) 9581-9588.
- [46] T. Wu, D. Lin, Y. Wu, X. Zhou, Q. Yan, W. Weng, H. Wan, In-situ FT-IR investigation of partial oxidation of methane to syngas over Rh/SiO₂ catalyst, *Journal of Natural Gas Chemistry*, 16 (2007) 316-321.
- [47] L. Qian, W. Cai, L. Zhang, L. Ye, J. Li, M. Tang, B. Yue, H. He, The promotion effect of hydrogen spillover on CH₄ reforming with CO₂ over Rh/MCF catalysts, *Applied Catalysis B: Environmental*, 164 (2015) 168-175.
- [48] H. Shen, X. Wu, D. Jiang, X. Li, J. Ni, Identification of active sites for hydrogenation over Ru/SBA-15 using in situ Fourier-transform infrared spectroscopy, *Chinese Journal of Catalysis*, 38 (2017) 1597-1602.
- [49] K. Ebitani, J. Konishi, H.J.J.o.C. Hattori, Skeletal isomerization of hydrocarbons over zirconium oxide promoted by platinum and sulfate ion, 130 (1991) 257-267.
- [50] K. Ebitani, J. Tsuji, H. Hattori, H.J.J.o.C. Kita, Dynamic modification of surface acid properties with hydrogen molecule for zirconium oxide promoted by platinum and sulfate ions, 135 (1992) 609-617.
- [51] N. Satoh, J. Hayashi, H. Hattori, Kinetic study of hydrogen adsorption on sulfated zirconia-supported platinum, *Applied Catalysis a-General*, 202 (2000) 207-213.
- [52] H. Hattori, T.J.C.S.f.A. Shishido, Molecular hydrogen-originated protonic acid site as active site on solid acid catalyst, 1 (1997) 205-213.
- [53] R. Ueda, T. Kusakari, K. Tomishige, K. Fujimoto, Nature of spilt-over hydrogen on acid sites in zeolites: Observation of the behavior of adsorbed pyridine on zeolite catalysts by means of FTIR, *J. Catal.*, 194 (2000) 14-22.
- [54] A. Guntida, K. Suriye, J. Panpranot, P.J.T.i.C. Praserttham, Comparative Study of Lewis Acid Transformation on Non-reducible and Reducible Oxides Under Hydrogen Atmosphere by In Situ DRIFTS of Adsorbed NH₃, (2018) 1-12.

- [55] C.H. Kline, V.J.I. Kollonitsch, E. Chemistry, CATALYTIC ACTIVITY OF TUNGSTEN. II, 57 (1965) 53-60.
- [56] D.G. Barton, S.L. Soled, E. Iglesia, Solid acid catalysts based on supported tungsten oxides, *Top. Catal.*, 6 (1998) 87-99.
- [57] M.I. Zaki, N.E. Fouad, S.A.A. Mansour, A.I. Muftah, Temperature-programmed and X-ray diffractometry studies of hydrogen-reduction course and products of WO₃ powder: Influence of reduction parameters, *Thermochim. Acta*, 523 (2011) 90-96.
- [58] S.J. Choung, S.W.J.I. Weller, E.C.P. Design, Development, Oxygen chemisorption and olefin disproportionation activity of tungsten oxide/silica, 22 (1983) 662-665.
- [59] R. Westhoff, J.J.J.o.C. Moulijn, Reduction and activity of the metathesis catalyst WO₃/SiO₂, 46 (1977) 414-416.
- [60] D.J. Moodley, The metathesis activity and deactivation of heterogeneous metal oxide catalytic systems, North-West University, 2003.
- [61] J.C. Mol, P.W.J.H.o.H.C.O. van Leeuwen, Metathesis of alkenes, (2008) 3240-3256.
- [62] S.J. Huang, S.L. Liu, Q.J. Zhu, X.X. Zhu, W.J. Xin, H.J. Liu, Z.C. Feng, C. Li, S.J. Xie, Q.X. Wang, L.Y. Xu, The effect of calcination time on the activity of WO₃/Al₂O₃/HY catalysts for the metathesis reaction between ethene and 2-butene, *Applied Catalysis a-General*, 323 (2007) 94-103.
- [63] E.L. Lee, I.E. Wachs, In situ Raman spectroscopy of SiO₂-supported transition metal oxide catalysts: An isotopic O-18-O-16 exchange study, *Journal of Physical Chemistry C*, 112 (2008) 6487-6498.
- [64] E.I. Ross-Medgaarden, I.E. Wachs, Structural determination of bulk and surface tungsten oxides with UV-vis diffuse reflectance spectroscopy and Raman spectroscopy, *Journal of Physical Chemistry C*, 111 (2007) 15089-15099.
- [65] S. Lwin, I.E. Wachs, Olefin Metathesis by Supported Metal Oxide Catalysts, *Acs Catalysis*, 4 (2014) 2505-2520.
- [66] X.L. Yang, W.L. Dai, R.H. Gao, K.N. Fan, Characterization and catalytic behavior of highly active tungsten-doped SBA-15 catalyst in the synthesis of glutaraldehyde using an anhydrous approach, *J. Catal.*, 249 (2007) 278-288.
- [67] R.H. Bliss, B.F.J.I. Dodge, E. Chemistry, Vapor-Phase Hydration of Ethylene, 29 (1937) 19-25.

- [68] B. Scheffer, P. Molhoek, J.J.A.c. Moulijn, Temperature-programmed reduction of NiO_WO₃/Al₂O₃ hydrodesulphurization catalysts, 46 (1989) 11-30.
- [69] V.M. Benitez, N.S. Figoli, About the importance of surface W species in WO_x/Al₂O₃ during n-butene skeletal isomerization, Catal. Commun., 3 (2002) 487-492.
- [70] M. Suvanto, J. Raty, T.A. Pakkanen, Catalytic activity of carbonyl precursor based W/Al₂O₃ and CoW/Al₂O₃ catalysts in hydrodesulfurization of thiophene, Applied Catalysis a-General, 181 (1999) 189-199.
- [71] J.C. Reyes, M. Avalosborja, R.L. Cordero, A.L. Agudo, Influence of Phosphorus on the Structure and the Hydrodesulfurization and Hydrodenitrogenation Activity of W/Al₂O₃ Catalysts, Applied Catalysis a-General, 120 (1994) 147-162.
- [72] S.H. Zhu, X.Q. Gao, Y.L. Zhu, Y.W. Li, Promoting effect of WO, on selective hydrogenolysis of glycerol to 1,3-propanediol over bifunctional Pt-WO_x/Al₂O₃ catalysts, Journal of Molecular Catalysis a-Chemical, 398 (2015) 391-398.
- [73] B.H. Cooper, B.B.L. Donnis, Aromatic saturation of distillates: An overview, Applied Catalysis a-General, 137 (1996) 203-223.
- [74] E. Furimsky, F.E. Massoth, Deactivation of hydroprocessing catalysts, Catal. Today, 52 (1999) 381-495.
- [75] C.S. Song, Designing sulfur-resistant, noble-metal hydrotreating catalysts, Chem. Tech., 29 (1999) 26-30.
- [76] A. Stanislaus, B.H. Cooper, Aromatic Hydrogenation Catalysis - a Review, Catalysis Reviews-Science and Engineering, 36 (1994) 75-123.
- [77] L.J. Hu, G.F. Xia, L.L. Qu, C. Li, Q. Xin, D.D. Li, Strong effect of transitional metals on the sulfur resistance of Pd/HY-Al₂O₃ catalysts for aromatic hydrogenation, Journal of Molecular Catalysis a-Chemical, 171 (2001) 169-179.
- [78] M.A. Asensi, A. Corma, A. Martinez, Skeletal isomerization of 1-butene on MCM-22 zeolite catalyst, J. Catal., 158 (1996) 561-569.
- [79] D. Nuntasri, P. Wu, T. Tatsumi, High selectivity of MCM-22 for cyclopentanol formation in liquid-phase cyclopentene hydration, J. Catal., 213 (2003) 272-280.

- [80] S.L. Liu, X.J. Li, W.J. Xin, S.J. Xie, P. Zeng, L.X. Zhang, L.Y. Xu, Cross metathesis of butene-2 and ethene to propene over Mo/MCM-22-Al₂O₃ catalysts with different Al₂O₃ contents, *Journal of Natural Gas Chemistry*, 19 (2010) 482-486.
- [81] S. Watmanee, K. Suriye, P. Prasertdam, J. Panpranot, Effect of Surface Tungstate W₅₊ Species on the Metathesis Activity of W-Doped Spherical Silica Catalysts, *Top. Catal.*, 61 (2018) 1615-1623.
- [82] S. Huang, S. Liu, W. Xin, J. Bai, S. Xie, Q. Wang, L. Xu, Metathesis of ethene and 2-butene to propene on W/Al₂O₃-HY catalysts with different HY contents, *J. Mol. Catal. A: Chem.*, 226 (2005) 61-68.
- [83] K. Gayapan, S. Sripinun, J. Panpranot, P. Prasertdam, S. Assabumrungrat, Effect of pretreatment atmosphere of WO_x/SiO₂ catalysts on metathesis of ethylene and 2-butene to propylene, *RSC Advances*, 8 (2018) 11693-11704.
- [84] V. Logie, G. Maire, D. Michel, J.-L. Vignes, Skeletal isomerization of hexenes on tungsten oxide supported on porous α -alumina, *J. Catal.*, 188 (1999) 90-101.
- [85] J. Yori, C. Vera, J. Parera, n-butane isomerization on tungsten oxide supported on zirconia, *Applied Catalysis A: General*, 163 (1997) 165-175.
- [86] V. Benitez, N. Figoli, About the importance of surface W species in WO_x/Al₂O₃ during n-butene skeletal isomerization, *Catal. Commun.*, 3 (2002) 487-492.
- [87] H. Liu, L. Zhang, X. Li, S. Huang, S. Liu, W. Xin, S. Xie, L. Xu, Production of propene from 1-butene metathesis reaction on tungsten based heterogeneous catalysts, *Journal of Natural Gas Chemistry*, 18 (2009) 331-336.
- [88] S. Maksasithorn, P. Prasertdam, K. Suriye, M. Devillers, D.P. Debecker, WO₃-based catalysts prepared by non-hydrolytic sol-gel for the production of propene by cross-metathesis of ethene and 2-butene, *Applied Catalysis A: General*, 488 (2014) 200-207.
- [89] S. Zhu, X. Gao, Y. Zhu, J. Cui, H. Zheng, Y. Li, SiO₂ promoted Pt/WO_x/ZrO₂ catalysts for the selective hydrogenolysis of glycerol to 1, 3-propanediol, *Applied Catalysis B: Environmental*, 158 (2014) 391-399.

- [90] N. Liu, S. Ding, Y. Cui, N. Xue, L. Peng, X. Guo, W. Ding, Optimizing activity of tungsten oxides for 1-butene metathesis by depositing silica on γ -alumina support, *Chem. Eng. Res. Des.*, 91 (2013) 573-580.
- [91] Q. Zhao, S.-L. Chen, J. Gao, C. Xu, Effect of tungsten oxide loading on metathesis activity of ethene and 2-butene over WO_3/SiO_2 catalysts, *Transition Met. Chem.*, 34 (2009) 621-627.
- [92] X.-L. Yang, R. Gao, W.-L. Dai, K. Fan, Influence of tungsten precursors on the structure and catalytic properties of $WO_3/SBA-15$ in the selective oxidation of cyclopentene to glutaraldehyde, *The Journal of Physical Chemistry C*, 112 (2008) 3819-3826.
- [93] L. Wang, Y. Wang, Y. Cheng, Z. Liu, Q. Guo, M.N. Ha, Z. Zhao, Hydrogen-treated mesoporous WO_3 as a reducing agent of CO_2 to fuels (CH_4 and CH_3OH) with enhanced photothermal catalytic performance, *Journal of Materials Chemistry A*, 4 (2016) 5314-5322.
- [94] X.-L. Yang, W.-L. Dai, R. Gao, K. Fan, Characterization and catalytic behavior of highly active tungsten-doped SBA-15 catalyst in the synthesis of glutaraldehyde using an anhydrous approach, *J. Catal.*, 249 (2007) 278-288.
- [95] P. Biloen, G. Pott, X-ray photoelectron spectroscopy study of supported tungsten oxide, *J. Catal.*, 30 (1973) 169-174.
- [96] H. Liu, K. Tao, H. Yu, C. Zhou, Z. Ma, D. Mao, S. Zhou, Effect of pretreatment gases on the performance of WO_3/SiO_2 catalysts in the metathesis of 1-butene and ethene to propene, *Comptes Rendus Chimie*, 18 (2015) 644-653.
- [97] A. Shpak, A. Korduban, M. Medvedskij, V. Kandyba, XPS studies of active elements surface of gas sensors based on WO_3-x nanoparticles, *J. Electron. Spectrosc. Relat. Phenom.*, 156 (2007) 172-175.
- [98] M. Seifollahi Bazarjani, M. Hojamberdiev, K. Morita, G. Zhu, G. Cherkashinin, C. Fasel, T. Herrmann, H. Breitzke, A. Gurlo, R. Riedel, Visible light photocatalysis with $c-WO_3-x/WO_3 \cdot xH_2O$ nanoheterostructures in situ formed in mesoporous polycarbosilane-siloxane polymer, *J. Am. Chem. Soc.*, 135 (2013) 4467-4475.

- [99] J. Song, Z.-F. Huang, L. Pan, J.-J. Zou, X. Zhang, L. Wang, Oxygen-Deficient Tungsten Oxide as Versatile and Efficient Hydrogenation Catalyst, *ACS Catalysis*, 5 (2015) 6594-6599.
- [100] O.Y. Khyzhun, XPS, XES and XAS studies of the electronic structure of tungsten oxides, *J. Alloys Compd.*, 305 (2000) 1-6.
- [101] Z. Wang, W. Wang, L. Zhang, D. Jiang, Surface oxygen vacancies on Co₃O₄ mediated catalytic formaldehyde oxidation at room temperature, *Catalysis Science & Technology*, 6 (2016) 3845-3853.
- [102] X. Li, X. Li, T. Zhu, Y. Peng, J. Li, J. Hao, Extraordinary Deactivation Offset Effect of Arsenic and Calcium on CeO₂-WO₃ SCR Catalysts, *Environmental science & technology*, 52 (2018) 8578-8587.
- [103] M.J. Manto, P. Xie, C. Wang, Catalytic dephosphorylation using ceria nanocrystals, *ACS Catalysis*, 7 (2017) 1931-1938.
- [104] Z. Paal, P. Menon, Hydrogen effects in metal catalysts, *Catalysis Reviews Science and Engineering*, 25 (1983) 229-324.
- [105] Y. Zhang, Y. Zhou, J. Shi, S. Zhou, X. Sheng, Z. Zhang, S. Xiang, Comparative study of bimetallic Pt-Sn catalysts supported on different supports for propane dehydrogenation, *J. Mol. Catal. A: Chem.*, 381 (2014) 138-147.
- [106] A. Guntida, K. Suriye, J. Panpranot, P. Praserthdam, Comparative Study of Lewis Acid Transformation on Non-reducible and Reducible Oxides Under Hydrogen Atmosphere by In Situ DRIFTS of Adsorbed NH₃, *Top. Catal.*, 61 (2018) 1641-1652.
- [107] X. Wu, L. Zhang, D. Weng, S. Liu, Z. Si, J. Fan, Total oxidation of propane on Pt/WO_x/Al₂O₃ catalysts by formation of metastable Pt δ^+ species interacted with WO_x clusters, *J. Hazard. Mater.*, 225 (2012) 146-154.
- [108] H. Xu, M. Sun, S. Liu, Y. Li, J. Wang, Y. Chen, Effect of the calcination temperature of cerium-zirconium mixed oxides on the structure and catalytic performance of WO₃/CeZrO₂ monolithic catalyst for selective catalytic reduction of NO_x with NH₃, *RSC Advances*, 7 (2017) 24177-24187.

- [109] M. Zaki, N. Fouad, S. Mansour, A. Muftah, Temperature-programmed and X-ray diffractometry studies of hydrogen-reduction course and products of WO₃ powder: Influence of reduction parameters, *Thermochim. Acta*, 523 (2011) 90-96.
- [110] M. Daniel, B. Desbat, J. Lassegues, B. Gerand, M. Figlarz, Infrared and Raman study of WO₃ tungsten trioxides and WO₃·xH₂O tungsten trioxide hydrates, *J. Solid State Chem.*, 67 (1987) 235-247.
- [111] Z. Xiao, Q. Zhang, T. Chen, X. Wang, Y. Fan, Q. Ge, R. Zhai, R. Sun, J. Ji, J. Mao, Heterobimetallic catalysis for lignocellulose to ethylene glycol on nickel-tungsten catalysts: Influenced by hydroxy groups, *Fuel*, 230 (2018) 332-343.
- [112] K. Gayapan, S. Sripinun, J. Panpranot, P. Prasertdam, S. Assabumrungrat, Effects of calcination and pretreatment temperatures on the catalytic activity and stability of H₂-treated WO₃/SiO₂ catalysts in metathesis of ethylene and 2-butene, *RSC Advances*, 8 (2018) 28555-28568.
- [113] K. Gayapan, S. Sripinun, J. Panpranot, P. Prasertdam, S. Assabumrungrat, Effect of pretreatment atmosphere of WO_x/SiO₂ catalysts on metathesis of ethylene and 2-butene to propylene, *Rsc Advances*, 8 (2018) 11693-11704.
- [114] E.I. Ross-Medgaarden, I.E. Wachs, Structural determination of bulk and surface tungsten oxides with UV-vis diffuse reflectance spectroscopy and raman spectroscopy, *The Journal of Physical Chemistry C*, 111 (2007) 15089-15099.
- [115] J. Horsley, I. Wachs, J. Brown, G. Via, F. Hardcastle, Structure of surface tungsten oxide species in the tungsten trioxide/alumina supported oxide system from x-ray absorption near-edge spectroscopy and Raman spectroscopy, *J. Phys. Chem.*, 91 (1987) 4014-4020.
- [116] Y. Dai, Y. Li, B. Zhang, Facile Fabrication of Ultrathin Tungsten-MFI Zeolite Films with Enhanced Hydrophobicity, *Crystal Growth & Design*, 19 (2019) 4521-4525.
- [117] J. Yan, T. Wang, G. Wu, W. Dai, N. Guan, L. Li, J. Gong, Tungsten oxide single crystal nanosheets for enhanced multichannel solar light harvesting, *Adv. Mater.*, 27 (2015) 1580-1586.
- [118] J.-F. Wu, A. Ramanathan, A. Biancardi, A.M. Jystad, M. Caricato, Y. Hu, B. Subramaniam, Correlation of Active Site Precursors and Olefin Metathesis Activity in W-Incorporated Silicates, *ACS Catalysis*, 8 (2018) 10437-10445.

- [119] O. Klepel, W. Böhlmann, E. Ivanov, V. Riede, H. Papp, Incorporation of tungsten into MCM-41 framework, *Microporous Mesoporous Mater.*, 76 (2004) 105-112.
- [120] L. Hu, S. Ji, Z. Jiang, H. Song, P. Wu, Q. Liu, Direct synthesis and structural characteristics of ordered SBA-15 mesoporous silica containing tungsten oxides and tungsten carbides, *The Journal of Physical Chemistry C*, 111 (2007) 15173-15184.
- [121] L. Hu, S. Ji, T. Xiao, C. Guo, P. Wu, P. Nie, Preparation and characterization of tungsten carbide confined in the channels of SBA-15 mesoporous silica, *The Journal of Physical Chemistry B*, 111 (2007) 3599-3608.
- [122] H. Xu, M. Sun, S. Liu, Y. Li, J. Wang, Y. Chen, Effect of the calcination temperature of cerium–zirconium mixed oxides on the structure and catalytic performance of WO₃/CeZrO₂ monolithic catalyst for selective catalytic reduction of NO_x with NH₃, *RSC Advances*, 7 (2017) 24177-24187.
- [123] X. Wu, L. Zhang, D. Weng, S. Liu, Z. Si, J. Fan, Total oxidation of propane on Pt/WO_x/Al₂O₃ catalysts by formation of metastable Pt^{δ+} species interacted with WO_x clusters, *J. Hazard. Mater.*, 225-226 (2012) 146-154.
- [124] S. Vorakitkanvasin, W. Phongsawat, K. Suriye, P. Praserttham, J. Panpranot, In situ-DRIFTS study: influence of surface acidity of rhenium-based catalysts in the metathesis of various olefins for propylene production, *RSC Advances*, 7 (2017) 38659-38665.
- [125] C. Persson, Å. Oskarsson, C. Andersson, Tungsten (VI) complexes with bidentate coordination of the catecholate monoanion. Synthesis of [W (O) Cl₃ (O, HO • C₆H₄) • O (C₂H₅)₂] and synthesis and crystal structure of [W (O) Cl (O₂ • C₆H₄)(O, HO • C₆H₄) • O (C₂H₅)₂], *Polyhedron*, 11 (1992) 2039-2044.
- [126] A. Basrur, S. Patwardhan, S. Was, Propene metathesis over silica-supported tungsten oxide catalyst—Catalyst induction mechanism, *J. Catal.*, 127 (1991) 86-95.
- [127] S.J. Choung, S.W. Weller, Oxygen chemisorption and olefin disproportionation activity of tungsten oxide/silica, *Industrial & Engineering Chemistry Process Design and Development*, 22 (1983) 662-665.
- [128] A. Balerna, E. Bernieri, E. Burattini, A. Kuzmin, A. Lusi, J. Purans, P. Cikmach, XANES studies of MeO_{3-x} (Me= W, Re, Ir) crystalline and amorphous oxides, *Nuclear*

Instruments and Methods in Physics Research Section A: Accelerators, Spectrometers, Detectors and Associated Equipment, 308 (1991) 240-242.

[129] C.D. Baertsch, K.T. Komala, Y.-H. Chua, E. Iglesia, Genesis of Brønsted acid sites during dehydration of 2-butanol on tungsten oxide catalysts, *J. Catal.*, 205 (2002) 44-57.

[130] E. Iglesia, F.H. Ribeiro, M. Boudart, J.E. Baumgartner, Synthesis, characterization, and catalytic properties of clean and oxygen-modified tungsten carbides, *Catal. Today*, 15 (1992) 307-337.

[131] R. Bera, S. Koner, Incorporation of tungsten oxide in mesoporous silica: Catalytic epoxidation of olefins using sodium-bi-carbonate as co-catalyst, *Inorg. Chim. Acta*, 384 (2012) 233-238.

[132] S. Ansari, M.S. Ansari, S.P. Satsangee, R. Jain, WO₃ decorated graphene nanocomposite based electrochemical sensor: A prospect for the detection of anti-anginal drug, *Anal. Chim. Acta*, 1046 (2019) 99-109.

[133] T.I. Bhuiyan, P. Arudra, M.N. Akhtar, A.M. Aitani, R.H. Abudawoud, M.A. Al-Yami, S.S. Al-Khattaf, Metathesis of 2-butene to propylene over W-mesoporous molecular sieves: A comparative study between tungsten containing MCM-41 and SBA-15, *Applied Catalysis A: General*, 467 (2013) 224-234.

[134] S. Lwin, Y. Li, A.I. Frenkel, I.E. Wachs, Nature of WO_x Sites on SiO₂ and Their Molecular Structure-Reactivity/Selectivity Relationships for Propylene Metathesis, *ACS Catalysis*, 6 (2016) 3061-3071.

[135] J.-F. Wu, A. Ramanathan, W.K. Snavey, H. Zhu, A. Rokicki, B. Subramaniam, Enhanced metathesis of ethylene and 2-butene on tungsten incorporated ordered mesoporous silicates, *Applied Catalysis A: General*, 528 (2016) 142-149.

[136] J.G. Howell, Y.-P. Li, A.T. Bell, Propene Metathesis over Supported Tungsten Oxide Catalysts: A Study of Active Site Formation, *ACS Catalysis*, 6 (2016) 7728-7738.

[137] X.-L. Yang, W.-L. Dai, R. Gao, H. Chen, H. Li, Y. Cao, K. Fan, Synthesis, characterization and catalytic application of mesoporous W-MCM-48 for the selective oxidation of cyclopentene to glutaraldehyde, *J. Mol. Catal. A: Chem.*, 241 (2005) 205-214.

- [138] M. Morey, J. Bryan, S. Schwarz, G. Stucky, Pore surface functionalization of MCM-48 mesoporous silica with tungsten and molybdenum metal centers: perspectives on catalytic peroxide activation, *Chem. Mater.*, 12 (2000) 3435-3444.
- [139] M.A.A. Aziz, K. Puad, S. Triwahyono, A.A. Jalil, M.S. Khayoon, A.E. Atabani, Z. Ramli, Z.A. Majid, D. Prasetyoko, D. Hartanto, Transesterification of croton megalocarpus oil to biodiesel over WO₃ supported on silica mesoporous-macroparticles catalyst, *Chem. Eng. J.*, 316 (2017) 882-892.
- [140] A. Bendjeriou-Sedjerari, J. Sofack-Kreutzer, Y. Minenkov, E. Abou-Hamad, B. Hamzaoui, B. Werghi, D.H. Anjum, L. Cavallo, K.W. Huang, J.M. Basset, Tungsten(VI) Carbyne/Bis(carbene) Tautomerization Enabled by N-Donor SBA15 Surface Ligands: A Solid-State NMR and DFT Study, *Angew. Chem. Int. Ed. Engl.*, 55 (2016) 11162-11166.
- [141] A. Chirkin, V. Lavrenko, M. Malysheva, L. Kuznetsova, Composition and structure of functional groups on the surface of tungsten disilicide powder, *Powder Metall. Met. Ceram.*, 51 (2012) 1-6.
- [142] S. Boonpai, S. Wannakao, K. Suriye, V. Márquez, J. Panpranot, B. Jongsomjit, P. Praserttham, A.T. Bell, Influence of surface Sn species and hydrogen interactions on the OH group formation over spherical silica-supported tin oxide catalysts, *Reaction Chemistry & Engineering*, 5 (2020) 1814-1823.
- [143] A.A. Azmi, A.H. Ruhaimi, M.A.A. Aziz, Efficient 3-aminopropyltrimethoxysilane functionalised mesoporous ceria nanoparticles for CO₂ capture, *Materials Today Chemistry*, 16 (2020).
- [144] G. Wang, H. Zhang, H. Wang, Q. Zhu, C. Li, H. Shan, The role of metallic Sn species in catalytic dehydrogenation of propane: Active component rather than only promoter, *J. Catal.*, 344 (2016) 606-608.
- [145] G. Wang, H. Zhang, Q. Zhu, X. Zhu, X. Li, H. Wang, C. Li, H. Shan, Sn-containing hexagonal mesoporous silica (HMS) for catalytic dehydrogenation of propane: An efficient strategy to enhance stability, *J. Catal.*, 351 (2017) 90-94.
- [146] T. Iida, A. Takagaki, S. Kohara, T. Okubo, T. Wakihara, Sn-Beta Zeolite Catalysts with High Sn Contents Prepared from Sn-Si Mixed Oxide Composites, *ChemNanoMat*, 1 (2015) 155-158.

- [147] K. Wongsaprom, R.-a. Bornphotsawatkun, E. Swatsitang, Synthesis and characterization of tin oxide (SnO₂) nanocrystalline powders by a simple modified sol–gel route, *Appl. Phys. A*, 114 (2013) 373-379.
- [148] J. Zhu, B.Y. Tay, J. Ma, Synthesis and mechanism study of mesoporous SnO₂/SiO₂ composites, *J Nanosci Nanotechnol*, 6 (2006) 2046-2055.
- [149] H. Wang, H. Wang, X. Li, C. Li, Nature of active tin species and promoting effect of nickle in silica supported tin oxide for dehydrogenation of propane, *Appl. Surf. Sci.*, 407 (2017) 456-462.
- [150] X. Wang, H. Xu, X. Fu, P. Liu, F. Lefebvre, J.-M. Basset, Characterization and catalytic properties of tin-containing mesoporous silicas prepared by different methods, *J. Mol. Catal. A: Chem.*, 238 (2005) 185-191.
- [151] U.S. Taralkar, P. Kalita, R. Kumar, P.N. Joshi, Synthesis, characterization and catalytic performance of Sn-MCM-48 in solvent-free Mukaiyama-type aldol condensation reactions, *Applied Catalysis A: General*, 358 (2009) 88-94.
- [152] H. Zhu, D.H. Anjum, Q. Wang, E. Abou-Hamad, L. Emsley, H. Dong, P. Laveille, L. Li, A.K. Samal, J.-M. Basset, Sn surface-enriched Pt–Sn bimetallic nanoparticles as a selective and stable catalyst for propane dehydrogenation, *J. Catal.*, 320 (2014) 52-62.
- [153] Q. Liu, M. Luo, Z. Zhao, Q. Zhao, K-modified Sn-containing dendritic mesoporous silica nanoparticles with tunable size and SnO_x-silica interaction for the dehydrogenation of propane to propylene, *Chem. Eng. J.*, 380 (2020).
- [154] X. Fan, J. Li, Z. Zhao, Y. Wei, J. Liu, A. Duan, G. Jiang, Dehydrogenation of propane over PtSnAl/SBA-15 catalysts: Al addition effect and coke formation analysis, *Catalysis Science & Technology*, 5 (2015) 339-350.
- [155] B.K. Vu, M.B. Song, I.Y. Ahn, Y.-W. Suh, D.J. Suh, W.-I. Kim, H.-L. Koh, Y.G. Choi, E.W. Shin, Pt–Sn alloy phases and coke mobility over Pt–Sn/Al₂O₃ and Pt–Sn/ZnAl₂O₄ catalysts for propane dehydrogenation, *Applied Catalysis A: General*, 400 (2011) 25-33.
- [156] E.P. Reddy, L. Davydov, P.G. Smirniotis, Characterization of Titania Loaded V-, Fe-, and Cr-Incorporated MCM-41 by XRD, TPR, UV–vis, Raman, and XPS Techniques, *The Journal of Physical Chemistry B*, 106 (2002) 3394-3401.

- [157] J.A. Cecilia, E. Vilarrasa-García, C. García-Sancho, R.M.A. Saboya, D.C.S. Azevedo, C.L. Cavalcante, E. Rodríguez-Castellón, Functionalization of hollow silica microspheres by impregnation or grafted of amine groups for the CO₂ capture, *International Journal of Greenhouse Gas Control*, 52 (2016) 344-356.
- [158] C.-M. Yang, H.-A. Lin, B. Zibrowius, B. Spliethoff, F. Schüth, S.-C. Liou, M.-W. Chu, C.-H. Chen, Selective surface functionalization and metal deposition in the micropores of mesoporous silica SBA-15, *Chem. Mater.*, 19 (2007) 3205-3211.
- [159] J. Dijkmans, M. Dusselier, W. Janssens, M. Trekels, A. Vantomme, E. Breynaert, C. Kirschhock, B.F. Sels, An Inner-/Outer-Sphere Stabilized Sn Active Site in β -Zeolite: Spectroscopic Evidence and Kinetic Consequences, *ACS Catalysis*, 6 (2015) 31-46.
- [160] J. Zhang, L. Gao, Synthesis and characterization of antimony-doped tin oxide (ATO) nanoparticles, *Inorg. Chem. Commun.*, 7 (2004) 91-93.
- [161] P. Park, H.H. Kung, D.-W. Kim, M. Kung, Characterization of SnO₂/Al₂O₃ lean NO_x catalysts, *J. Catal.*, 184 (1999) 440-454.
- [162] A. Van Meerbeek, A. Jelli, J. Fripiat, Reduction of the surface of silica gel by hydrogen spillover, *J. Catal.*, 46 (1977) 320-325.
- [163] P. Meriaudeau, A. Thangaraj, C. Naccache, S. Narayanan, Interaction of hydrogen with Pt-Silicalite, *J. Catal.*, 148 (1994) 617-624.
- [164] V. Zholobenko, L. Kustov, V.Y. Borovkov, V. Kazansky, A new type of acidic hydroxyl groups in ZSM-5 zeolite and in mordenite according to diffuse reflectance infrared spectroscopy, *Zeolites*, 8 (1988) 175-178.
- [165] Z. Chao, T. Wu, J. Ye, G. Chen, H. Wan, ¹H MAS NMR characterization of hydrogen over silica-supported rhodium catalyst, *Science in China Series B: Chemistry*, 44 (2001) 103-112.
- [166] M. Dementyeva, T. Sheshko, Y.M. Serov, Synthesis of olefins from CO and H₂ at atmospheric pressure on Fe- and MnO₂-containing nanosystems, *Theor. Exp. Chem.*, 49 (2013) 46-51.
- [167] S.E. Collins, J.J. Delgado, C. Mira, J.J. Calvino, S. Bernal, D.L. Chiavassa, M.A. Baltanás, A.L. Bonivardi, The role of Pd-Ga bimetallic particles in the bifunctional

mechanism of selective methanol synthesis via CO₂ hydrogenation on a Pd/Ga₂O₃ catalyst, *J. Catal.*, 292 (2012) 90-98.

[168] R. Bhat, W. Sachtler, Potential of zeolite supported rhodium catalysts for the CO₂ reforming of CH₄, *Applied Catalysis A: General*, 150 (1997) 279-296.

[169] L. Qian, Y. Ren, H. Yu, Y. Wang, B. Yue, H. He, Controlled atmosphere ¹³C and ¹H MAS NMR study of reforming route of methane with carbon dioxide over Rh/SBA-15, *Applied Catalysis A: General*, 401 (2011) 114-118.

[170] X. Wang, Y.-c. Xie, Preparation and characterization of SnO₂-based composite metal oxides: active and thermally stable catalysts for CH₄ oxidation, *Catal. Lett.*, 75 (2001) 73-80.

[171] X.-L. Yang, W.-L. Dai, H. Chen, J.-H. Xu, Y. Cao, H. Li, K. Fan, Novel tungsten-containing mesoporous HMS material: its synthesis, characterization and catalytic application in the selective oxidation of cyclopentene to glutaraldehyde by aqueous H₂O₂, *Applied Catalysis A: General*, 283 (2005) 1-8.

[172] Z. Liu, J. Zhou, K. Cao, W. Yang, H. Gao, Y. Wang, H. Li, Highly dispersed nickel loaded on mesoporous silica: One-spot synthesis strategy and high performance as catalysts for methane reforming with carbon dioxide, *Applied Catalysis B: Environmental*, 125 (2012) 324-330.

[173] V. Parvulescu, C. Anastasescu, C. Constantin, B.-L. Su, Mono (V, Nb) or bimetallic (V-Ti, Nb-Ti) ions modified MCM-41 catalysts: synthesis, characterization and catalysis in oxidation of hydrocarbons (aromatics and alcohols), *Catal. Today*, 78 (2003) 477-485.

[174] B. Rakshe, V. Ramaswamy, A. Ramaswamy, Crystalline, microporous zirconium silicates with MEL structure, *J. Catal.*, 163 (1996).

[175] D. Lenz, W.C. Conner Jr, J. Fraissard, Hydrogen spillover on silica III. Detection of spillover by proton NMR, *Journal of Catalysis;(USA)*, 117 (1989).

VITA

NAME Sirawat Boonpai

DATE OF BIRTH 23 July 1993

PLACE OF BIRTH SARABURI

INSTITUTIONS ATTENDED Chulalongkorn University

HOME ADDRESS 713/1 M.11, Sung Noen, Sung Noen, Nakhon Ratchasima, Thailand, 30170

PUBLICATION

- 1) S. Boonpai, K. Suriye, B. Jongsomjit, J. Panpranot, P. Prasertdam, Catal. Today, 358 (2020) 370–386.
- 2) S. Boonpai, S. Wannakao, J. Panpranot, B. Jongsomjit, P. Prasertdam, J. Phys. Chem. C, 124 (2020) 15935-15943.
- 3) S. Boonpai, S. Wannakao, K. Suriye, V. Márquez, J. Panpranot, B. Jongsomjit, P. Prasertdam, A.T. Bell, React. Chem. Eng., 5 (2020) 1814-1823.

AWARD RECEIVED

- 1) SCG Chemicals Co., Ltd. Fully Funded Ph.D. Scholarship
- 2) PTT Exploration and Production Public Company Limited (PTTEP) Scholarship
- 3) Thai Oil Public Company Limited Scholarship